# RF-EMF Radiation Exposure and Radio Resources Management in 5G Wireless Network.


By

**Adedotun Temitope Ajibare**

Supervisor:
**Dr Daniel Ramotsoela.**

This dissertation is submitted in partial fulfilment of the academic requirements for the Master of Science in Engineering to the Department of Electrical Engineering, Faculty of Engineering and Built Environment University of Cape Town.

As the candidate's supervisor, I have approved this dissertation for submission.

Name: Dr Daniel Ramotsoela

Signature:

Date:

# Declaration

I know the meaning of plagiarism and declare that all the work in the document, save for that which is properly acknowledged, is my own. This dissertation has been submitted to the Turnitin module and I confirm that my supervisor has seen my report and any concerns revealed by such have been resolved with my supervisor.

I present the dissertation for examination for the Degree of MSc Eng. in Electrical Engineering. I also grant the University a free license to reproduce the above thesis in whole or in part, for the purpose of research.

Name: Adedotun Temitope Ajibare

Signature: Signed by candidate

Date: 23/12/2021

# Dedication

To Almighty God - The Alpha ($\alpha$) and the Omega ($\Omega$).

To my Parents - For your impeccable value for education.

# Abstract

The fifth generation (5G) mobile network is expected to solve the challenge of heavy network traffic demand associated with mobile communication networks. Mobile communication network is characteristically heterogeneous with several base stations and numerous users with diverse demands. With the limited radio resources, there will be an infeasibility challenge in the network as the system capacity is unable to support the users' target quality of service (QoS) requirements. To bring solution to the limited resources, heavy traffic demands and congestion problems; an efficient management of resources such as; the transmit power, time, physical resource blocks (PRBs), frequency (sub-channels) is required.

Deciding on how to efficiently allocate, manage, and control the resources dynamically among several slices and users in an isolated multi-tenancy scenario without compromise on the QoS/quality of experience (QoE) of user is very important. Also important is the consideration of the network challenges such as; interference (on user equipment (UE)) and radiofrequency electromagnetic field (RF-EMF) radiation exposure (a health challenge on user) emitted in both the uplink and downlink of wireless networks, especially the 5G mobile network. Therefore, this research aims to assess the impacts of these challenges, develop and evaluate efficient radio resources management schemes and algorithms. Schemes that will effectively guarantee the users' QoS in terms of the data rate and reduced the interference and radiation exposure of the users in the network. Thus, this dissertation proposes four major solutions in 5G mobile networks.

Firstly, a 5G network resource allocation scheme is proposed. A QoE resource allocation problem is formulated as an optimisation problem, the proposed scheme solves the problem using Mixed Integer Non-Linear Program (MINLP). It jointly incorporates admission control and a heuristic mechanism that takes the QoS constraints, the slice's and user's priorities into consideration to enhance resource utilisation efficiency, improve the throughput of users, and consequently, the QoE of users.

In addition, this research also proposed a novel slicing carrier assignment scheme (SCAS), a joint power and sub-channel allocation scheme in a 5G network to reduce the co-users interference in the network. In SCAS, an optimisation

problem is formulated to minimise the downlink transmit power while guaranteeing a minimum data rate requirement for the slice and user subject to QoS constraints, interference thresholds, gNB power budget and the sub-channel orthogonality constraints. The scheme assigns sub-channels to users considering the transmit power level of the neighbouring sub-channel before allocating the sub-channel to users by comparing the transmit power threshold of the slice to which the user belongs.

Thirdly, this work investigates the impact of radiofrequency (RF) electromagnetic fields (EMF) radiation exposure induced by wireless networks, most importantly 5G cellular networks for both the uplink and downlink radio emissions using exposure-index open-loop power control algorithm (EOPCA), a novel simulation method that quantifies the realistic electromagnetic exposure of the human user. The exposure index (EI) is used to characterize the EMF exposure taking into account the power density, specific absorption rate (SAR), the electric field strength as well as considering other factors such as the environment, the conductivity and the mass density of the tissue. The radiations emitted from APs and UEs were simulated, analyzed and compared with the threshold set by the International Commission on Non-Ionizing Radiation Protection (ICNIRP) for the understanding of radiation impact.

Lastly, this work investigates the effect of minimising the EI and SAR induced in the 5G mobile networks and its impact on the QoS of the users in the network. It proposed a power control algorithm that solves an optimisation problem formulated to minimise the EI while guaranteeing the QoS requirement of users. Given that the radiated SAR and EI are characterized by power density in the wireless network, the proposed algorithm controls the transmit and the received powers subject to interference, power and QoS constraints. The performance of the proposed schemes were evaluated and compared with standards and other algorithms in the literature. The results show that the enhanced network efficiency, improved users' QoS, reduced users' interference and reduced radiation exposure (SARs and EIs) on the users in 5G network while satisfying the required QoS in terms of the data rate. Furthermore, the results reveal that both SAR and EI are tolerable and fall within the thresholds set by the ICNIRP and other regulators.

# Acknowledgements

I thank Almighty God for making it possible for me to complete the degree, especially the research. I am grateful to my supervisor Dr. Daniel Ramotsoela, for his guidance and support throughout the entire research.

I am especially grateful to my colleagues, Dr 'Dayo Oladejo, Dr Lateef Akinyemi, Mr Stephen Ekwe and Mr Mfon Charles for their constant show of love, support and constructive criticisms throughout my research.

Most importantly, I thank my enduring, loving, and supportive family, especially my wife, kids, and parents for always being there for me. You are limited and special editions.

# Table of Contents

# List of Figures

# List of Tables

# List of Acronyms

**1G** - First Generation

**2G** - Second Generation

**2.5G** - Second-and-a-half Generation

**2.75G** - Second-and-three-quarters Generation

**3GPP** - Third Generation Partnership Project

**4G** - Fourth Generation

**5G** - Fifth Generation

**AN** - Access Network

**AP** - Access Point

**APD** - Amplitude Probability Distribution

**API** - Application Programming Interface

**B** - Bandwidth

**BER** - Bit Error Rate

**BS** - Base station

**C5GNA** - Conventional 5G Network Algorithm

**CAPEX** - Capital Expenditures

**CCI** - Co-Channel Interference

**CN** - Core Network

**CP** - Control Plane

**CSI**- Channel State Information

**D2D** - Device-To-Device

**DL** - Downlink

**DP** - Data Plane

**DRL** - Dosimetric Reference Limit

**E2E** - End-To-End

**EDGE** - Enhanced Data rate for GSM Evolution

**EI** - Exposure Index

**EIPCA** - Exposure Index Power Control Algorithm

**EM** - Electromagnetic

**eMBB** - enhanced Mobile Broadband

**EOPCA** - Exposure-index Open-loop Power Control Algorithm

**ERL** - Exposure Reference Level

**FCC** - Federal Communications Communication

**FDD** - Frequency Division Duplex

**gNB** - gNodeB

**GSM** - Global System for Mobile Communications

**GPRS** - General Packet Radio Services

**HetNet** - Heterogeneous Network

**IBN** - Institute for Building Biology + Sustainability

**IEEE** - Institute of Electrical and Electronics Engineers

**ICNIRP** - the International Commission on Non-Ionizing Radiation Protection

**IMT** - International Mobile Telecommunications

**InP** - Infrastructure Provider

**IoT** - Internet of Things

**ISI** - Inter-Symbol Interference

**ITU** - International Telecommunication Union

**KPI** - Key Performance Indicator

**LEXNET** - Low Electromagnetic Field Exposure Networks

**LoS** - Line-of-Sight

**LTE -** Long Term Evolution

**LTE-A** - LTE-Advanced

**MAC** - Media Access Control

**MANO** - Management and Orchestration

**mMTC** - Massive Machine Type Communications

**MINLP** - Mixed-Integer Non-Linear Program

**MVNO** - Multiple Virtual Network Operator

**NF** - Network Function.

**NFV** - Network Functions Virtualisation

**NFV-MANO** - NFV Management and Orchestration

**NGN** - Next Generation Networks

**NOMA** - Non-Orthogonal Multiple Access

**NSI** - Network Service Instance

**Ofcom** - The Office of Communications

**OFDMA** - Orthogonal Frequency Division Multiple Access

**ONF** - Open Networking Foundation

**OPEX** - Operating Expenditure

**PPE** - Personal Protective Equipment

**PRAAC** - Prioritized Resource Allocation and Admission Control

**PRB** - Physical Resource Blocks

**QCI** - QoS Class Identifier

**QoE** - Quality of Experience

**QoS** - Quality of Service

**RA** - Resource Allocation

**RAN** - Radio Access Network

**RAT** - Radio Access Technology

**Rx** - Receiver

**SA** - Spectrum Analyser

**SAR** - Specific Absorption Rate

**SCAS** - Slicing Carrier Assignment Scheme

**SC-FDMA** - Single Carrier-Frequency Division Multiple Access

**SDN** - Software Defined Networks

**SINR** - Signal-to-Interference-and-Noise-Ratio

**SLA** - Service Level Agreement

**SNR** - Signal-to-Noise-Ratio

**SON** - Software Organising Networks

**SP** - Service Provider

**TN** - Transport Network

**TTI** - Transmission Time Interval

**TX** - Transmitter

**UE** - User Equipment

**UPF** - User Plane Function

**URLLC** - Ultra-Reliable Low-Latency Communications.

**VAR** - Volume Absorption Rate

**VM** - Virtual Machine

**VN** - Virtual Network

**VNF** - Virtual Network Function

**VoIP** - Voice over Internet Protocol

# Chapter 1

# 1. Introduction

## 1.1. Background

The advent of the fourth industrial revolution (4IR) [1] in 2011 also referred to as Industry 4.0, has brought about many evolving technologies especially in wireless communication. The transformation of mobile communication started in the early 1980s with the first-generation (1G) mobile technology in Finland [2] and metamorphosed in the early 1990s to the digital second generation (2G), widely known as the Global System for Mobile Communications (GSM) [2]. The huge leap of the evolution of the 2G to the third-generation (3G) networks in the United States in 2003 was premised on the General Packet Radio Service (GPRS) [2]. In a similar trend, in 2009, the third-generation (3G) of mobile networks was enhanced into an all-IP packet-switched network leading to the fourth generation (4G) of mobile networks [2]. These advancements in the technologies in mobile networks from one generation to another brought about changes not only in the nomenclature but also significant improvements in the Quality of Service (QoS), the Quality of Experience (QoE), the capacity and of course the efficiency of networks [3]. However, the increase in the number of user devices and the sophistication of these user devices, as well as the 'big' data which is forecast [3], [4], [5] by many experts and major stakeholders in both industry and academia to be on an astronomical increase. As a result of this projection and the anticipated demand for wireless radio resources, the 4G network has evolved with better QoS requirements to a new generation of mobile networks in 2020. Following the similar trends in nomenclature, this new generation is the fifth-generation (5G) of mobile networks.

The 5G network is motivated by and is expected to meet the QoS requirements of industry 4.0 (the verticals), such as the high number of connected devices, low energy consumption, low latency, and high data rates [6]. Currently,

5G network operates in the sub-6 GHz frequency band and it is expected that future 5G networks will be deployed using the promising millimetre wave (mm-wave) communications band of 28 and 39 GHz. Such high operating frequencies reduces the coverage areas of the Access Points (APs) in the network. Therefore, there will be a corresponding increase in the number of radio APs and multiple-input-multiple-output (MIMO) antennas [7] to make up for the reduced coverage area [7]. This proliferation of APs and antenna has increased the interference and also the exposure concerns and have geared interests towards many researches and investigations [8], [9], [10] on the induced electromagnetic (EM) radiations originating from the mobile network.

The RF electromagnetic radiation has been classified as non-ionizing radiation as its photons do not have enough energy to break bonds or ionize biological molecules [11]. Moreover, there is a need for proper network planning and examination of the levels of radiation exposure in the 5G network taking into account its different effects of transmitter (Tx) and receiver (Rx) on users, This investigated level of radiation exposure characterized from the electric field strength ($E$) and the magnetic field strength ($H$), should be compared with the threshold set by the international regulatory bodies such as the International Commission on Non-Ionizing Radiation Protection (ICNIRP) [12], United State (US) Federal Communications Communication (FCC) [13], and the Institute of Electrical Electronics Engineers (IEEE) [14].

These radiation exposure limits are defined using the power density, (S), the Specific Absorption Rate (SAR), or the Exposure Index (EI); a metric developed by the European Union (EU) Low Electromagnetic Field Exposure Networks (LEXNET) [15].

The realisation of 5G networks will be made possible with enabling technologies such as Network Slicing (NS), Software Defined Networking (SDN), Network Function Virtualisation (NFV) and Mobile Edge Computing (MEC) [16], [17]. NS is a fusion of the enabling technologies of 5G networks. A 5G sliced network is a mobile communication system that involves the abstraction of multiple isolated logical networks running on a single physical network to support a wide range of verticals (such as manufacturing, transportation systems, energy utilities, health care facilities, public safety institutions, media and entertainment) with different set of QoS requirements. A NS framework is made possible by both

SDN and NFV [5]. The diverse set of services provided by Network Slicing as a dedicated virtual network is known as NS [18]. The 5G network has significant merits when compared to existing networks, on account of logical networks that give better performance when compared to the one-size-fits-all model. It is expected that 5G networks will provide different requirement-based services in the form of network slices. These network slices are classified based on QoS requirements, such as enhanced Mobile Broadband (eMBB), Ultra-Reliable Low-Latency Communication (URLLC), and massive Machine Type Communication (mMTC) [19].

Moreover, NS through virtualisation capability enhances the flexibility, agility, efficiency, and manageability networks of the 5G network. It optimises the utilisation of physical network resources. Through NS and virtualisation, the concept of multi-tenancy in which different Mobile Virtual Network Operators (MVNOs) share the underlying physical network of the Infrastructure Providers (InP), is achievable in 5G networks and this will bring about other benefits, such as profit maximisation for both the MVNOs and InP and resource efficiency [18].

Resource sharing and management among these slice tenants and their users are important. Mobile network resources are allocated primarily through static partitioning and dynamic partitioning, respectively. In static partitioning, a fixed share of the network resource is allocated to MVNOs irrespective of the traffic condition of the network and QoS demands. In dynamic partitioning, network resources are allocated to MVNOs by consideration of the stochastic characteristic of the network traffic and QoS demands. Moreover, dynamic partitioning results in an agile and efficient network. As a result, designing a dynamic resource allocation and admission scheme is necessary. The scheme will have an algorithm that can reconfigure and migrate network resources despite the required isolation in the network.

Also in a shared spectrum, due to the high transmit power of some slice users as a result of the QoS requirements of the slice, such as high data rates allocated to these users, co-channel interference will exist in the network. To mitigate the problem of interference caused by both spectrum resources sharing and the high transmit power, dynamic slicing; and a scheduling scheme using joint power and a sub-channel is proposed. Based on the QoS requirement of the use case, it is expected that the various slices will require a different level of transmit power. Sub-channels are allocated by the scheduler based on the transmit power to

minimise interference in the entire network. This dissertation, therefore, addresses three major areas in the 5G network resource management, namely resource allocation, interference, and radiation mitigation as shown in Fig. 1.1.

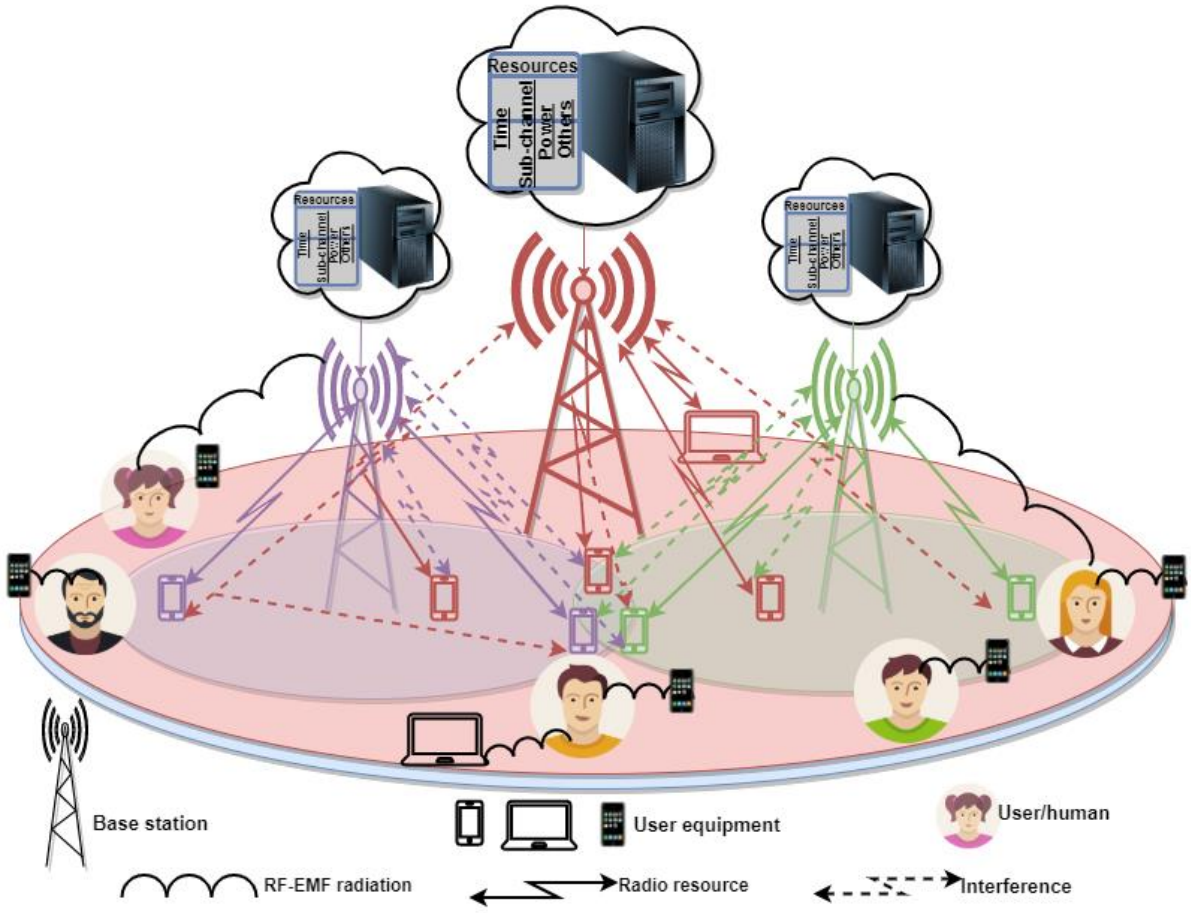


*Figure 1.1: Schematic illustration of the radio resource, interference and RF-EMF radiation management in 5G network.*

Firstly, this work focuses on the development of an admission control scheme for effective allocation of network resources in 5G sliced networks, while considering both priorities among slices (inter-slice priorities) and priorities among users belonging to the same slice (intra-slice priorities). This prioritized resource allocation and admission control (PRAAC) scheme is formulated as a Mixed Integer Non-Linear Program (MINLP) that solves the resource allocation problem [20] jointly with admission control to deal with infeasibility issues in optimisation when considering new user equipment (UE) requests based on their priorities and slice data rate (i.e., QoS) threshold. The proposed heuristic mechanism aims to enhance resource utilisation efficiency, increase the overall system performance, improve

users' throughput, and consequently, the users' QoE, by considering their QoS constraints and priorities. Results obtained show that the proposed scheme improves the users' QoE when compared to the traditional resource allocation (RA) method.

To meet the adaptive resource allocation problem and reduce the interference challenge, this dissertation also examines the problem of interference created as a result of shared resources at the base station. It investigates the joint power and sub-channel allocation scheme in 5G networks with the aim of reducing the co-users interference in the network. It proposes a novel slicing carrier assignment scheme (SCAS), in which an optimisation problem is formulated by guaranteeing a minimum data rate requirement for each slice. In assigning sub-channels to slice users, the scheme considers the transmit power level of the neighbouring sub-channels before allocating a sub-channel to users. The proposed scheme compares the transmit power threshold of the slice to which the user belongs subject to the QoS constraints and Channel State Information (CSI) of the sub-channel. With the aid of a slice scheduler (algorithm), the sub-channel constraints reduce interference, thereby increasing the channel's Signal-to-Interference-Noise-Ratio (SINR), throughput and the overall network efficiency. Simulation results demonstrates that the proposed scheme reduces interference experienced by the users in the network, and enhances network efficiency.

Also, to mitigate the radiation induced by both the uplink (UL) and downlink (DL) transmissions in wireless communication, this work analyses the radiation exposure emitted by wireless networks using a computational method, by simulating the system models of heterogeneous 4G and 5G networks and characterizing the power density, the SAR, and the EI generated by the induced RF-EMF exposure of the user's location in the network area. An open-loop fractional power control concept (OLPC) that controls the UE transmit power $P_{tx}$ for the uplink transmission was incorporated into the proposed scheme.

Furthermore, the impact of having the power controlled in the network will reduce UE transmit and received power, hence, minimise EMF exposure and at the same time reducing the interference [21] in the network. This work also proposes a power control and optimisation algorithm that minimises the characterised EI in the form of the power density in a simulated 5G network. To avoid an unreasonable trade-off between radiation exposure and required QoS amongst users in the

network, the minimisation is subject to maintaining acceptable QoS with low EMF in UL and DL transmissions.

## 1.2. Problem Definition and Research Motivation

The 5G is expected to be a virtualised multitenancy network where several MVNOs will be sharing the same physical Radio Access Network (RAN) provided by a single InP. These shared network resources are limited, scarce and costly [22]; there is a need for dynamic resource sharing in 5G virtualised multitenant networks due to varying QoS requirements, the network traffic, costs, and the diverse characteristics of its different MVNOs.

Also, due to the many MVNOs, slices, and users sharing the spectrum with high transmit power to meet their expected QoS targets, there will be more interference in the heterogeneous network (HetNet). Moreover, it is also expected that with a 5G network, there will be a proliferation of APs and massive Multiple-In Multiple-Out (MIMO) antennas thereby causing more radiofrequency electromagnetic fields (RF-EMF) radiation in and around the network coverage areas.

### 1.2.1. Problem Definition

Therefore, this research has identified three (3) major challenges;

- Issue of resource sharing among different MVNO's slices, and users.
- Increase in the network interference among users, and.
- Increase in RF radiation exposure to users in the network coverage area.

### 1.2.2. Research Motivation

As a result of the problems defined above, there is motivation to study and address these challenges with an efficient RF-EMF radiation exposure and radio resources management in 5G network. The motivations of this research as highlighted as follows:

- There is a need to design a practical, efficient, flexible, and dynamic resource allocation and admission control algorithms that account for different users' traffic demands. These algorithms would have the ability to migrate and reconfigure slice resources to improve the overall performance and reduce both the InP and the MVNOs Operating Expenditure (OPEX).

- Additionally, there is a need to develop a scheme that will allocate sub-carriers to user equipment based on the minimum required transmit power of the slice they belong to. This would minimise the total transmit power and resultantly, the co-user interference in the network.

- Furthermore, there is a need to investigate, compute, and analyse the effect of the electromagnetic exposure radiated from the 5G wireless network to (human) users. Also, these characterised exposures should be compared with the limits advised by the regulatory bodies.

- Lastly, there is a strong motivation to provide RF-EMF exposure mitigation methods (such as power control scheme and power optimisation algorithm), increase health awareness, and abate the controversies surrounding 5G radiofrequency radiation exposure to users.

## 1.3. Research Questions

The research questions in this dissertation are as follow:

- How can radio resources be fairly assigned to the various users and slices with their intra-slice and inter-slice priorities in a dynamic multitenant 5G network?

- How can the interference be minimised using joint power control and sub-channel assignment while allocating resources to the different users and slices in a 5G network?

- How can the RF-EMF radiation exposures be assessed, evaluated and mitigated in an ultra-dense 5G network environment?

- How can the network resources (such as frequency, power, time, and distance) be optimised and used to minimise the RF-EMF radiation exposures in the 5G network without compromising the QoS of users?

## 1.4. Research Aim and Objectives

This work's aim is to develop schemes that allocate radio and network resources efficiently to users in a 5G network with reduced network interference and RF-EMF radiation exposure.

The research objectives of this dissertation is as follows:

- To develop a resource allocation and admission control scheme for a virtualised multitenant 5G network using slice's and users' priorities to meet needed QoE requirements of users and maximize the overall network resources.
- To design a dynamic slicing and scheduling scheme for 5G networks using joint power and sub-carrier allocation that both mitigates the users' interference and increases network capacity.
- To investigate the effects of lower transmit power and lower SINRs in the network, develop a scheme that uses an effective power control mechanism in reducing the RF-EMF radiation exposure in a 5G network and maintain acceptable QoS with low EMF in both UL and DL transmissions.
- To develop a scheme that uses an optimisation problem to minimise the total EI of users in the network by minimising the transmit and received powers in the network.
- To implement and evaluate the proposed schemes in a simulated 5G networks environment.

## 1.5. Research Methodology

In this research, 5G virtual networks were modelled in a simulated wireless network environment. The research work aims to optimise radio resources while mitigating RF-EMF exposure and interference in a 5G network, for the system efficiency, enhancement of the users' QoE and health.

This research comprises basically optimisation solutions to the problems earlier defined. Many works of literature were reviewed to provide the needed background of the subject. And a couple of related works were reviewed along the problem's and the proposed solution's line. An admission control method was jointly incorporated for the resources allocation scheme. Additionally, analytical derivations and theoretical formulations, as well as computer simulations were engaged in solving for the RF-EMF exposure from the network. Three of the formulated problems were solved with optimisation tools and methods and the experiments were simulated using MATLAB. The MINLP optimisation approach was chosen as the optimisation tool. The evaluation of the proposed solutions to the problems formulated shows that the optimisation tools and methods improved the QoS, the QoE, mitigated and reduced both the interference and radiation exposure experienced by the users. Hence, this justifies the choice of methodological approach employed in this study. The proposed schemes were solved by first recognizing the problem, defining the problem, constructing a model, solving the problem, validating the solution, and implementing the solution.

## 1.6. Scope and Limitations

This dissertation is in partial fulfilment, therefore, its scope is constrained to some limitations such as complexity, time, and resources. All the proposed solutions in this dissertation are considered for the 5G network which is expected to be ultra-dense and heterogeneous. However, without loss of generality, the first two schemes (PRAAC and SCAS) were simply modelled using the downlink of the AP where a single gNodeB (gNB) is considered. Furthermore, this single RAN and its resources belong to a single InP that provides services to different MVNOs. These MVNOs provide services to their own UE based on the agreed Service Level Agreement (SLA) they subscribe to, as in a multi-tenancy setup.

The slices used in this dissertation are based on three main 5G use cases; that is, the mMTC, the eMBB, and the URLLC [23]. Each UE can only request service from the single slice it subscribes to at a time. In the considered scheme, the priorities of the slice are set based on the importance of the QoS required, while the priorities of the user are set based on a prior bargain made with the Service Provider (SP) which might be in terms of the SLA or contract signed. Moreover, in the first scheme, signal-to-noise-ratio was considered as it assumed no interference among the users.

In analysing the radiation exposure, we considered both the downlink and uplink transmissions of a HetNet. However, this research was limited to analysis through computer simulation only and could not do field measurement with the use of a spectrum analyser (SA) or dosimeter because of the cost and the time of getting one.

The biological details of RF-EMF radiation exposure to humans are not considered as this is basically a research work from wireless networks point of view. The research assumed constant values for some environmental and biological scenarios such as tissue temperature, tissue conductivity, permittivity, body mass density [24].

## 1.7. Contributions to knowledge

The major contributions recorded in the course of this study have been peer-reviewed in some international technical publications that are highlighted later in this section. The contributions are summarised as follows:

- A prioritized resource allocation and admission control scheme has been proposed and developed. This scheme incorporates admission control and iteratively maximized the QoE of UEs considering the QoS constraints and priorities to deal with infeasibility challenges and enhance both the QoS and QoE of the users and ultimately the overall network resources. The resource allocation and admission control problem is formulated as an optimisation problem. The proposed scheme proffered an MINLP solution to this problem by dynamically assigning radio resources to a multitenant network with slices and users based on their agreed SLA. The MINLP maximizes a derived QoE of users in the network with intra-slice priorities, inter-slice priorities, and some QoS constraints. The performance of the

PRAAC scheme is examined via different parameters and metrics such as data rate, QoE. The scheme is compared with an algorithm in the literature.

- A joint-power and sub-channel allocation scheme has been developed. The proposed scheme incorporates the idea of orthogonality of sub-channels in the frequency domain and applied it to a virtualised sliced network where different transmit power is required for diverse types of service/slice that has different QoS requirements. With a centralised scheduler/controller, the proposed scheme dynamically admit users and allocates the most suitable sub-channel(s) and other network resources. The proposed scheme uses MINLP, an optimisation solution to the problem of co-user's interference in 5G networks. It minimises the total downlink transmit power of the users in the cell, subject to QoS constraints, interference limits and the CSI. Resultantly, it minimises the overall interference in the network. The performance of the PRAAC scheme is examined via different parameters and metrics such as data rate, tolerable interference, transmit power. The evaluation of the scheme demonstrates functional QoS of UEs and reduced network interference when compared with works in the literature.

- A novel method of assessing, evaluating, and analysing the 5G mobile network's induced RF-EMF has been developed. The scheme used the computational method to evaluate the radiation exposures in the uplink and downlink of both the 4G and the 5G networks. Furthermore, this study also proposed a mitigation method that incorporates an open-loop fractional power control concept (OLPC) that controls the UE transmit power $P_{tx}$ for the uplink transmission. With this, the SAR and EI of the users in the networks were evaluated. The performance of the proposed algorithm Exposure-index Open-loop Power Control Algorithm (EOPCA) is compared in the uplink and downlink transmissions of both the 4G and the 5G networks. Also, the radiation exposures were checked against the standard limits advised by the regulatory bodies.

- An EI power control algorithm (EIPCA) was proposed. The EIPCA solves a formulated optimisation problem that sum all the radiation exposures of users in the network, this is solved with MINLP. The MINLP is solved by minimising the total EI of users in the network while achieving the target QoS of these users. The EIPCA minimises the EI through the transmit and received powers in the network with some QoS constraints. The proposed scheme investigated the trade-

off between reducing the RF-EMF radiation exposure and achieving the expected data rate. Through simulation analysis, the evaluation and validation of the proposed algorithm were corroborated with the target QoS values and the radiation exposure thresholds.

The list of publications associated with the contributions of this dissertation is as follows:

1. Adedotun Temitope Ajibare and Olabisi E. Falowo, “Resource Allocation and Admission Control Strategy for 5G Networks Using Slices and Users’ Priorities”. *In Proceedings of the 14th IEEE Africon - 2019 International Conference*, pp. 25-27, September 2019, Accra, Ghana.
2. Adedotun Temitope Ajibare and Olabisi E. Falowo, “Dynamic Slicing and Scheduling for 5G Networks Using Joint Power and Sub-Carrier Allocation”. *In Proceedings of the 22nd Southern Africa Telecommunication Networks and Applications Conference* (SATNAC 2019), pp. 32-37, 1-4 September 2019, Zimbali, KwaZulu-Natal, South Africa.
3. Adedotun Temitope Ajibare, Daniel Ramotsoela, Lateef Akinyemi and Sunday Oladejo, “RF-EMF Radiation Exposure Assessment of 5G Networks: Analysis, Computation and Mitigation Methods”. *In Proceedings of the 15th IEEE Africon International Conference*, pp 215-220, September 2021, Arusha, Tanzania.
4. Adedotun Temitope Ajibare and Daniel Ramotsoela, “A Radiofrequency Electromagnetic Wave Radiation Exposure Minimisation Method in 5G Network: A Perspective of QoS Trade-Offs". *In Proceedings of the International Conference on Electrical, Computer and Energy Technologies* (IEEE ICECET 2021), December 2021, pp 1-6, Cape Town, South Africa.

## 1.8. Dissertation Outline

This chapter is the introduction to the dissertation, it presents the topic and its sub-elements. It gives a concise introduction to the wireless networks, the 5G networks, network slicing, radio resources sharing, interference, and radiofrequency EMF radiation. It outlined the research questions, objectives, methodology, scope and limitations as well as the contributions to knowledge made so far. The rest of the dissertation is structured as follows:

Chapter 2 presents the review of the literature. It describes and examines 5G network and it several enabling technologies such as NFV, SDN, NS, and edge computing. Subsequently, it describes exhaustively the 5G wireless network issues, resource management, and network planning as regards the three solutions proffered in this dissertation, namely network resource sharing, interference management, RF-EMF radiation exposure mitigation. It further explains resource allocation, admission control, slice scheduler, radiation and exposure metrics in a typical 5G network scenario. It contains the literature review of all the challenges discussed and the associated proposed solutions in this dissertation. Many authors works were reviewed with the potential research area surveyed, their methodologies presented, and the strength of their works stated. It also critically pointed out the challenges in their research. This gives more understanding of the challenges, the created gaps, and the required solutions in the research topic/area. Moreover, the chapter dwells on other authors schemes with which the proposed solutions in this dissertation were benchmarked.

Chapter 3 presents an admission control scheme for effective allocation of network resources for sliced 5G networks, considering both the user's and the slice's priorities. The scheme is developed to efficiently allocate, manage, and control the slice resources dynamically in an isolated multitenancy scenario. Therefore, the chapter proposes a heuristic mechanism with an admission control method that improves QoE, enhance resource utilisation efficiency and improve the throughput of users. Additionally, Chapter 3 shows the evaluation and performance of the proposed algorithm when compared with other schemes. It demonstrates the reliable performance of the proposed scheme in terms of the increase in the QoE of users, as well as efficient resource utilisation when data rate was used as the performance metric.

Chapter 4 investigates the joint power and sub-channel allocation scheme in a sliced 5G network. A novel SCAS was developed, this proposed scheme minimises the transmit power in the downlink transmission subject to the interference thresholds, the QoS constraints, the sub-channel orthogonality constraints, and the gNB power budget. This scheme examines the transmit power level of the neighbouring sub-channels and compares it with the transmit power threshold of the slice the requesting user belongs to before assigning a sub-channel to the user. This, therefore, minimises the co-tier interference among many users in the

network. Like the first proposed scheme, Chapter 4 presents the performance and evaluation of this scheme, results show that the proposed scheme demonstrates a reasonable level of tolerable interference among users in the network. This tolerable interference has a great impact on the data rate as well as the number of admitted users, the transmit power, and notably the efficiency of the network.

Chapter 5 analyses the effect of RF-EMF radiation exposure induced from mobile networks, case-studying the 5G network from both the uplink and downlink transmission links. This radio emissions impact is investigated using a novel EOPCA by simulating the quantified realistic electromagnetic exposure to the (human) user. The EI is characterized by the radiation exposure from the UEs and APs considering the power density, the electric field strength, the mass density of the tissue, the conductivity of tissue, and the specific SAR. The chapter analyses and compares the numerical results with the threshold set by the IEEE and the ICNIRP. Also compares the exposure from uplink and downlink, as well as the different RAT to understand the radiation impact.

Again, Chapter 6 investigates the effect of minimising the EI as well as the SAR induced by the 5G wireless network and its impact on the QoS of the users in the network. It presents a power control algorithm with an optimisation solution that minimises the EI subject to power, QoS, interference constraints while the required users QoS is guaranteed. Lastly, evaluation results of the proposed scheme show that the SAR and EI on users in the 5G network reduce while satisfying the QoS requirements. Chapter 6 compares the results with the thresholds ICNIRP and IEEE.

Finally, the conclusion of the entire dissertation alongside the recommendations for future works are offered in Chapter 7. This dissertation presents its findings in the form of the solutions proffered to the challenges in RF-EMF radiation exposure and radio resources management in a 5G wireless network. It proposes resource allocation schemes on how the limited radio and network resources are maximized, and also how to reduce/mitigate the challenges of interference and radiation exposure in the network. The full structure of the dissertation is depicted as in Fig. 1.2.

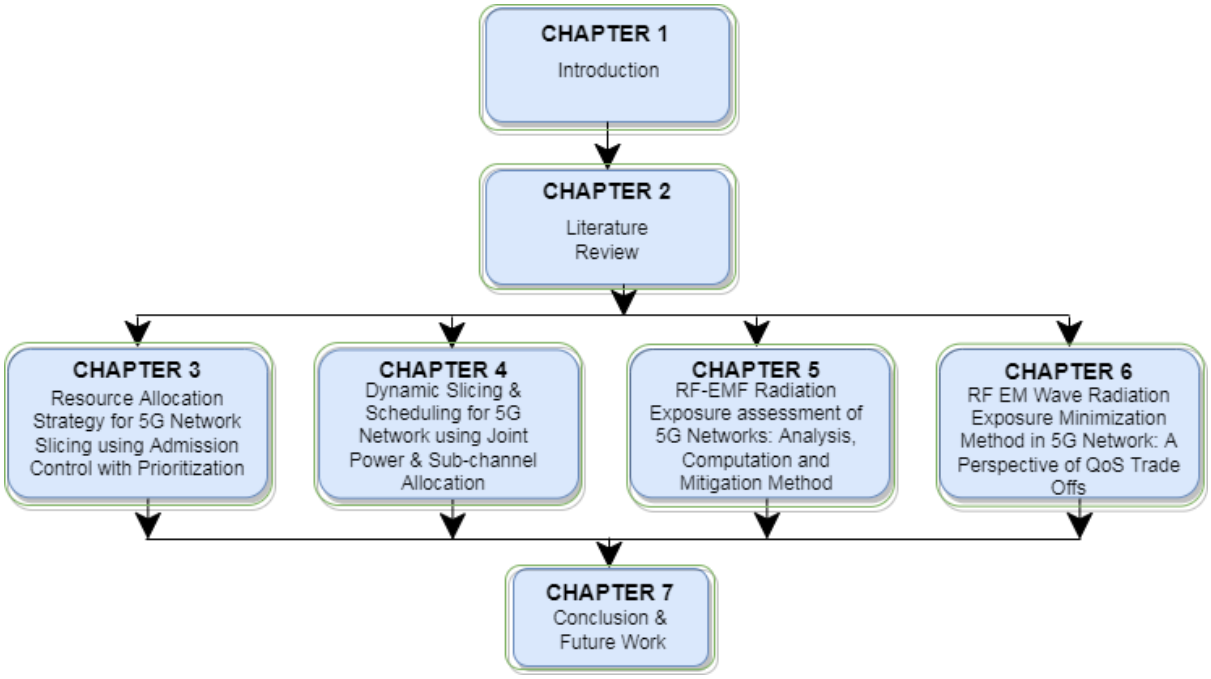


*Figure 1.2: The full structure of the dissertation.*

## 1.9. Summary

Chapter 1 gives a brief introduction to wireless communication, the 5G network and its technologies, and the RF-EMF radiation exposure in wireless networks. It discusses how the network can be planned and managed, especially how the radio and network resources can be shared among users in a dynamic and isolated way. It reiterates the motivations behind this topic, it echoes the major challenges in wireless communication as resource sharing, interference, and RF-EMF radiation exposure. This is more so because the 5G network is multitenancy, heterogeneous and ultra-dense. It also explains the need for proper network planning and efficient management of network resources as major solutions to these network challenges. It also explicitly defines how this dissertation aims to solve the challenges as described in Section 1.4 by presenting the objectives of the dissertation and also the methodology behind the solution as stated in Section 1.5. The scope and limits of this work were stated before outlining the major contributions in the course of this research and as published in some IEEE index conferences papers. Lastly, Section 1.8 briefly outlines the format of the dissertation.

# Chapter 2

# 2. Literature Review

This chapter presents in detail the background of the technologies on which this work is based. It describes 5G Network and its proposed architecture, NS and its enablers in the wireless network such as SDN, NFV and MEC. It also discusses how these enabling technologies complement one another to offer network slices to tenants. A review of related works is carried out on resource allocation, slice scheduler and admission controller in NS.

## 2.1. 5G Mobile Networks

The world has experienced different evolutions and generations with regard to telecommunication networks. For the mobile network, the introduction of the 1G in 1981, and the second generation (2G) network, which was launched as GSM in 1991 was a huge success. The 2G network was later upgraded into a second-and-a-half generation (2.5G) network widely referred to as GPRS, and later into a second-and-three-quarters generation (2.75G) network [25] otherwise known as the Enhanced Data rate for GSM Evolution (EDGE). The introduction of GPRS and EGDE are major steps in the advancement of GSM to the 3G networks that was launched in 2003. In 2009, the 4G became the wireless standard using an all-IP packet-switched network. The Advanced Long Term Evolution (LTE) otherwise known as the 4G network uses the International Mobile Telecommunication-Advanced (IMT-Advanced) technology [25].

The motivations for the 5G network are the current users' demand for extremely low latency required for cloud computing and demand for the high data rate to support video applications, which the current 3G and 4G technologies cannot provide. Cisco, in one of their recent reports [4], predicted that by 2022,

network data traffic will be around 278.1 Exabytes monthly and the number of connected devices to the internet would be about 13.1 billion and this would be more than the world population. By 2022, the estimated monthly data traffic would be about 8 times what it was seven years earlier. Fifth-generation (5G) mobile networks are now being deployed commercially as of early 2020.

According to the industry and academia, 5G network will provide users with 1000 times the bandwidth of the current 4G network as well as 100 times the data rate of the current mobile network to support the applications in smart devices [18]. Also, different techniques such as Terahertz band mobile communication [22] will be used in 5G to fulfil users' requirements.

The core driver of 5G networks is the ability to support a range of verticals such as healthcare, media, automotive, energy, and manufacturing. These verticals are derived from the use cases with diverse service requirements. Compared with what the older generation networks 5G networks can offer more diverse services than the present generations of networks that use a "one-size-fits-all" service structure. Thus, they are incapable of meeting the different service expectations that verticals require with respect to scalability, mobility, reliability, latency, availability, security, and throughput [22].

It is clear that with this huge growth in demand for data services, there is a need for a new generation network with higher capabilities and expectations as summarized below. Fig. 2.1 below summarises the specifications of the 5G network as regards the use cases.

- 10–100 times higher user's data rate (10Gb/s peak data rates)
- 10 times longer battery life for low-power devices (10 years on battery)
- 10–100 times higher number of connected devices
- Five times reduced end-to-end (E2E) latency (<1ms radio latency)
- 1000 times higher mobile data volume per area
- High-speed (up to 500 km/h) mobility.

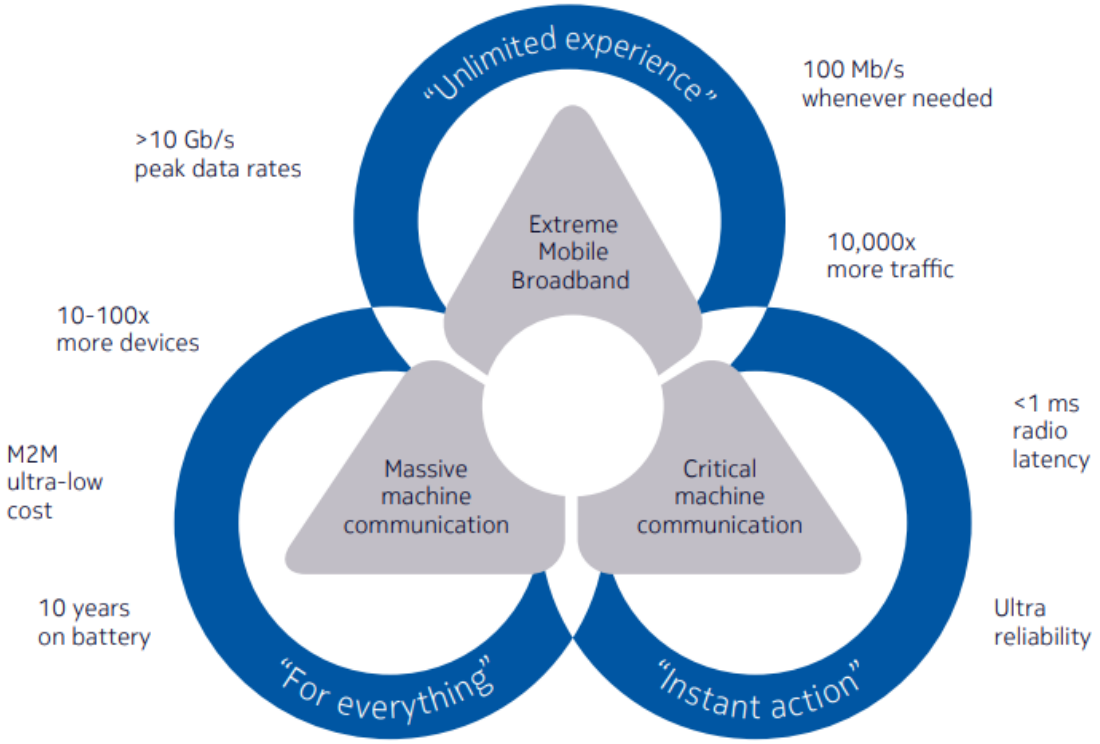


*Figure 2.1: The expected specification of 5G in terms of the requirements [26].*

To achieve these goals, the 5G network must have the following characteristics: (1) it should be extremely smart and flexible [25]; (2) it should have an spectrum management scheme that is efficient [25]; (3) it should improve efficiency with minimal cost [25]; (4) it should be supportive of billions of devices from different sources of Internet of Things (IoT) (solution provided in IPv6) [25]; and (5) it should be backwardly compatible and integrate with older generation networks, which give a high rate of communication coverage with low latency [25]. To determine how 5G system performance affects the QoE of end-users, specific evaluation metrics such as latency data rate are needed. Table 2.1 shows the User's QoE indicators based on the QoS already discussed.

*Table 2.1: Quality of Experience indicators for 5G networks [25].*

| **QoE Indicators** | **Requirements** |
|---|---|
| Throughput | 5 Gbps in data-level and user-level |
| Latency | D2D latency lesser than 1ms |
| Availability | ≈100% |
| Reliability | 99.999% |

5G enabling Technologies will include the following approaches which could aid both the structural and constituent design for 5G:

1. Device-centric architecture
2. Millimetre-wave (mmWave)
3. Massive multiple-in multiple-out (MIMO)
4. Core provision for machine-to-machine (M2M)/(D2D) communication
5. Non-Orthogonal Multiple Access (NOMA)
6. NFV
7. SDN
8. C-RAN/MEC/Fog computing
9. Network slicing etc. [25] [27] [6].

## 2.2. Network Slicing in 5G Mobile Networks

5G NS structure is suggested with the virtualisation of wireless networks in LTE-Advanced (LTE-A) networks [28], where the physical resources are virtualised for efficient allocation of the network resources. This structure brings flexibility. The framework is basically the physical resource layer, resource allocation scheme layer, virtual network layer, and the slice layer.

NS has been defined as multiple E2E logical networks that are isolated from each other but run on a commonly shared physical infrastructure. The multiple logical networks (slices) provide different services capability to meet various users' negotiated service requirements [18]. Network slicing requires a paradigm change in system architecture, framework, and design. NS spans across the access networks (AN), the transport network (TN), the core network (CN), and terminal domains [29]. i.e., NS in 5G networks involves slicing the core network, RAN and including the end-user equipment. Fig 2.2 shows the concept of 5G Network Slicing as Network-as-a-service (NaaS) model and the slices for various users.

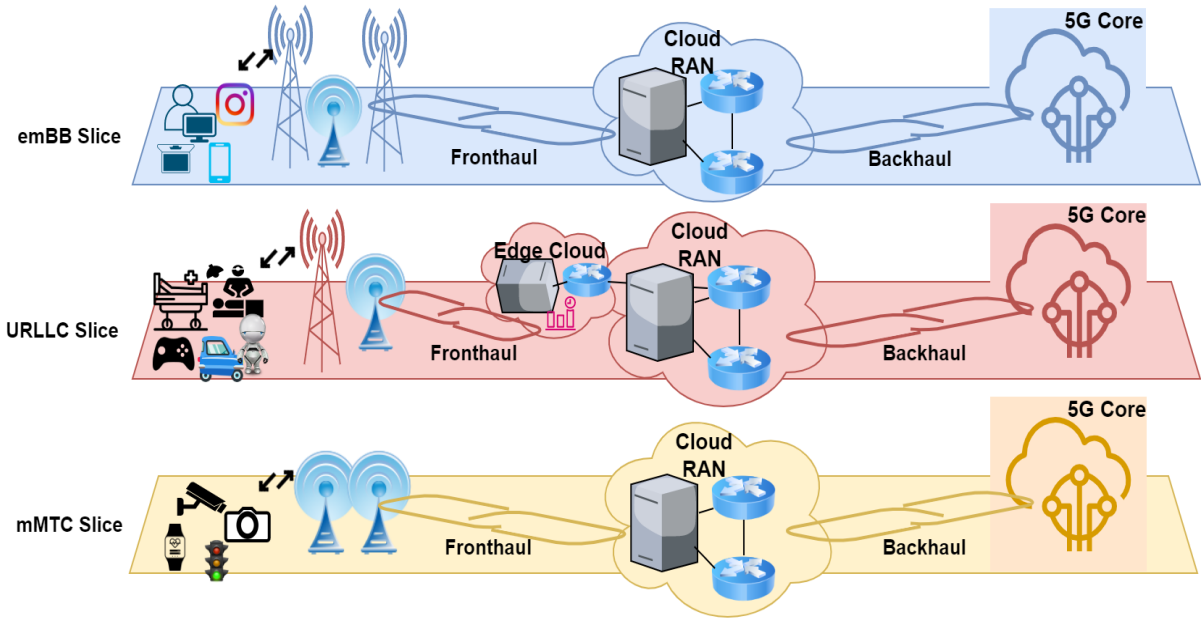


Figure 2.2: Conceptual illustration of network slicing (NaaS Model).

These created network, functions in the form of logical networks that provide different services to a diverse group of users are known as Network Slices. Network slices can be defined as E2E virtual networks consisting of a pool of network functions logically operating on a single physical network infrastructure, each virtual network is tailored to provide different services. It can be created on-demand and must be flexible enough to concurrently allow different use cases from several tenants on the shared infrastructure. Network functions are efficiently and dynamically customised to virtual network slices based on their corresponding QoS requirements. A Network slice is logically isolated from other slices, it is an independent network that has its traffic patterns, topologies, rules and more importantly its virtual resources, but resources can be shared among them.

The softwarisation of the network provides programmability, flexibility, modularity, and security that makes creating several network slices that are well secured possible. The softwarisation is realisable through the key technologies such as NFV, SDN and MEC [22] to form virtualised, softwarised, and cloudified 5G networks. These are later discussed in Section 2.3.

Justifications for Network Slicing

Owing to the significant advantages of 5G Sliced networks compared with the previous generations of networks, slicing is considered based on the following reasons:

- With the logical networks provided by slicing, it provides better network performance especially in terms of QoE of users than the traditional networks.
- Also, network slicing provides scalability for the network slices as the number of admitted users as well as the QoS requirements in the network change.
- Network Slicing brings in multitenancy where different MVNOs are involved in the network and tends to increase the radio resources utilisation. This idea will decrease both the capital expenditures (CAPEX) and the OPEX which therefore increase the profit of a network [30].
- Network slicing provides isolation of slices and tenants network resources. This means that slice configurations are independent of each other, thus, it enhances the security and reliability of the slices and tenants.
- Lastly, network slicing optimises the utilisation and allocation of these network resources with the aid of its service-based network slices [18].

### 2.2.1. The Slicing framework in 5G Mobile Network

In this section, the proposed framework for the 5G network slicing is discussed. The 5G network is based on NS and enabling technologies such as SDN, NFV, and MEC. Fig. 2.3 shows the network slicing architecture for 5G networks with the three main layers.

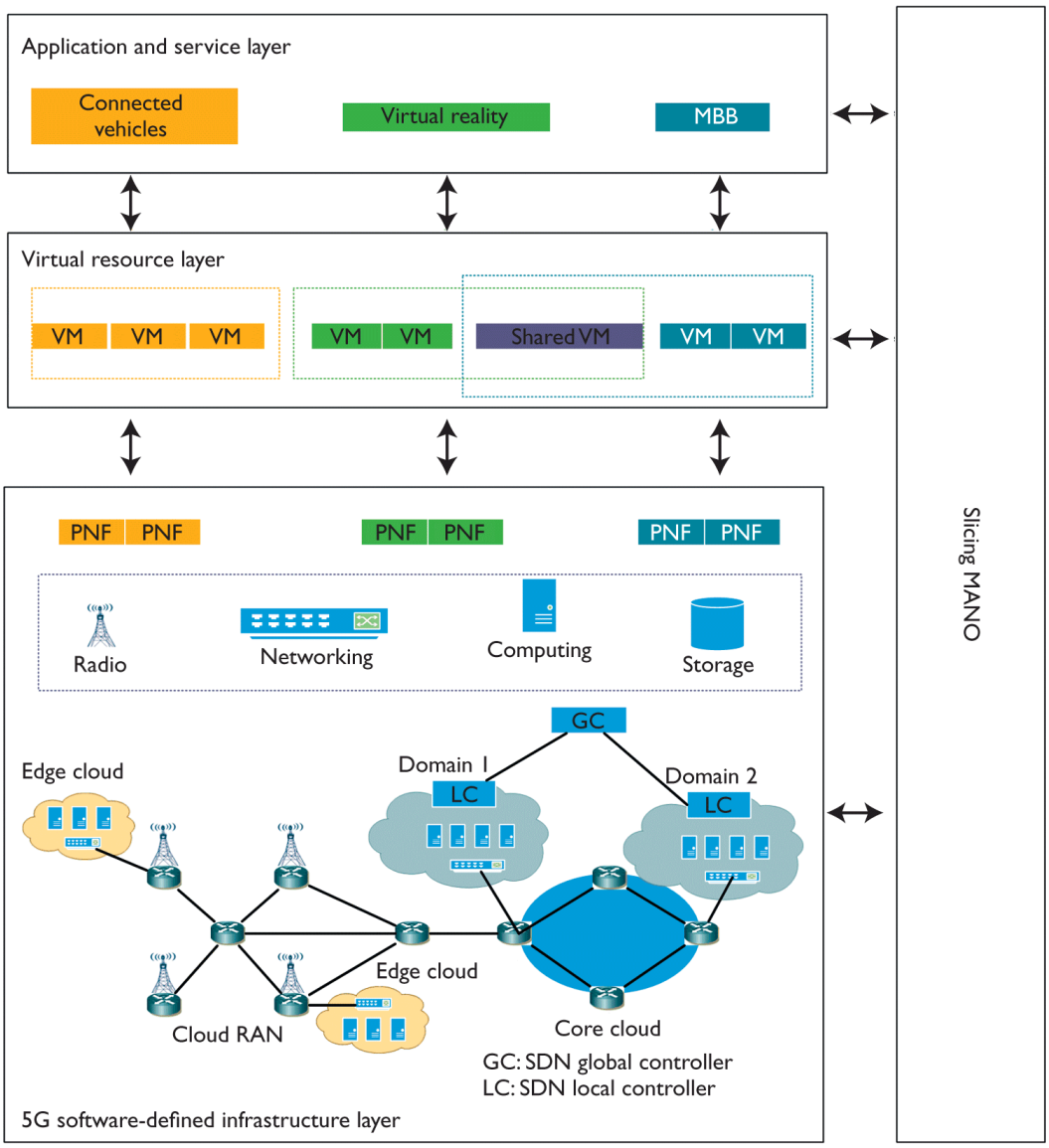


*Figure 2.3: 5G network slicing framework [18].*

The framework contains a 5G software-defined infrastructure (5G-SDI) layer, virtual resource layer, application and service layer, and slicing management and orchestration (MANO) functional component [18].

**5G software-defined infrastructure layer.**

The bottom layer is the 5G software-defined infrastructure layer. This layer is made of multi-domain 5G software-defined physical infrastructures, control and management that

- provides an abstraction of resources and allows a dynamic and flexible resource allocation.

• helps the virtualisation of infrastructure resources that form the slices; and

• allows both the InP and the MVNOs to manage virtual resources.

**Virtual resource layer**,

In the virtual resource layer, the physical resources that have been virtualised such as radio, storage, computing, and network run as VNFs on VM instances which are used as network slices.

**Service/Application layer**

The Service/Application layer consists of heterogeneous service instances such as M2M, critical communication, and eMBB which has been defined based on different service requirements as the use cases in 5G networks. These service instances are assigned to all the MVNOs in the network. Each of the MVNOs can have one or more service types in the network. The network slices are designed to be dynamic and scalable as the service needs change with time. Network slices are differentiated mainly by their services or QoS requirements, a network slice might provide services to instances with similar on-demand QoS requirements [16], [18].

**Slicing MANO**

The slicing MANO is another major part of the framework. It is built in a way similar to the NFV-MANO [16]. Slicing MANO orchestrates and manages the network slices, abstracted virtual resources and the underlying physical resources of the network. Its functions are sub-divided and are performed by sub-layers known as slices orchestrator, VNF manager and Virtual Infrastructure Manager (VIM).

The architecture is organized in a hierarchy with each domain having a local SDN controller and all the controllers in the different domains are connected with a centralised controller. Cloud RAN and MEC could also be employed to cloudify the network resources. VNFs in the URLLC (i.e., remote surgeries) slice and VNFs in the eMBB slice are positioned in edge and centralised core cloud, respectively [18] [22].

### 2.2.2. 5G NS Use Cases

The 5G network is expected to support a different verticals and use cases [12]. The International Telecommunication Union (ITU) and Fifth Generation-Public Private Partnership (5G-PPP) have identified three broad use cases: (i) eMBB, (ii) mMTC, and (iii) uRLLC [19], [25]. The major differences among these use cases translate to a set of diverse requirements as explained in Fig. 2.2 such as data rate, reliability, power efficiency, mobility, latency, connection density, and traffic density. These diverse requirements are not supported by the one-size-fits-all structure. The use cases are briefly explained below.

**Enhanced Mobile Broadband**: The eMBB deals with the user-centric use cases that gives internet access to multimedia contents, services and data. This use case will require novel applications with enhanced requirements such as bandwidth, latency, and density to improve on the present mobile broadband services. The eMBB use case is characterised to have extreme user data rates and traffic higher density than other use cases. eMBB slice will support streaming services such as YouTube videos, video calls. These services require high megabytes, a high number of devices and continuous transmission.

**Ultra-reliable low-latency communications**: The URLLC has strict service requirements such as latency, throughput, and availability [19]. URLLC slice services include: vehicle collision avoidance in autonomous driving and transportation safety, the use of a robot in remote medical surgery, wireless control in production processes, and smart grid. URLLC slice is characterised by its sensitive communication, heavy data traffic, stringent low latency, and high mobility requirements.

**Massive machine-type communications**: The mMTC or a machine-to-machine (M2M) type communication use case is characterized by its high connection density requirement and frequent transmission of data. It is a sensitive data communication slice use case that employs sensors to measure parameters and send information to data centres. Its huge amount of connected devices usually transmit fairly low volume of non-delay-sensitive data. Also, mobility management are reduced to the minimum in this slice. As a result of these factors, the devices have long battery life and are required to be at a low cost [19]. Examples of information are patient BP, patient temperature, room temperature, the fuel level in a generator, and level of content stored in a refrigerator.

These diverse use cases' needs/demands are mapped to suitably tailor network services in NS as shown in Fig. 2.4.

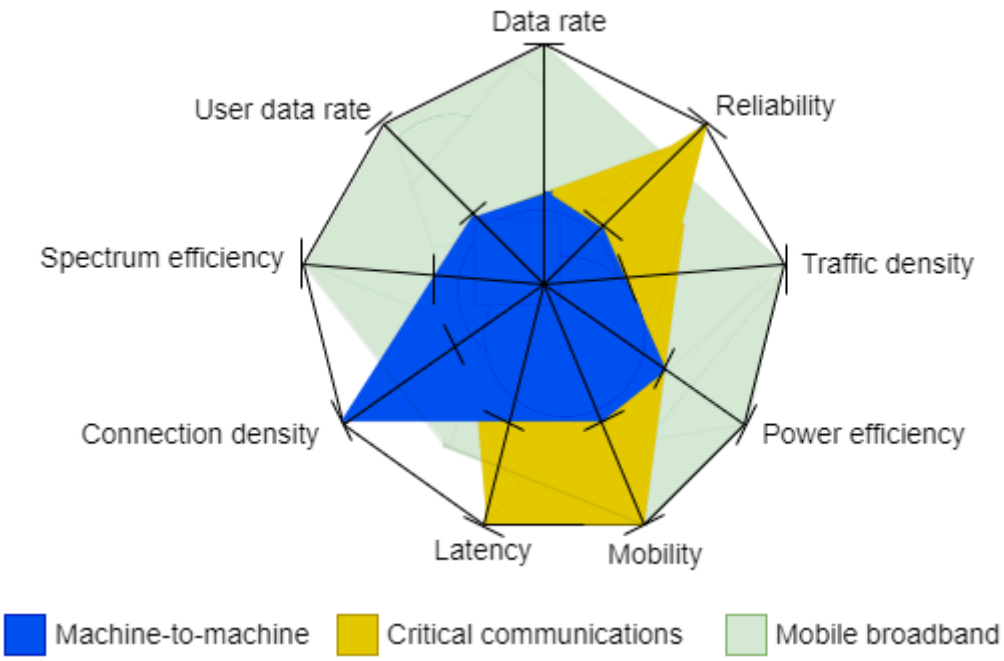


*Figure 2.4: Key 5G use cases and their requirements relating to network slicing [16].*

## 2.3. 5G Networks Enabling Technologies

In the following subsections, the main enabling technologies of achieving 5G networks are discussed. The technologies expected for 5G networks have been discussed in section 2.1, but the main enabling technologies include SDN, NFV, and MEC [31]. These technologies are expected to make a significant impact on NS and 5G deployment. The 5G network is expected to maximize the InP's revenue by the reduction in cost of equipment, power, and space through softwarisation and virtualisation. Additionally, resource utilisation efficiency is expected to be increased [18].

### 2.3.1. SDN as an Enabler of Network Slicing

Software-Defined Network is defined by one of the standardisation bodies and organisation Open Network Foundation (ONF) [32] as "*the physical separation of the network control plane from the forwarding plane, and where a control plane controls several devices*". SDN primarily decouples the network control plane from the data plane. The network control functions are independently run as

applications in centralised controllers logically placed in the network [18], and assigns traffic to network elements in the separated data plane of the network. SDN fosters network flexibility and scalability. Thus, enhanced programmability, centralised management of the network. It also increases the reliability, adaptability, cost-effectiveness, and better the overall experience of users [33].

SDN is an emerging network architecture has changed the traditional network architecture where both the control plane and the data plane were packed in proprietary hardware, from the hardware-based network into a software-based network. As shown in Fig. 2.5, the SDN controller [33] manages and optimises network resources through the standardised interfaces known as southbound SDN protocols such as OpenFlow [34], ForCES [35] and PCE [36].

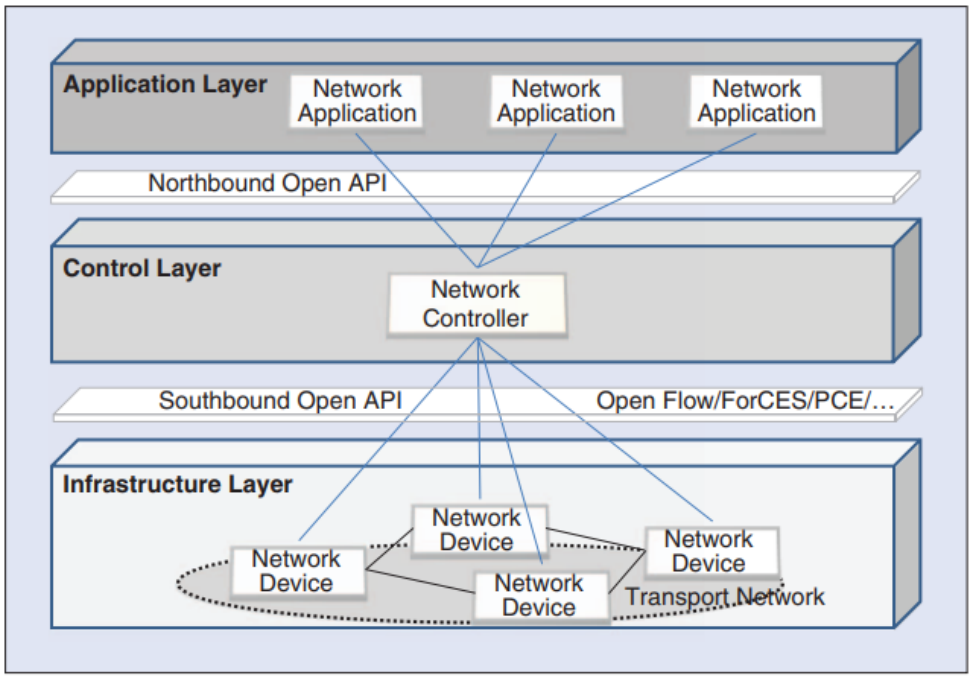


*Figure 2.5: Overview of SDN architecture [31].*

In [37], ONF describes the SDN architecture in three main parts which are infrastructure layer, control layer, and application layer as shown in Fig.2.5.

DATA/PHYSICAL PLANE: The data/physical plane or infrastructure layer consists of the network devices such as physical switches and virtual switches which are managed in the control plane. This layer is accessed by the southbound Open API which is mostly OpenFlow. In 5G networks, the gNodeB is in the physical plane and is in charge of packet forwarding and collection to the control plane.

CONTROL LAYER/PLANE: The control plane integrates all the network resources and RANs. Through a set of SDN controllers in the control plane, it manages the network forwarding behaviour through an open interface. The controller interacts with its interfaces which are: southbound, northbound and east/westbound interfaces [33].

APPLICATION PLANE/LAYER: This layer is made up of the end-user business applications/services. It is the product of an SDN network which is given in the form of network capabilities and services. The network applications are in the form of slices or use cases that inform the control plane about the requirement of the slices through the Northbound Open API [31]. With this architecture, the SDN controller through the northbound interface provides resources of the network to the application layer logical switch.

### 2.3.2. NFV as an Enabler of Network Slicing

The NFV concept entails the decoupling of network functions (NF) from a costly proprietary hardware device and running them on less expensive application software/virtual machines (VM) in a standardised device [33]. These NFs executed in software components are called virtual network functions. NFV enables the decoupling of network functionality of the physical networks. NFV aids the migration of networks to new technologies while supporting legacy technologies. Moreover, it also supports the isolation and sharing of radio and network resources [33].

Virtualisation is the abstraction of network resources, it is an important technology to implement NS [18]. It introduces a new business model that enables efficient resource sharing among slices, with the InP and the MVNOs (i.e., Tenants) as the novel actors. The virtualisation of the mobile network is associated with reduced CAPEX and OPEX, efficient network resources utilisation; increase user's satisfaction; agility and innovation; and flexible network management scheme. The NFV architecture is illustrated as shown in Fig. 2.6.

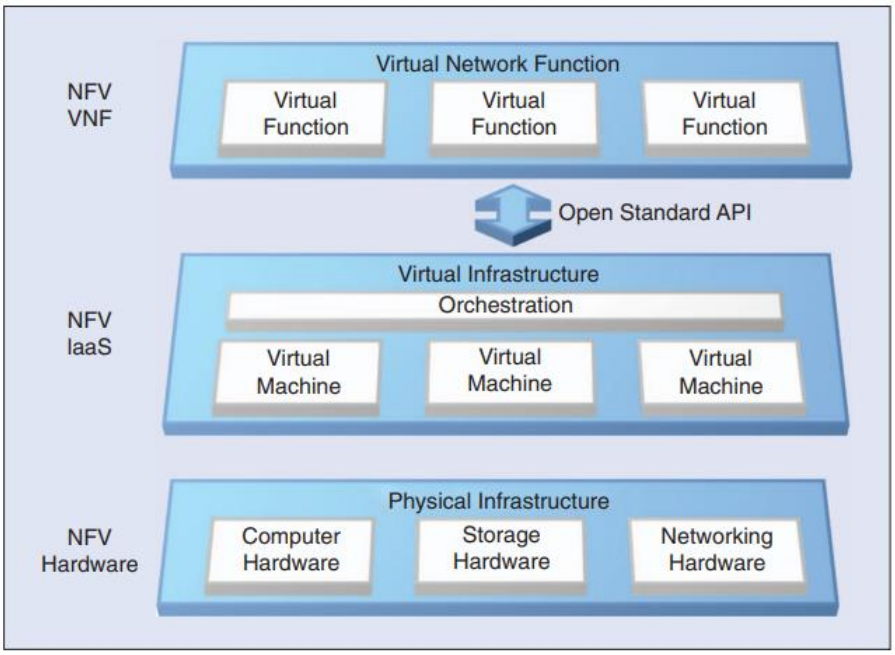


*Figure 2.6. Overview of NFV architecture [31].*

The network function of the physical infrastructure device is implemented in a software application running in the VMs. These VMs are created on high volume dedicated servers connected with high volume switches which are automated by orchestration. Fig. 2.7 compares the conventional network with SDN and NFV architectures. As shown, it makes the creation and management of slices to be performed easily when VNFs can be taken away from hardware and run centrally [38].

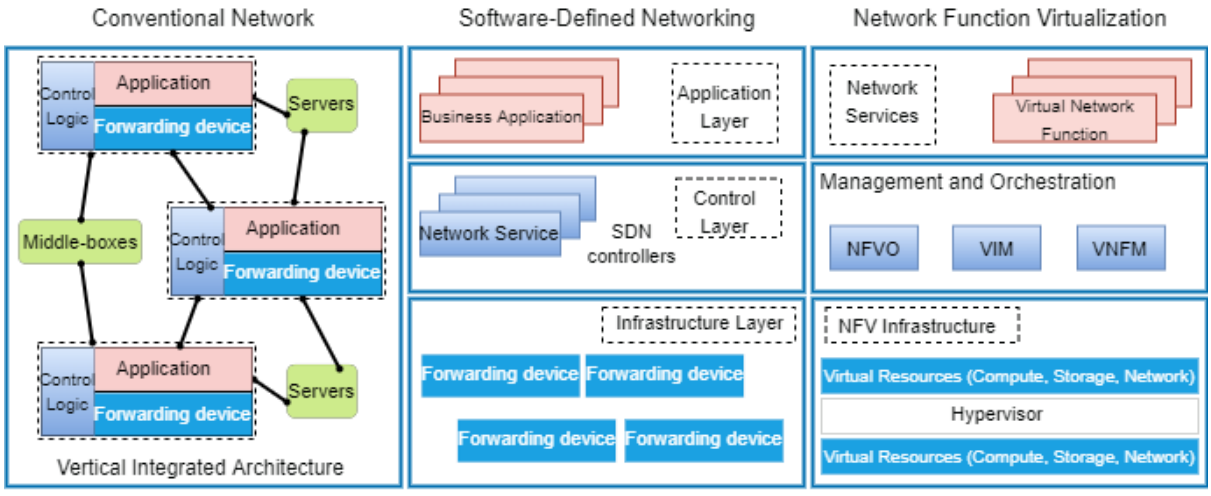


*Figure 2.7. Comparison of the conventional network, SDN, and NFV architectures. [22]*

### 2.3.3. MEC as an Enabler of Network Slicing

Mobile Edge Computing, also known as Multiple-access Edge Computing [39] and edge cloud processing will support 5G access networks, especially for services and use cases that are delay-sensitive such as URRLC and mMTC by deploying the User Plane Function (UPF) in an edge cloud [40]. MEC will offer services at the edge network to give users proximity to the network functions. As such, it reduces the delay and enhances the performance of the network. It also allows the edge server to exploit the storage, computation, and dynamic service creation within a given network slice by allowing multi-tenancy [30], as the VFNs and applications are decentralised at the edge cloud [39].

Traditionally, data traffic from the core network are routed through a base station and the contents are delivered to users [41]. Devices deployed at the mobile edge solely act as mobile APs [41]. Thus, they only provide network connectivity and do not provide computing or storage resources for mobile UEs [41]. However, in MEC, new devices are deployed and co-hosted at base station towers to offer computing and storage capabilities at the edge as shown in Fig. 2.8. The UE connects through the base station and the user's radio signal is routed via the backhaul to the core network. The MEC Servers are positioned close to the base station and hence to the mobile users. Thus, moves the computational efforts from the internet to the mobile edge, hence, reduces the network stress [40]. Users' requests are directly handled and responded to by the services hosted on MEC servers at the network edge and not through the core network. Hence, increasing the bandwidth capacities and lowering the network latency [41], these are important for the slices in 5G networks.

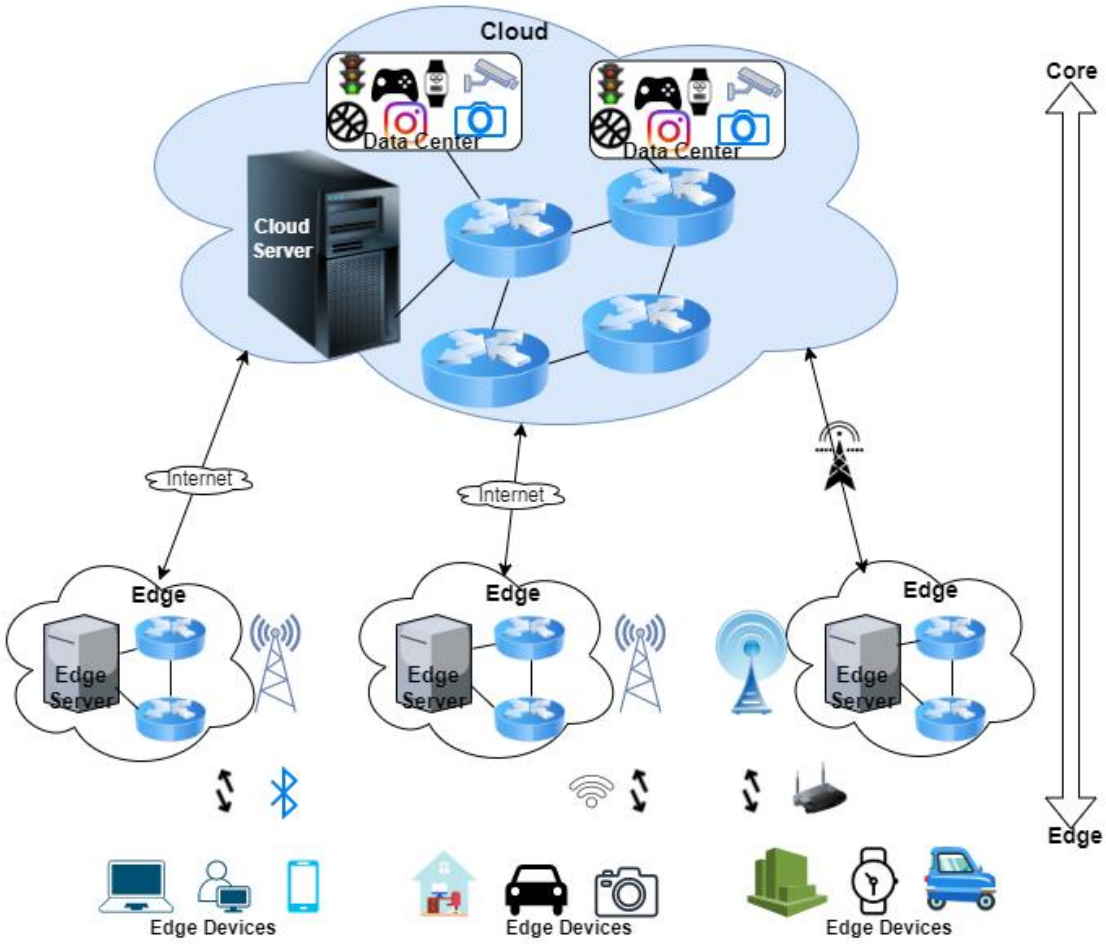


*Figure 2.8. MEC-enabled 5G architecture.*

## 2.4. Resource Allocation in 5G Wireless Networks

Resource allocation is needed in 5G network to facilitate dynamic, and effective assignment of network resources that satisfies the various QoS requirements [42]. This is necessary because the network resources are scarce, virtualised, and are of diversified services [43]. One of the fundamental challenges [18] in 5G networks is how to assign the isolated resources efficiently to network slices with different QoS requirements. 5G heterogeneity will also add to the complexities of resource allocation, especially for densely shared heterogeneous APs. Therefore, well-managed, flexible and efficient resource allocation schemes that consider other factors such as radiation and interference awareness are needed [44]. In literature, many resource allocation schemes have been proposed with respect to the different parameters such as data rate, power, interferences, channel conditions, bandwidth, SLAs, or a combination of them [33].

Radio resources can be shared either by the fixed partitioning method or dynamically. Static sharing provides a dedicated chunk of resources which is easy to achieve and give network resource isolation but has the demerit of inefficient use of network resources. While dynamic sharing of the resources among different virtual slices provides efficient use of radio resources. However, due to the dynamic nature of network traffic, the dynamic resource sharing among slice users makes network resource usage more efficient. In sharing radio; computational; and other network resources there is a need for a dynamic scheduling mechanism that will assign these resources among the different RAN slices adequately to avoid overprovisioning or inadequacy that might affect performance [44].

### 2.4.1. Radio Resources Allocation

In a wireless network, resources could be in the form of radio-frequency, time, power and space, but majorly, radio-frequency is considered. The radio access technologies (RATs) decide when devices can access and transmit in the network with their medium access control (MAC) functions. The main technologies used in LTE are the 3GPP LTE standard and the IEEE 802.11 standard [45] and could be assumed that 5G networks could use these current standards to access the medium as well. Using the 3GPP LTE standard, medium access is implemented with Single Carrier-Frequency Division Multiple Access (SC-FDMA). On the downlink channels, resource allocation is implemented in the time/frequency domain using Orthogonal Frequency Division Multiple Access (OFDMA).

As shown in Fig. 2.9, in the time domain using Frequency Division Duplex (FDD) mode, the downlink channels in the air interface are divided into frames of 10ms, each frame consists of 10 sub-frames which are called the Transmission Time Interval (TTI). (i.e., 1 frame = 10 TTIs = 10 sub-frames).

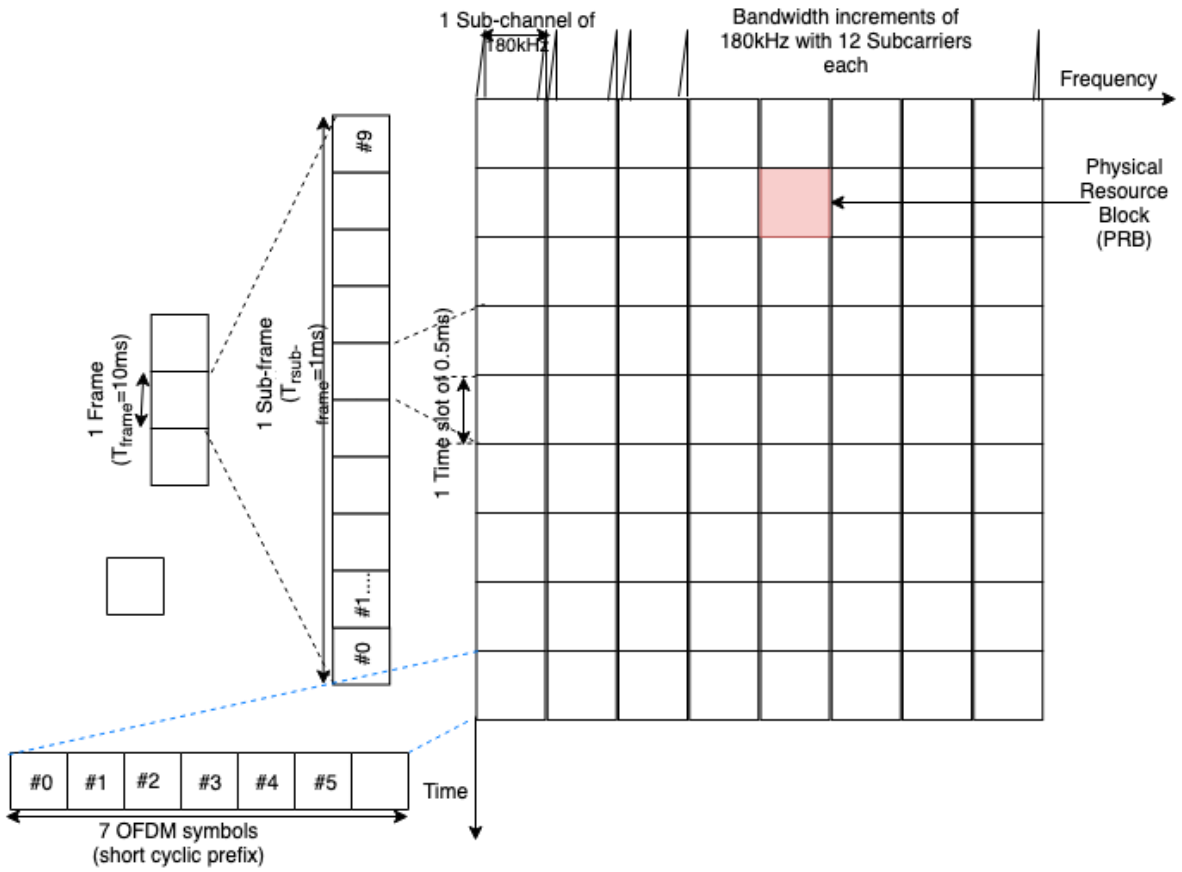


*Figure 2.9: LTE time-frequency frame.*

Each sub-frame or TTI is divided into time slots of 0.5ms which carries 7 OFDM symbols in the default configuration of short cyclic prefix and 6 OFDM symbols in the extended cyclic prefix. (i.e., 1 sub-frame = 1TTI = 2 time slots = 0.5ms).

In the frequency domain, the system bandwidth is divided into sub-channels of 180 kHz [45], each having 12 sub-carriers. Meaning that each sub-carrier has an equal bandwidth of 15 kHz. The number of sub-channels in the network depends on the total available bandwidth. The Physical Resource Block (PRB) is the basic resource unit of allocation in the wireless network and it is made up of 1 time slot and 1 sub-channel in the time and frequency domains respectively. A PRB is 12 OFDM subcarriers transmitting for the duration of one time Slot (0.5ms). 12 subcarriers x 7 symbols = 84 symbols (or resource elements) comprise a normal PRB. There are 72 symbols in a Resource Block with the extended CP.

$$PRB = 1\text{Timeslot}(T) * 1\text{Subchannel}(C) = T * C \tag{2.1}$$

where total PRBs in the channel is the total number of sub-channels.

Therefore, the PRB is a function of sub-channels in the network. Allocation/assignment decision is usually done for each user using a certain amount of PRBs in the time and frequency domain which is implemented at every TTI to make the best use of the resources. This task of resource allocation or assignment to users is referred to as scheduling. In 5G networks, a scheduler is required to orchestrate, control and decide how these assignments are carried out taking into consideration the fairness, in some cases the priorities, SLA and more importantly the QoS requirements of slices on demand.

## 2.5. The Admission Controller

The 5G network is expected to solve the problem of high traffic and dense demand in wireless communication [6]. However, with the limited resources, there will be an infeasibility challenge in the network as the system capacity is unable to support their target QoS requirements [20]. Therefore, there is a need to have admission control schemes [46] that will bring about a solution to the congestion problem in the network. Admission control which considers priorities [47] is required in both slice creation and user resource requests to maximize admitted UE.

Admission control has been thoroughly investigated in the literature [48], [49], [50], [51]. However, the admission control of slices or a group of users in virtualised networks is relatively new [52], [53], [54], [55], [56], [57]. The admission control scheme could be broadly classified into centralised or distributed; single-class or multiple-class; and rate-based method or the channel-state-based method.

- Firstly, as centralised or distributed [49]. The distributed admission controller is less complicated and more appropriate for single independent admission control. However, the centralised controller achieves better network efficiency though results to a longer delay. But for virtualised slices and their set of users, the higher overall network efficiency makes it better.
- Also, it can be classified as either single-class or multiple-class admission controllers [49]. 5G network slices will come with different QoS needs, hence the multiple-class method will support higher flexibility of slice QoS requirements, unlike the single-class admission control method.
- Lastly, the other classes of admission control are the rate-based method and the channel-state-based method [49]. In the latter method, new requests are

admitted only if the channel quality is greater than the users QoS requirements. Whereas, in the rate-based method, the user is only admitted if the available resource can provide for its target rate.

Figure 2.10 illustrates the admission control/resource allocation module with the admission decisions based on solving the admission request problem.

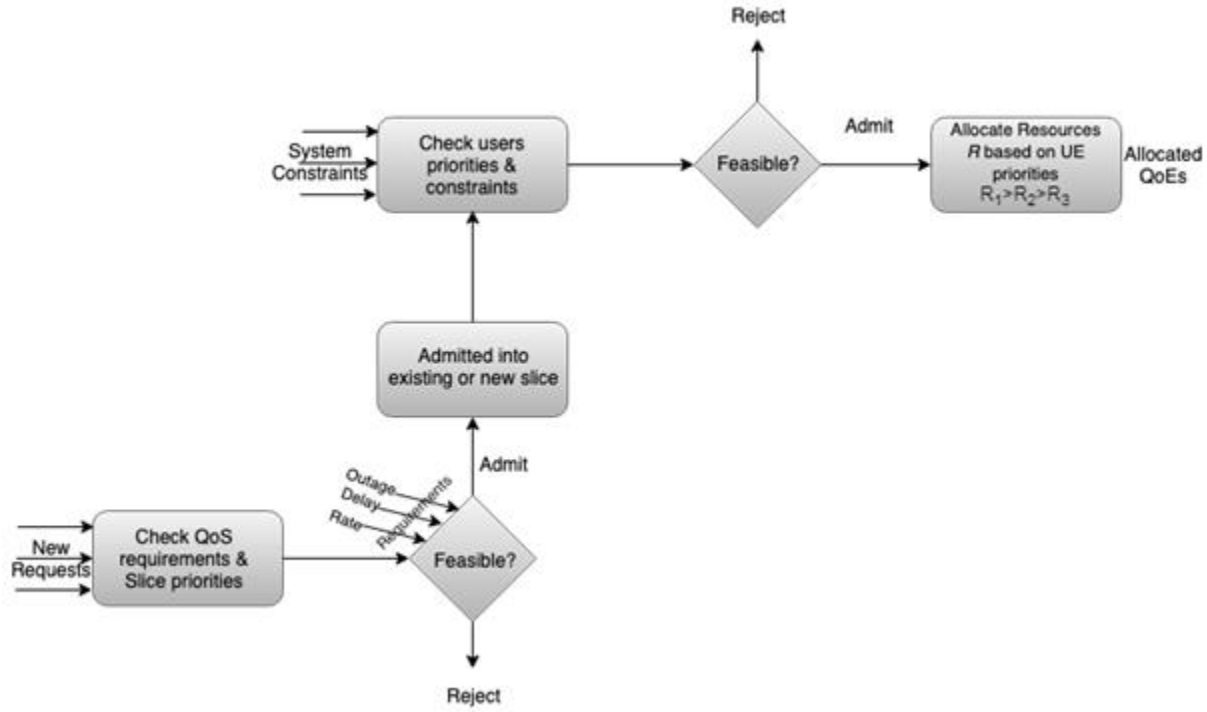


*Figure 2.10. New request admission control process.*

New network slices are created on-demand as MVNOs send service requests to the InP. After consideration and decisions are made, SLA is agreed upon, and the network slice is created and maintained by the slice MANO. As shown in Fig. 2.11, the operators' policies, services templates, orchestrator and SLA are embedded in the slice MANO. The slice MANO has to address the optimisation challenges of allocating slices by first using existing network service instance (NSI) where necessary to optimise the utilisation of the network resources. And if no existing NSI can be used, it creates a new NSI. Also, it has to update the requirements when NSI is shared. The admission control method avoids congestion and infeasibility whereas the resource allocation method optimises the network utilisation while meeting the SLAs of each slice instance.

The system must be able to adapt to some inconsistent and non-stationary dynamics of the network [58], such as high demand in the request of a particular

slice over a short period. For example, a significant increase in traffic of eMBB around festive periods, most especially the early hours of the first day of a new year. The admission control schemes must put into consideration some features such as utilisation, cost, flexibility, and scalability to guarantee the target QoS for both new and existing slices subject to the limited network resources to optimise the admission and resources allocation.

Over time, intelligent admission control [59] has given so many benefits to InP. There are different methods in which intelligent admission control can be realised in a network, examples of these methods are Neural networks [60], which is biologically inspired algorithms designed to learn from observing data. Big data analytics [61], which uses complex techniques of very large data sets to determine hidden patterns. Q/Machine learning [62], a model-free reinforcement learning algorithm. Game theory [63], a mathematical model for strategic interaction among competing players; and Heuristic optimisation [42], a more quickly technique for solving complex problems.

The user admission control is similar to that of the slice other than user request is tailored to one of the already existing slices QoS requirements. Admission control decides if to admit an incoming slice/user request or not. The decision is done by considering factors such as available channel bandwidth, maximizing resource utilisation, satisfying QoS requirements and priorities. Slices requirements are elastic. i.e., parameters are ranged from maximum to minimum. Therefore, slices with higher priority are first allocated and granted the required amount of resources which tends toward the maximum. Whereas slices with lower priority are allocated lesser resources but still within their target QoS requirements and an update of resource allocation is done. Another factor to be considered in admission control and resource allocation is the delay [64]. The time dynamics required for admitting a request into the network in terms of latency is very important and should be < 1ms [23], [65].

## 2.6. The Slice Scheduler

The slice scheduler or controller is responsible for assigning sub-channels and other radio resource allocation to users and slices in the network. It generally functions at the MAC layer of the gNB the 5G networks base station [66]. The SDN/NFV-enabled 5G architecture is expected to operate in the slicing-MANO

earlier discussed in Section 2.2.1. The primary functions are to perform PRB assignment to slices/among slices, and perform traffic balancing by controlling the traffics that are transmitted to the base station [38].

There are various types of schedulers in the literature such as SDN controller implemented in NS-3 [66]. This controller communicates with a Slice Optimiser to receive information regarding the slices and adapts the network slices according to the network state. Others are scheduler implemented as a "Hypervisor" [67] using the OPNET simulation tool. Lastly, a heuristic slicing and scheduling scheme [68] that allocates sub-channels to different Virtual Networks (VNs) based on their target rate. Fig. 2.11 represents the type of controller used in this work.

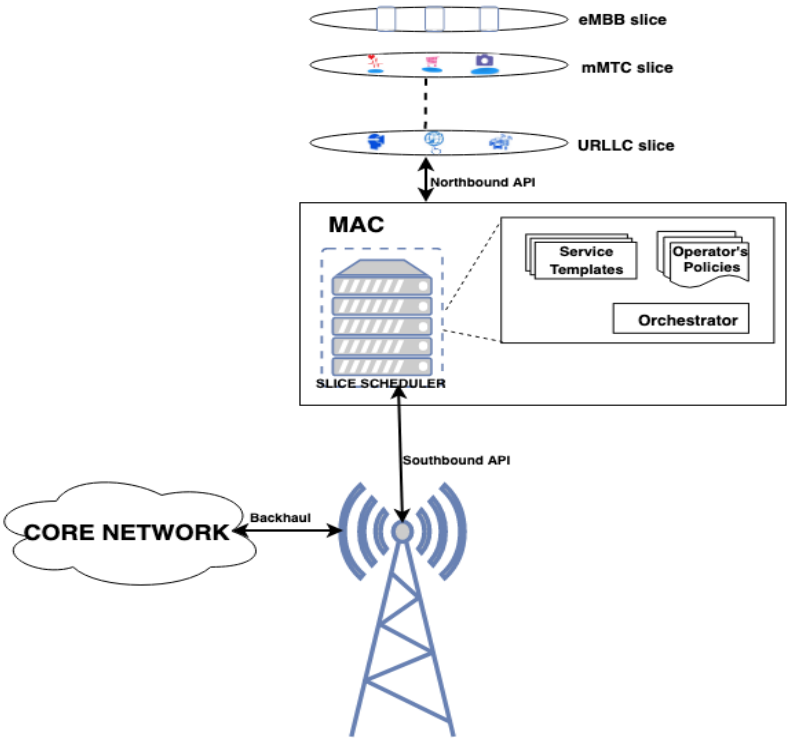


*Figure 2.11. Concept of slice scheduler in 5G sliced networks.*

The scheduler accommodates the resource allocation algorithms [66], [68]. Algorithms optimise, manage and orchestrate the network resources in the Slice Orchestrator. These algorithms set the schedulers apart, in many cases, the algorithm must be able to admit users when necessary, allocate resources to the UEs and dynamically adjust the number of sub-channels/resources according to QoS requirements [69], latencies of transmission [70], transmit power from or to UEs [71], the level of interference [72], and the Channel Quality Indicator (CQI)

[73], etc. The scheduler makes the scheduling decision and this is updated every scheduling period as discussed in section 2.4.1.

## 2.7. RF-EMF Radiation Exposure Management in Mobile Networks

Electromagnetic exposure's consequences to humans relate to the magnetic field strength, electrical field strength, instantaneous power, average power, absorbed energy, modulation format, carrier frequency duration of exposure and the kind of polarisation.

Investigation of electromagnetic fields especially from radiofrequency has been on for over 60 years, the research on the safety and health risk of RF-EMF radiations started in the 1940s. The first safety guideline was published in the 1960s and this has since been regularly revised and updated [74], however, a lot of unanswered questions have stirred up research and more investigations. This has brought about many published research works on the health effects of radiation exposure. In many works of literature reviewed, more authors concluded that there are weak or no adverse effects and health risks than the ones concluding adverse effects and health risks. They established that there is no credible evidence suggesting or linking the "adverse effect" on humans to exposures that are below the standard recommendation by IEEE Std. C95.1 [14]. As a result, it is unlikely to cause adverse health issues [75], while in some studies, some biological modifications are stated [76].

The evolution into 5G network has renewed the interest in the decreasing research on the RF-EMF exposure. Recent RF-EMF studies are toward efficient assessment and management of the exposure levels from 5G APs [77], [78], [79], [80], [81]. Many authors conducted preliminary measurements, while some did computational and numerical studies on the RF-EMF level coming out of these base stations. However, at the moment, none of these approaches can be said to be the standardized method. The results of their findings depend on several factors such as frequency, exposure duration, wave pattern, modulation pattern, sensitivity, reliability, biological cell and physiological status of the exposed model system [76].

Most measurements and simulations show that the RF-EMF levels are at small fractions of the maximum levels specified by the guidelines authorities such as ICNIRP, IEEE, and FCC. Since we cannot be too careful in ensuring safety and precaution, many schools of thought have suggested that the exposure level limits should be further reviewed downward to ensure more safety of human health provided the QoS of the users in the network is guaranteed. Countries like Belgium, China, Germany, etc. have adopted stricter regulations [81], [82].

Many studies [75], [76], [83] used animals in their experiments and have shown that the minimum cataractogenic SAR and power density required to cause adverse effects such as lens cataract is about 100 to 150 W/kg and 150 mW/cm² respectively, for up to 100 minutes in the eyes and a temperature increase of up to 41°C [84]. Also, it is a fact that most research/results have shown that RF radiations from user devices and APs are below the exposure limits. Nonetheless, there is still widespread public concerns about the adequacy of the existing guidelines. Thus, there is a need for constant study, review and update of these limits based on findings [84].

### 2.7.1. Exposure Mitigation Methods

There are different methods used in mitigating exposure. They include administrative controls, the use of personal protective equipment (PPE), and engineering controls [75]. This research concentrates on the engineering control method which is the preferred technique in mitigating exposure in the network. Engineering control approaches include antenna beamforming, incident power/power density control, optimisation etc.

Authors in [75] created a synopsis, a reference document to the IEEE Std C95.1™-2019 [14]. The IEEE Std C95.1™-2019 is published by IEEE as the standard that specified exposure measures and limits that prevent unhealthy impacts that are related with EMF radiation in the frequency range between 0 Hz and 300 GHz [75]. W. H. Bailey *et al.* [75] explained the terms dosimetric reference limit (DRL) and exposure reference level (ERL) of persons in restricted environments and the general public in unrestricted environments. DRLs are defined in terms of in situ power density, SAR, and electric field strength in the body of the exposed person. While ERLs are expressed as magnetic field, electric field, incident power density, induced current, contact current, and contact voltage limits determined by

computational analysis and measurements external to the exposed person. The ERLs ensure that the DRLs are not exceeded.

In [77] the RF-EMF exposure level of twenty-five 5G APs were measured and analysed in a dense urban area of Telstra Australia. These APs employ the use of massive MIMO antennas for beamforming and optimisation of the signal strength at the user device. With the use of the Ericsson Network manager, about 13 million samples taken 24 hours over 7 days were obtained from the 5G APs during an average time of 6 minutes exposure. The result showed that the maximum time-averaged power in the direction of each beam is less than the maximum theoretical exposure. Also, the constant maximum power of a fixed beam contributes to the unrealistic evaluation of RF-EMF radiation.

To confirm that the RF-EMF exposures radiated from 5G APs stay within the ICNIRP limits, The Office of Communications (Ofcom), the United Kingdom‘s communication regulator recently carried out some RF-EMF exposure measurements and assessments at some locations near 5G APs [78]. The measurements were done in thirty-three 5G APs locations in the United Kingdom cutting across England, Wales, Northern Ireland, and Scotland. With the help of a field strength analyser (Narda SRM-3006) and an anisotropic electric field probe, the measured RF-EMF exposure values from these 5G-enabled APs are far less than the levels recommended by the ICNIRP standards. The highest level and the next highest level are 7.1% and 1.5%, respectively of the ICNIRP limits. Lastly, when compared to the ones the older generations are contributing, and with the ICNIRP reference levels, the total exposure contributed by 5G is currently low and it was found to be 0.23% as at when published.

Authors in [85], [86], [76], [83] conducted evaluation of radiofrequency exposure systems using biological evaluation methods. In [85], a study of the potential carcinogenicity and toxicity of the exposures of the 2G and the 3G mobile networks signals were conducted on rodents using 1512 mice and 1568 rats. Animal chambers that allow prolonged exposure were designed to house the rodents and the dose rate distribution in the body of the rodents were presented. In [86], the authors present a systematic review on the common radiofrequency exposure methods for both in vitro and the in vivo studies and they presented the advantages and disadvantages of both studies. This review presents assistance to

researchers in developing RF exposure experiments using both electromagnetic and biological methods.

The work of X Lisheng, *et al.* [24] studied the effect of RF EM radiation on human body sizes. They assessed compliance on the standard limits of different human body trunk models of a five-year-old, a ten-year-old, and an adult models using the finite-difference time-domain method at the frequency of 2450 MHz. The results show that with the increment in human body size, radiation decreases from –53dB to –116dB. Consequently, they recommended that different power levels of communication equipment should be set for users with different body sizes.

M. Cavagnaro, *et al.* in [87] studied the influence of exposure duration and metric in correlation with the temperature increase and absorbed energy. They used an anatomically voxel-based model of the human body. At several frequencies, the correlation of induced temperature elevation and the EM fields were evaluated. They presented their results using SAR and volume absorption rate (VAR) and noted that for both SAR and VAR, the best correlation between the temperature and the exposure durations (which was from 30 seconds to 30 minutes in an increment of 30 seconds) was between 1 and 2 minutes for most of the frequencies considered. It can be inferred from this that the increase in the induced temperature depends on the tissue's size and the exposure time, which all correlate with the exposure metrics. Additionally, for short exposure durations, SARs has a better correlation compared to VAR, while for longer exposure durations, it is the VARs that has a better correlation.

A new approach to safety evaluation was proposed in [88]. The authors used a SA and an amplitude probability distribution (APD) in conducting the leakage measurement of microwave electromagnetic fields and high frequencies, and the exposure levels were compared with the SAR derived over an average of 6 minutes and with the safety guidelines to ensure workers' safety. The finding of their investigation suggests the use of the APD measurement instead of the direct 6 minutes measurement for safety evaluation because the APD measurement can be obtained in less than 6 minutes. They derived a time-averaged SAR for the safety evaluation and they concluded that with the statistically averaged SAR, the intensities of the leaked field are not high to the extent of causing thermal hazards for the users in the high-frequency and microwave EMFs environment.

The authors [81] presented the outcomes of EMF exposure measurements carried out at places around 5G-enabled APs. They proposed a comprehensive exposure assessment methodology using a common SA in measuring/calculating in-situ the time-averaged instantaneous exposure and the theoretical maximum exposure from 5G APs operating at 3.5 GHz. They believe the methodology applies to any 5G network be it operating using any sub-6 GHz frequencies or within the millimeter-wave range. They validated their 5-step measurement methodology in the line of sight (LOS) of a 3.5 GHz 5G base station in Dusseldorf, Germany. They stated that all the exposure values are quite below the regulatory bodies' reference limit of 61V/m for the frequency 3.5GHz used.

The authors in [89] stated that to ensure compliance with the exposure guidelines, the uncertainties in the computation and measurements should be reported, they analyse two sources of uncertainties in RF-EMF namely; repeatability and spatial interpolation. With the use of a SA and a monopole-type antenna, the electric fields and their associated uncertainties were randomly measured in an area in having three medium-wave radio broadcasting transmitters. Also, two approaches were presented namely the additive approach and the direct-comparison approach. In the additive approach, the uncertainties are added to the results of the assessment before the exposure level are compared to the exposure limits, while in the direct-comparison approach, the measured exposure levels are compared directly with the exposure limits, even if the uncertainties are large. The results suggested that the additive approach is more appropriate.

The authors in [90] developed a method that calculates the incident PD and derives an expression for SAR matrices by approximating the near-field gain and by modelling the total electric field transmitted from the transmitter in near-field effects. The results from the simulated 28 GHz millimeter-wave exposure setup validated that model could estimate exposure with high accuracy. Authors in [91] did the comparison of the external field strength and the SARs using a human model in an electromagnetic field for intermediate frequency of 100kHz to 10MHz they derived the relationship between external field strengths and the local SARs and suggested a review of the IEEE and ICNIRP standard/guidelines. In addition, the current exposure limit levels for all the older generations pre-5G network must

be also taken into consideration when measurements, calculations, or simulations are done [81].

### 2.7.2. Exposure, Absorption and Dose

There are many confusions about exposure and absorption in the literature though are used interchangeably, but there is still a fundamental difference between exposure and absorption. In RF-EMF radiation, exposure is the amount and duration of radiation that gets to the body surface, while absorption is the intensity/amount of radiant energy absorbed by the body tissue. Also, dose rate/dosage is the radiant energy absorbed per unit time [92].

### 2.7.3. Frequency, Power, Time and Distance as a Factor

As earlier stated, the level of electromagnetic fields around APs and wireless devices depend on the frequency, the power, the duration, and the distance. It is a fact that only when in use, wireless communication devices pose a potential risk of exposure to users, and the closer the device, the more the emitted radiation. However, RF exposure can be reduced by reducing the time spent using the device, especially the mobile phone, and also by increasing the distance between the user's head and the device.

To determine the safety **distance** for electromagnetic exposure from an AP antenna, the electromagnetic fields (*E*-fields and *H*-fields), or the SARs should be evaluated and compared with the reference limits [93]. This is important as part of network planning, therefore it is always necessary to investigate the safety distances before siting a base station in the network. It is quite easier and faster to use the EM-fields than the SARs.

In [93], the authors measured the electromagnetic fields and the SARs for occupational exposure of a 900MHz base station using a network analyser (Rohde & Schwarz ZVR). The safety distances determined from the EM-fields and the SARs were compared and were found to be in excellent agreement. Also, the reference

limits from the regulatory bodies were compared and the electromagnetic exposures from the antenna were found to be stricter than the limits.

For accuracy' s sake, it is important to measure both the electric and magnetic fields within the near field of the source, however, only the electric field which is the dominant field is usually considered because the AP's antenna is an electric source [93]. Also, the maximum electric field and the magnetic field are not at the same location, that is; the point of the minimum electric field in the antenna is the same as the point of the maximum magnetic field, and vice-versa [94].

Having a standard average **time** for the exposure limits is very crucial in preventing the health and safety risks caused by excessive heating. Unreasonably long averaging time will allow excessive short-term exposures, while unreasonably short averaging time will be too conservative and will exclude exposures that have short-term variations. So the question is how long should a user be allowed to be exposed in an EMF environment at a given exposure level?

In developing the exposure limits in 1966, the committee that developed the first RF-EMF exposure limits arrived at 6 minutes (0.1 hours) averaging time considering the exposure's thermal effect on tissue. Thomas S. Ely (1924-2015), a member of the committee stated that he *"was trying to come up with a number with as few significant figures as I could, considering the precision of what we were dealing with. A minute was too short — an hour was too long*" [95]. This contributes to the subsequent and the present exposure limits' averaging time of 6 minutes.

K. R. Foster *et al.* [96] considered determining an appropriate "averaging time" in RF-EMF exposure limits to prevent unhealthy impacts. They simulated the exposure from a communication waveform of frequencies between 1 to 300 GHz, with the transient temperature fluctuations. The results of the experiment conform to the current choice of 6 minutes as the averaging time of RF exposure limits in the existing generations. However, they suggested a review for the averaging time of RF exposure limits for the mm-wave frequencies.

Table 2.2 (modified from [96]) shows the averaging time for the exposure limits for frequencies ranging from 0 kHz to 300 GHz in both the restricted (occupational) and unrestricted (general public) environments.

*Table 2.2. Averaging time for the exposure limits [96].*

| **Standards/Guidelines** | **General Public limit (minutes)** | **Occupational limit (minutes)** |
|---|---|---|
| FCC (447498 D04) Interim General RF Exposure Guidance v01 (2021) | 30 [c] (mobile UEs/far-field exposure)<br>30[c] (portable UEs) | 6 [c] (mobile UEs/far-field exposure)<br>6[c] (portable UEs) |
| IEEE Std. C95.1™-2019 IEEE Standard for Safety Levels with Respect to Human Exposure to Electric, Magnetic, and Electromagnetic Fields, 0Hz-300GHz | 0.1 - 30 MHz<br>6 [c] | 10.1 - 3 GHz<br>6 [c] |
| | 30 - 100 MHz<br>$0.636\ f_M^{1.337}$ [a c] | |
| | 100 MHz - 5 GHz<br>30 [c] | |
| | 5 - 30 GHz<br>$150/f_G$ [b c] | 3 - 30 GHz<br>$19.63/f_G^{1.079}$ [b c] |
| | 30 - 100 GHz<br>$25.24/f_G^{0.476}$ [b c] | 30 - 300 GHz<br>$2.524/f_G^{0.476}$ [b c] |
| | 100 - 300 GHz<br>$5048/[(9\,f_G - 700)f_G^{0.476}]$ [b c] | |
| ICNIRP Guidelines for limiting exposure to electromagnetic fields (100kHZ-300GHz) (2020) | <10 GHz<br>6 [c]<br>10 - 300 GHz<br>$68/f_G^{1.05}$ [b c] | <10 GHz<br>6 [c]<br>10 - 300 GHz<br>$68/f_G^{1.05}$ [b c] |

a $f_M$ freq. in MHz
b $f_G$ freq. in GHz
c all times are in minutes

The time variation of emitted exposures from the wireless networks is characterized by the daily and weekly variations of traffic which depends on the number of connected users in these networks. In [79], the authors investigated how exposures change over time due to the existence of peak and off-peak hours in the daily exposure, also, the existence of weekdays and weekends in the weekly exposure. The objectives of their study were to determine when the exposure levels are expected to be maximum, to identify the worst-case exposure and its compliance with the set limits, and to assign resources dynamically and optimally. P. De Lellis *et al.* presented a time-series analysis model that uses measured data to construct a predictor for the RF-EMF exposure. The results observed that exposure is highest during a specific time of the day compared to the night, and

showed that exposure is periodically different on weekdays when compared to weekends. With the above, the worst-case radiated exposure was determined.
As a result, the predictor can be used along with a self-organizing network (SON) or an SDN to reassign resources efficiently from the APs where there is an increase in radiated exposure due to the high number of users to other APs where there are fewer users. This would optimise the operation of the wireless network,

Also, the authors in [80] investigated and showed that the exposure level from a base station is not constant and varies with time due to the variation in traffic load. They developed an approach that uses a SA to measure the transmit power from the APs at different times of the day, and analyses the correlation of the measured exposure in time and space. The self-correlation were done for an AP in the time series, while the cross correlations were done for multiple APS in the same area. The minimum and maximum electric fields were found to be 1.18 and 2.36 V/m, respectively. They also concluded that due to traffic variation, the exposure higher levels are between (9h – 23h) while the lower levels are between (23h – 9h). Also, they found out that the lifestyle of users is more consistent than the traffic, therefore, the spatial correlation is bigger than the time correlation.

**Power** and power control are important topics in radio resource management. In wireless networks, powers are transmitted from both uplink (UEs to the APs) and downlink (the APs to UEs) transmissions. Controlling both the uplink and downlink transmit powers has been a major consideration in many works of literature [97], [98], [99], [100]. Power control is usually used to optimise the power of the desired received signals while limiting interference and radiofrequency-electromagnetic force (RF-EMF) radiation.

The transmit power is directly proportional to the received SINR and the RF-EMF radiations. Therefore, a proper power control scheme [100] is required for both uplink and the downlink to dynamically adjust the transmit power of wireless communication networks to optimise and ensure target SINR level; and minimise both the RF-EMF exposure and the interference [21]. Power control scheme is extensively dealt with in Chapter 5.

### 2.7.4. Safety Factors, Standard Limits, Guidelines and Metrics

5G network is expected to take the advantage of high throughput of the millimeter wave technology, thus, the above 6GHz to 28GHz (millimeter wave) frequency band is the ideal candidate for 5G wireless network propagation. Beamforming is a major consideration for millimeter wave communication, the design of this beamforming is done in such a way that it caters for the limitations of millimeter wave channels. However, there is still the challenge of RF-EMF radiation exposure to users. Though exposure occurs at all the radio frequencies, nevertheless, the level varies as the radiation absorbed by the user from AP and wireless devices are frequency dependant.

The adverse effects of heating caused by exposure are the rationales behind having different safety factors for different frequency ranges. For frequencies below 100 kHz, the concern is strictly electrostimulation. For frequencies between 100kHz to 5MHz, the concerns are both electrostimulation and heating, while for frequencies above 6GHz, the concerns are electrostimulation, local heating and whole-body heating of the tissue surface [90]. Therefore the exposure limits are defined to guide against the effects of electrostimulation between the frequencies of 0Hz and 5MHz and guide against the effects of electrostimulation, local heating and whole-body heating between the frequencies of 100 kHz and 300 GHz [75].

Different standard metrics and thresholds have been adopted by the regulatory bodies. The ICNIRP [101], the FCC [13], and the IEEE *Std. C95.1* [14] adopted SAR as the metric for lower frequencies from 100kHz to 6GHz. The ICNIRP's SAR limit is 2W/kg for local exposure and 0.08W/kg for the whole-body exposure average over 6 minutes for 10g of tissue [90], while the FCC's SAR threshold is 1.6W/kg for a local exposure average over 6 minutes for 1g of tissue [90]. The FCC limits are only with the power of law in the United States of America. However, many countries have adopted these stricter safety guidelines in ensuring public health and safety from wireless network operations and other RF emitting equipment [102].

For higher frequencies in the millimeter-wave band, radiation exposure behaviour is different from the lower frequencies explained above. Thus, the FCC used power density as the exposure metric instead of the SAR. The limit is frequency (wavelength) dependent. This is because the millimeter-wave penetration into the human body is limited, i.e., less than one millimeter [103]. Therefore, causes a low level of absorption below the tissue surface such as the skin and the

eyes, but a high level of deposited energy in the tissue's surface (skin) which elevate the skin temperature and not the body core temperature. Consequently, millimeter-wave is nonlethal as it is restricted to surface heating of the skin, and it is measured with the incident power density (PD) as the appropriate standard metrics [90], [14].

Apart from the incident power density and the SAR, the external field strength most especially the electric field strength (E-field) is also used as a metric for compliance reasons to guide against the health risks of users. The electric field strength has recommended limits that correspond to the limits of SARs; however, these limits are different in the various frequency range (of 0Hz to 300GHz) as published in the standard/guidelines [91].

Table 2.3 applies to local SAR, whole-body SAR, and Local power density exposures for frequencies ranging from 100kHz to 300GHz in both the restricted (occupational) and unrestricted (general public) environments. The values are clearly stated, hence, do not require formulas to determine the limits. The table is modified from Table 5 of IEEE standards [104] and Table 2 of ICNIRP guidelines [101].

*Table 2.3. The basic exposure restrictions (100 kHz - 300 GHz) [104], [101].*

| Exposure conditions | Frequency range | General Public limit (unrestricted environments) | Occupational limit (restricted environments) |
|---|---|---|---|
| **Whole-body exposure SAR (W/kg)[a]** | 100 kHz - 6 GHz | 0.08 | 0.4 |
| | >6 - 300 GHz | 0.08 | 0.4 |
| **Local exposure (head and torso) SAR (W/kg)[b]** | 100 kHz - 6 GHz | 2 | 10 |
| | >6 - 300 GHz | NA[c] | NA[c] |
| **Local exposure (limbs and pinnae) SAR (W/kg)[b]** | 100 kHz - 6 GHz | 4 | 20 |
| | >6 - 300 GHz | NA[c] | NA[c] |
| **Local $S_{ab}$ (W/m²)[d]** | 100 kHz - 6 GHz | NA[c] | NA[c] |
| | >6 - 300 GHz | 20 | 100 |

a Whole-body average SAR is to be averaged over 30 minutes and local exposure over 6 minutes (see Table 2.2 for averaging time).
b Local SAR is averaged over a 10g cubic mass of tissue.
c "NA" means "not applicable" thus, it should not be considered.
d Local $S_{ab}$ should be averaged over a square 4cm² surface area of the body. Above 30GHz, the exposure averaged over a square 1cm² surface area is restricted to two times that of the 4cm² restriction.

Table 2.4 (culled from Tables 9 and 10 of IEEE standards [104]) shows the local exposures for frequencies ranging from 100 kHz to 6GHz in both the restricted (occupational) and unrestricted (general public) environments. In this frequency range, formulas are used to determine the exposure ERL.

*Table 2.4. Whole-body exposure ERLs (100kHz - 300GHz) for occupational and general limits [104].*

| **Exposure conditions** | **Frequency range (MHz)** | **Electric field strength ($E$)[a,b,c] (V/m)** | **Magnetic field strength ($H$)[a,b,c] (A/m)** | **Power density ($S$)[a,b,c] (W/m²)** | | **Averaging time (min)** |
|---|---|---|---|---|---|---|
| | | | | $S_E$ | $S_H$ | |
| **General Public limit (unrestricted environments)** | 0.1 - 1.34 | 614 | $16.3/f_M$ | 1000 | $100000/f_M^2$ | 30 |
| | 1.34 - 30 | $823.8/f_M$ | $16.3/f_M$ | $1800/f_M^2$ | $100000/f_M^2$ | 30 |
| | 30 - 100 | 27.5 | $158.3/f_M^{1.668}$ | 2 | $9400000/f_M^{3.336}$ | 30 |
| | 100 - 400 | 27.5 | 0.0729 | 2 | | 30 |
| | 400 - 2000 | — | — | $f_M/200$ | | 30 |
| | 2000 - 300 000 | — | — | 10 | | 30 |
| **Occupational limit (restricted environments** | 0.1 - 1.0 | 1842 | $16.3/f_M$ | 9000 | $100000/f_M^2$ | 30 |
| | 1.0- 30 | $1842/f_M$ | $16.3/f_M$ | $9000/f_M^2$ | $100000/f_M^2$ | 30 |
| | 30 - 100 | 61.4 | $16.3/f_M$ | 10 | $100\,000/f_M^2$ | 30 |
| | 100 - 400 | 61.4 | 0.163 | 10 | | 30 |
| | 400 - 2000 | — | — | $f_M/40$ | | 30 |
| | 2000 - 300 000 | — | — | 50 | | 30 |

a far-field plane-wave exposures.
b $f_M$ is the freq. in MHz.
c E, H, and S values are calculated with the RMS values.

Table 2.5 (culled from Tables 9 and 10 of IEEE standards [104]) shows the local exposures for frequencies ranging from 100 kHz to 6GHz in both the restricted (occupational) and unrestricted (general public) environments. In this frequency range, the formulas are used to determine the exposure ERL.

*Table 2.5. Local exposure ERLs (100kHz - 6GHz) for occupational and general limits.*

| **Exposure conditions** | **Frequency range (MHz)** | **Electric field strength ($E$) [a,b,c] (V/m)** | **Magnetic field strength ($H$) [a,b,c] (A/m)** | **Power density ($S$) [a,b,c] ($W/m^2$)** | **Power density ($S$) [a,b,c] ($W/m^2$)** |
|---|---|---|---|---|---|
| | | | | $S_E$ | $S_H$ |
| **General Public limit (unrestricted environments)** | 0.1-1.34 | 1373 | $36.4/f_M$ | 5000 | $500000/f_M^2$ |
| | 1.34-30 | $1842/f_M$ | $36.4/f_M$ | $9000/f_M^2$ | $500000/f_M^2$ |
| | 30-100 | 61.4 | $353/f_M^{1.668}$ | 10 | $47000000/f_M^{3.336}$ |
| | 100-400 | $21.2 \times f_M^{0.232}$ | $0.0562 \times f_M^{0.232}$ | $1.19 \times f_M^{0.463}$ | |
| | 400-2000 | — | — | $1.19 \times f_M^{0.463}$ | |
| | 2000-6000 | — | — | 40 | |
| **Occupational limit (restricted environments)** | 0.1-1.0 | 4119 | $36.4/f_M$ | 45000 | $500000/f_M^2$ |
| | 1.0-30 | $4119/f_M$ | $36.4/f_M$ | $45000/f_M^2$ | $500000/f_M^2$ |
| | 30 - 100 | 137.3 | $36.4/f_M$ | 50 | $500\,000/f_M^2$ |
| | 100 - 400 | $47.3 \times f_M^{0.232}$ | $0.125 \times f_M^{0.232}$ | $5.93 \times f_M^{0.463}$ | |
| | 400 - 2000 | — | — | $5.93 \times f_M^{0.463}$ | |
| | 2000 - 6000 | — | — | 200 | |

a peaks values are averaged over 6 min.
b $f_M$ is the freq. in MHz.
c E, H, and S values are calculated with the RMS values.

Table 2.6 (adapted from Table 11 of IEEE standards *[104]*) applies to exposure for frequencies from 6GHz to 300GHz in both the restricted (occupational) and unrestricted (general public) environments.

*Table 2.6. Local exposure ERLs (6GHz to 300GHz) [104].*

| **Frequency** | **Incident Power Density limit for the general public (unrestricted** | **Incident Power Density limit for occupational (restricted environments)** |
|---|---|---|

| | **environments) ($W/m^2$)[a,b,c]** | **($W/m^2$)[a,b,c]** |
|---|---|---|
| 6GHz | 40 | 200 |
| 6GHz - 300GHz | $55f_G^{-0.177}$ | $274.8f_G^{-0.177}$ |
| 300GHz | 20 | 100 |

a Incident power density is averaged over 6 min for local exposure.
b For 6 GHz - 300 GHz it should be averaged over an area of 4cm² of body surface with the shape of a square.
c $f_G$ is the freq. in GHz.

These standard limits are placed on the worst-case exposure and ensure that electromagnetic radiation exposure to a human does not cause any substantial temperature elevation or tissue heating. For frequencies between 2 and 300GHz with an averaging time of 30 minutes, some countries have specified stricter general public exposure limits *[82]*. Most notable is the German institute for building biology and sustainability (IBN) which is a thousand-fold lesser than the abovementioned standards. The IBN in their 2015 Standard of Building Biology Measurement Technique (SBM-2015) *[105]* specified the power density exposure limit as less than 0.1 μW/m². Also, 0.1 W/m² was set by the Chinese ministry of health *[106]* and the Belgium and Brussel adopted 20.6 V/m *[81]*.

SAR is expressed as a measure of electromagnetic power absorbed in human tissue per unit mass. The value of SAR depends largely on the averaging mass or volume, the larger the mass or volume of an exposed body, the lower the SAR on the body [84], and the absorption is a function of the electric field. It is worthy of note that the squared electric field magnitude in the human body is proportional to both the incident power density $S$ ($W/m^2$) and the SAR [94] as seen in Eqs. (2.2) and (2.3).

$$SAR = |E|^2 * \frac{\sigma}{\rho} \tag{2.2}$$

$$S = \frac{|E|^2}{Z_o} \tag{2.3}$$

where $E$ [V/m] is the induced electric field inside the human body, $\sigma$ [S/m] is the conductivity of the human body, $\rho$ [kg/m³] is the density of the human body, and $Z_o$ is the characteristic impedance of vacuum (free space) which is $120\pi\Omega$ = 377Ω. SAR [W/kg] is a metric used in the study of dosimetry. Dosimetry is the measurement or assessment of the RF energy introduced into the system and absorbed whenever a biological body is exposed to EM-field radiation [107], [108].

## 2.8. Related Work

Recently, the management of network resources has attracted many researchers both in industries and academia on how the resources in wireless networks can be efficiently managed to give better utilisation of network resources and safer networks.

Here are some of the relevant studies relating to resource allocation in mobile networks on the study in **Chapter 3**. The authors in [109] propose a Genetic Algorithm (GA) Intelligent Latency-Aware Resource allocation scheme. (GI-LARE). The theory of NS was investigated for the users' QoS requirements (data rate and latency QoS). Therefore, they classified the slices mainly with the eMBB slice (bandwidth-hungry use case) and the mMTC (latency-dependent use case). A latency-aware dynamic resource allocation problem is formulated as a utility optimisation problem and solved using Monte Carlo numerical simulations. Comparisons were carried out with the static allocation scheme and a branch and bound method in a 5G HetNet, and results show that the genetic algorithm schemes outperform the static scheme.

Also in [110], S. Haryardi *et al.* propose a new perception that the efficiency of a network is dependent on the resource allocation fairness level. They noted that when there is a major change in the traffic of each gNB in a 5G ultra-dense network, there will be a high-performance loss. The authors propose a new method to evaluate an index called Harmony-in-Gradation Index and coefficient to preserve the network performance. This formula maintains the ratio of a gNB load to its backhaul link capacity in each gNB to have a value close to each other. They categorized the resource allocation levels as perfect, fair, unbalanced and unfair, while the network performance was categorized as perfect, good, less good and poor. Results show that when the traffic is not proportional, it affects the transmit power of each APs causing unfair resource allocation and hence poor network performance. Therefore, the fairness level is closely linked to the network efficiency.

A game-theoretic approach to resource allocation was introduced in the work of R. Xie *et al.* [111]. The authors proposed a competitive game theory optimisation approach to solve the optimisation problem of sharing hierarchical caching resources among MVNOs in order to maximize revenue. The problem was decomposed into two independent caching resource sharing problems in the RAN and core networks. Then, the optimal solutions are solved and the global solution is attained, simulation results show that the expected revenue was maximized. A

joint congestion control and dynamic resource allocation was proposed in [112] adopting the Sparse Code Multiple Access (SCMA) technique for Physical Uplink Shared Channel (PUSCH) resources to improve the number of successful communications and guarantee lower energy consumption in the network. SCMA was adopted because is the most promising NOMA technique to support mMTC connectivity with small-size data.

Furthermore, the importance of priority in a wireless network has been studied in many works of literature. The authors in [113] study the statistical priority-based multiple access protocol (SPMA) which uses fixed priority thresholds in determining the reliability and latency (success rate) of packets at each node. The priorities are classified according to the packet's degree of urgency e.g. the latency tolerance. P. Liu *et al.* improve the performance of the statistical priority-based multiple access protocol (SPMA) by proposing an adaptive priority-setting strategy for the SPMA. This adaptive priority-setting strategy accounts for the change of transmission rates due to the change of channel condition at each network node. The adaptive priority-setting brings optimal transmission that ensures a 99 percent first-time success rate for packets of the highest priority, thereby giving high reliability and low latency in the network.

N. Bansal *et al.* in [114] did a comparative study among the priority algorithms and secondly between the priority and non-priority task scheduling algorithms of cloud computing. The algorithms enumerate the priority of tasks according to their specific attributes and then sort tasks by priority. By calculating the total allocation costs for each scheduling algorithm, the priority-based algorithms have good performances, however, the non-priority based algorithm gives the best performance in terms of less waiting time in allocating tasks. Similarly, authors in [115] propose an algorithm in a heterogeneous grid environment that minimises the processing cost and gives better performance in terms of the number of tasks carried out. This algorithm provides flexibility in the prioritisation of tasks in some conditions such that lower priority tasks can be allocated available resources before higher priority ones. For example, the algorithm after initially scheduling the tasks using the traditional priority-based method, if it finds out that the available resources cannot accommodate the next task due to not enough computational resources, the scheduler finds the next

lower priority job (other than the original higher priority task) that can satisfy the available computational requirement.

The authors in [116] propose an efficient and deadline-aware priority-driven congestion control (PCC) protocol in data centres. The PCC grants deadline-sensitive traffic the higher priorities. The PCC calculates the priority of the traffics in line with he traffics' the size and deadline of the transmitted data. Then adapts the congestion window in line with the computed traffic priority. This scheme improves the user-perceived QoS in the form of the throughput of high-demand traffics and completion time of time-sensitive traffics of transferred data.

A RA and admission control is formulated as an optimisation problem, subject to some QoS constraints and is proposed in [20]. The mechanism is designed to admit users with different priorities to maximize the number of users. Nevertheless, priorities are only used among the users, therefore, this work does not differentiate in scenarios where users are subscribed to services having different priorities. In [117], admission control policies have been implemented by InPs applying forecasting techniques using traffic analysis and prediction per network slice. This approach accepts provided the required QoS of the new service/user does not affect the QoS of the services in the network. The authors in [118] have proposed a hybrid offline-online resource allocation strategy. The mechanism proposes an iterative slice provisioning algorithm that adjusts the minimum slice requirements based on CSI.

In all the works reviewed, the inter-slice as well as intra-slice were not considered. A heuristic-based admission control mechanism is proposed in [119], network resources are dynamically assigned to different users/slices. They consider the inter-slice and intra-slice, however, their work has not considered multi-tenancy where different SPs belong to the same InP.

Here are some of the relevant and recent studies on power management and flexible scheduling pertaining to resource allocation in virtual wireless networks, works relating to the study in **Chapter 4**.

The authors in [45] discuss major works in the field of wireless network virtualisation. They review important topics such as the challenges and performance metrics in their survey. In [66], the authors propose a component

called Slice Optimiser which communicates and receive information about the network slices from an SDN controller. The Slice Optimiser which is an extension to the LTE's RAN uses the received information and adapts the slices according to the network state. The authors rely on SDN architecture, the slice optimiser with the SDN controller, all these are implemented in NS-3.

The authors in [120] propose a framework that leverages on the QoS Class Identifier (QCI) and security requirements in negotiating, selecting and assigning virtualised networks to the requesting applications or users in 5G Networks. In [121], V. Sciancalepore, *et al* describe a network slicing management and orchestration framework that automates, configure and activate multiple network infrastructure resource domain. However, the authors of [120] and [121] have not validated their proposed frameworks with either simulation or experiments.

In [122], the authors present a slice scheme where a Wireless Virtualised Network is sliced into two service-based slices with resource-based and rate-based services. The scheme aims to maximize the total rate of WVN by guaranteeing minimum PRBs for each slice. However, the authors consider equal chain gain and assumed equal noise power over all sub-carriers. The authors in [58] propose a framework and formulated an RA problem in small cells that minimises the total downlink transmit power subject to their power, QoS, and interference thresholds of microcell users. In [68], the authors present a slicing and scheduling scheme to meet the different rates of VNs. Each VN is allocated a certain number of sub-channels to provide services to its users. This scheme focuses on isolation among the VNs. A. Pratap, *et al* in [123] proposed a RA scheme that minimises interference and maximizes spectrum reuse in 5G heterogeneous small cell networks keeping the user-level fairness into consideration. However, none of the authors has focused on the transmit power required for the various slices which are different as a result of their specific QoS requirements in minimising the co-users interference.

Furthermore, many works in the literature have investigated RF-EMF radiation exposure induced by wireless networks differently. This has made it to be a bit controversial especially after the start of the recent corona virus pandemic and the many conspiracy theories linking the 5G network and COVID 19. The research area has garnered increasing attention recently, therefore, some of the recent and relevant studies on RF-EMF radiation and its exposure in wireless networks are reviewed here.

Relating to **Chapter 5**, the authors in [124] presented a surrogate model that evaluates the RF-EMF exposures caused by both the UP and DL of a 4G network. They characterized the SAR of the RF-EMF for a particular location. However, the authors failed to analyse the EI, they only compared it with the standard SAR limits. In [10], the authors conducted tests and measured the radiations emitted from some APs in three selected locations in Dar-es-Salaam, and compared it with the guideline of ICNIRP. Kaijage *et al.* used a selective radiation meter and the data collected were analysed using MATLAB [125]. However, the exposure results did not depict global exposure and concentrated mainly on the downlink side of the radio emission.

The authors in [7] presented two different measurement set-ups. The first measures the RF-EMF radiations from a base station for a couple of days and the second measures the RF-EMF radiations of the user equipment to a human head. The authors considered very poor reception values (which ordinarily increase the radiation) and compared them with the standard health threshold. However, P. Mandl *et al.* did not state the required average time (of at least 6 minutes) of the measurements for each day. In [9], the authors showed how important the realistic power levels of UEs and LTE base stations were vital for the precise evaluation of RF-EMF exposures induced from wireless communication devices. The authors obtained their data from over 7000 UEs and 41 LTE APs in different environments. However, the results only revealed the estimated uplink exposure.

In [8], the authors presented a study on SAR characteristics on the number of antennas and the positioning of a PIFA antenna in a UE. The authors raised concerns of degradation of the device and higher average SAR values on users when the positioning of the antenna is on the upper part of the device. G. Koutias and T. Samaras in [126], presented a genetic algorithm optimisation technique that works with indoor network planning which minimises the exposure from both UEs and APs. Lastly, authors in [127] dealt with the evaluation of RF-EMF exposure induced by the wireless network and investigated the relationship between the transmitted and received power from both UEs and APs respectively. A. Gati, *et al.* concluded that the exposure to UEs is higher while the base station exposure is lower.

The rest of the reviewed works from the literature are relating to **Chapter 6** of the dissertation.

In [128], the author presented a study on the QoE and EMF trade-off and how to reduce EI in 5G mobile networks. Sarrebourse *et al.* in [129] proposed a new exposure metric EI, and deployed low-complexity dosimeters to measure and provide the exposure information in the city. In [130], the authors presented a study on whole-body and localised SAR and dose prediction. They calculated the absorbed doses with the measured SAR values by multiplying the time duration of the exposure and showed the influence of phone call duration on the total absorbed dose. The authors concluded that SAR is lowered when more APs with lower transmit power are installed. However, the absorption due to UL transmission of the other users is not accounted for. Authors in [131] presented the strategies of reducing the global EMF exposure, their exposure is closed tied to users' behaviour e.g. mobility of user increases exposure, since a user experience frequent handovers and mobility increases signalling. Other factors presented that influence exposure are the; user's profile, type of services, and duration.

In [132], the authors minimised EMF exposure while achieving a target QoS and maximized the network capacity while remaining below the legal thresholds. The EMF exposure is characterized by UL transmit power and DL power density, the small cells' inter-site distance (ISD) were varied using 50m, 100m, and 200m with the optimal network parameters. A 50m & 100m ISD cause a strong reduction in the DL EMF exposure. UL EMF exposure improves significantly when the distance between users and small-cells (SC) decreases. The authors concluded that 5G network brings APs nearer to the user, and lowers UL transmit power by using smaller APs. D. Plets *et al.* [130] presented an exposure prediction method based on the measured values, the power was then used in calculating and predicting the SAR values and also the EIs. The authors compared the induced exposure of UMTS macrocell, UMTS femtocell, and WiFi Voice over Internet Protocol (VoIP). It was concluded that WiFi radiates more exposure due to no power control algorithm. A macrocell is better and a femtocell is the best in terms of exposure emission. Authors in [133] suggested ways of managing and reducing EMF levels without compromising the users' QoS. Some of the methods suggested include; efficient handover management, RATs, populations, and power control. In [134], the authors proposed a user scheduling scheme that reduces EM emissions in the UL. They formulated a user scheduling/power assignment algorithm that minimised the RF-EMF exposure of users by minimising the total energy dissipated towards each user subject to transmitting a required number of bits.

### 2.8.1. The Research Gaps

After reviewing and identifying various works related to the problems defined and the solutions proposed, a brief of research areas made from the contributions, approaches, methodologies, merits, and challenges was presented. The identified research gaps in the reviewed works are as follows;

1. Most reviewed schemes in the literature used intra-slice priority only and without being done in a multi-tenancy environment. Few works applied admission control to their scheme and many did not apply the concept of virtualised (slices) 5G network. As a result, an admission control scheme is proposed considering the inter-slice priority as well as the intra-slice priority in a multi-slice and multi-tenancy scenario.
2. Also, in most reviewed work, the concept of users requiring different transmitting power is considered, but none applied it to slices that have different target rates. Most works of literature worked on older RAT such as the 4G network. This work addresses the research gap by focusing on 5G RAN. It proposes a dynamic joint power and subcarrier allocation algorithm which assigns sub-channels to slice users based on their transmit power, subject to the CSI and some QoS constraints.
3. Most authors in the literature measured the radiofrequency fields such as the power density, electric field, and magnetic field when evaluating the impact of RF-EMF radiation exposure induced by wireless networks. Also, none of the authors has considered both the 5G uplink and downlink networks. These identified research gaps are addressed by characterizing and evaluating the SAR and the EI from both the APs and UEs in the 5G wireless network using a power control scheme. It compared them with that of the 4G network and with the ICNIRP's thresholds.
4. Lastly, power control and optimisation solutions have been used severally by many authors in literature. However, none of the reviewed related works applied it to the minimisation of RF-EMF radiation exposure using the EI. This research identified the gap and capitalised on the relationship between power density and radiation exposure at a user's location. Therefore proposed an RF-EMF exposure reduction scheme to

reduce the total EI in a 5G network which minimises the total EI subject to QoS, interference, transmit power, and other constraints.

## 2.9. Summary

This chapter presented the literature overview of the wireless networks from the 1G up to the 5G networks. The chapter explained exclusively the drivers, the expectations, the enabling technologies and the specifications of the 5G wireless network. Also, 5G based framework, its use cases, and network slicing as differentiating factor 5G wireless network from other exiting RATs were discussed. NFV, SDN, and MEC were discussed as the other supporting technologies.

Chapter 2 defined the main challenges in the proposed 5G wireless network as resource sharing, interference, and radiation exposure mitigation. The chapter explained radio resources allocation, admission controller, the slicing scheduler, power control, interference, and RF-EMF radiation exposure fundamentals and management in wireless networks.

Finally, Chapter 2 reviewed many related works in the literature and identified the existing contributions, approaches and research gaps. Subsequently, the ideas that meet these gaps correspondingly are presented by proposing the schemes that provide solutions to the formulated problems of resource allocation, interference and radiation exposure mitigations.

# Chapter 3

# 3. Resource Allocation Strategy for 5G Network Slicing Using Admission Control with Prioritisation.

## 3.1. Introduction

Radio resources are very scarce, therefore, there is a need to utilise and efficiently manage the available isolated resources among the different MVNOs. Radio resources can be allocated based on several network parameters such as data rate, interference levels, transmit power, bandwidth, pre-defined contracts (i.e., SLA), traffic load, channel conditions [40] [38]. In this chapter, a resource allocation and admission control scheme is proposed for 5G slice networks.

The recent increase in global data usage is due to the advancement in the capabilities of UEs and the development of applications that consume high bandwidth. This has caused an unprecedented increase in the demand for radio-frequency resources in wireless networks lately. As predicted by Cisco [4], the monthly global data traffic would exceed 278.1 Exabytes by 2022. Also, Cisco predicted that by 2023, the number of internet users would be 5.3 billion, and the number of connected devices would is estimated to be around 29.3 billion and of which 11% will be 5G connected [4]. However, the 5G network is expected to address these issues by meeting the QoS requirements such as the high number of connected devices, low energy consumption, low latency, and high data rates [6] which the present generations of wireless networks would not be able to satisfy.

In 5G slice networks, it is worthy of note that the network will be virtualised and this will bring about a multi-tenancy scenario. In multi-tenancy as depicted in Fig. 3.1, MVNOs (otherwise referred as tenants) share the same physical RAN

provided by a single InP. Hence efficient resource management by the InP is very important. Network resources can be shared statically or dynamically [16]. Due to the dynamic nature of network traffic, the design of agile and dynamic RA and admission control algorithms that manage the various network traffic loads is critical in ensuring reduction in the OPEX improving the overall network performance [18].

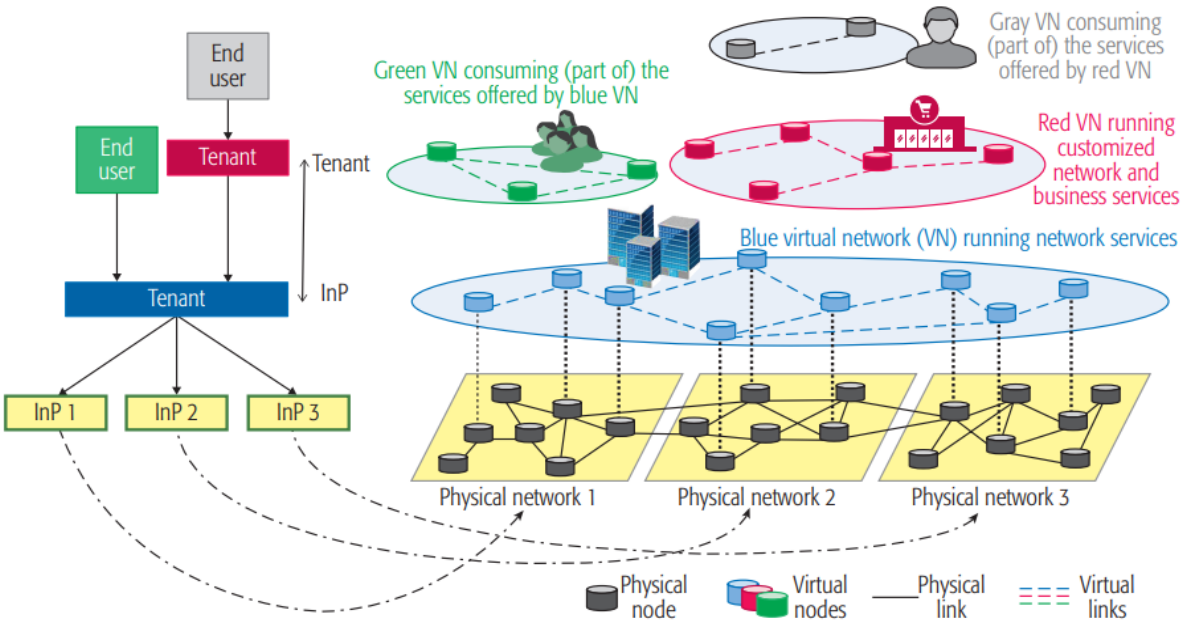


*Figure 3.1: 5G network slicing depicting InPs and MVNOs in a multi-tenancy scenario as virtualisation actors [22].*

As a result, a prioritized RA and admission control algorithm for downlink transmission in a gNodeB RAN is proposed. Herein, the UEs QoS requirements in terms of minimum and maximum data rate, bandwidth capacity limitations, intra-slice and inter-slice prioritisation are considered. The intra-slice priority also known as users' priority is the priority of users belonging to the same slice whereas the inter-slice priority (i.e. slice priority) is the priority of different slices that belongs to the same network. These priorities are defined based on the users and slices significance by the MVNO and/or the InP.

For overall system performance and to maximize the users' QoE, the RA problem is formulated as an MINLP optimisation problem [20]. Moreover, admission control is employed, jointly with the RA, to deal with infeasibility issues in the optimisation problem in scenarios where it is impossible to support all UEs with the available network resources, and in case of a new UE request.

The key contributions of this chapter are summarised as follows:

- A RA scheme is formulated as an optimisation problem. This offers a solution based on the PRAAC approach, where it iteratively maximizes the QoE of UEs which dynamically allocate resources to slices and users based on their QoS constraints and priorities. Different from [10], the scheme is based on multitenancy slices where different MVNOs belonging to the same InP provide services for different UEs. Moreover, it incorporates AC, jointly with RA, to deal with infeasibility issues.
- Prioritisation at both user and slice levels is considered. The priorities which together with the QoS constraints are used for both the admission control and resource allocation algorithms to enhance the QoE of UEs.

This chapter is structured as follows: Section 3.2 describes the proposed system model. The assumptions and mathematical formulation are described in Section 3.3. The description of the proposed algorithm and the performance evaluation are presented in Sections 3.4 and 3.5, respectively. Section 3.6 summarises the chapter.

## 3.2. Notations

In this subsection, the relevant notations used in the entire chapter are described. Table 3.1 highlights the list of notations.

*Table 3.1: List of notations*

| Symbol | Description |
|---|---|
| $m$, $M$ | MVNO, MVNO set |
| $s$, $S$ | Slice, Slice set |
| $u$, $U$ | User, User set |
| $u^{s,m}$ | User $u$ in slice $s$ and MVNO $m$ |
| $g$ | gNodeB |
| $c$, $C$ | Sub-channels, set of sub-channels |
| $b^c$ | Bandwidth of the generic sub-channel $c$ |
| $B$ | Total Bandwidth of the InP |
| $P^{\mathrm{T}}$ | Total transmit power of the gNodeB |
| $p^c$ | Transmit power of the sub-channel $c$ |
| $R_{\mathrm{s}}^{min}$, $R_{\mathrm{s}}^{max}$ | Minimum data rate, maximum data rate |
| $R^{TH}$ | Network threshold data rate |
| $p_{\mathrm{s^m}}$ | Priority of the slice $s$ in MVNO $m$ |
| $r_{\mathrm{u^s}}$ | Priority of the user $u$ in slice $s$ |
| $X_{u^{s,m}}$ | Log-normal shadow fading pathloss of user $u$ |
| $d_{u^{s,m}}^{g}$ | Distance between the user and the gNodeB |
| $\mathrm{PL}_{u^{s,m}}^{\mathrm{g}}$ | Pathloss between the gNodeB and the user |
| $h_g$ | gNB height |
| $f_c$ | Carrier frequency in MHz |
| $N_0$ | Noise spectral density |
| $\delta_{u^{s,m}}^{\mathrm{c}}$ | Binary allocation index of $u$ in the sub-channel |
| σ | Shadow fading pathloss component standard deviation in $dB$ |
| $H_{u^{s,m}}^{g}$ | Channel gain of user $u$ in slice $s$ and MVNO $m$ from the gNodeB |
| $\gamma_{u^{s,m}}^{c}$ | Signal to Noise Ratio of user $u$ in slice $s$ and MVNO $m$ |
| $\mathcal{R}_{\mathrm{u^{s,m}}}^{\mathrm{c}}$ | Data rate of user $u$ in slice $s$ and MVNO $m$ |
| $\mathfrak{Q}_{u^{s,m}}$ | QoE of user $u$ in slice $s$ and MVNO $m$ |
| $\mathfrak{Q}^{new}$ | New QoE request |
| $\Omega^{u^{s,m}}$ | Set of PRBs allocated to the user $u^{s,m}$ |

| | |
|---|---|
| $N_{PRB}^{m}$ | Minimum number of PRBs assigned to MVNO $m$ |

## 3.3. System Model and Assumptions

In this work, a system model where a single gNodeB is operated by an InP is considered for a proposed 5G sliced virtual network system as shown in Fig. 3.2 below.

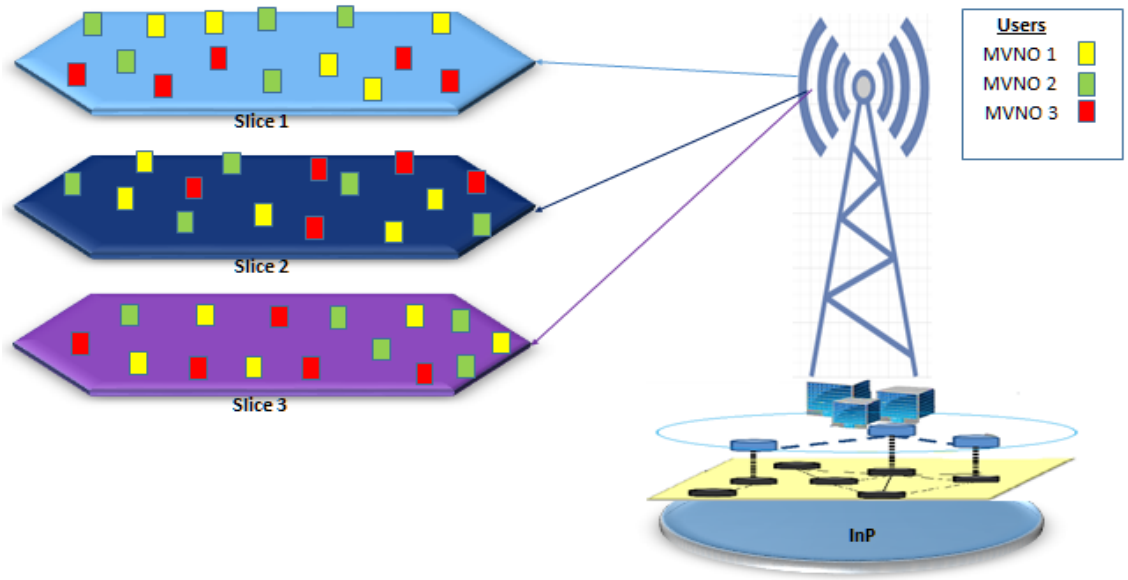


*Figure 3.2: System model of the proposed scheme.*

It is assumed that the gNodeB $g$, is operated by an InP with a coverage area of 500m radius and offers infrastructure services to a set of MVNOs $M$. An MVNO $m \in M$ have an SLA with the InP. The MVNOs have an independent set of slices $S$ from the InP's virtual network resources. Hence, each slice $s \in S$ has its set of user equipment $U$ services are rendered to. The gNodeB's bandwidth $B$ MHz is divided into a set of sub-channels, $C$, where the bandwidth, $b^c$, of the generic sub-channel $c$ is given as $B/|C|$. Moreover, the sub-channels are allocated to the MVNOs such that $c \in C$ with a total bandwidth size of $B$ MHz. In the time domain, $T$ sub-frames refer to as TTI of 1ms which makes up a frame structure. These sub-frames and subcarriers make up the available PRBs in the network. The total transmit power $P^{\mathrm{T}}$ of the gNodeB $G$, is presumed to be equally and uniformly distributed across the sub-channels C, i.e., $p^c = P^{\mathrm{T}}/C$. In this system model, each slice $s \in S$ requests admission in terms of QoS constraints that are associated with the slice in the form of the minimum and maximum data rates, $R_s^{min}$ and $R_s^{max}$, respectively. Each slice $s \in S$ has a priority, $p_{s^m}$, where the sum of the inter-slice priorities of all the slices $S$

associated with an MVNO $m \in M$ is equal to one (i.e., $\sum_{s \in \mathbf{S}} p_{\mathrm{s^m}} = 1$). Also, each user $u \in U$ is subscribed to a slice $s \in S$ has an intra-slice priority $r_{\mathrm{u^s}}$, where $\sum_{u \in \mathbf{U}} r_{u^s} = 1$. Thus, the pathloss between the gNodeB and a user is given by [135]:

$$PL^{g}_{u^{s,m}(dB)} = 40(1 - 4 * 10^{-3} h_g)\log_{10}\left(\frac{d^{g}_{u^{s,m}}}{1000}\right) - 18\log_{10}(h_g) + 21\log_{10}(f_c) + 80 + \log_{10}(X_{u^{s,m}}) \tag{3.1}$$

where $X_{u^{s,m}}$ is the log-normal shadow fading pathloss of user $u$ in *dB*. Additionally, $d^{g}_{u^{s,m}}$ is the distance between a user $u \in U$ and the gNodeB $g$, $h_g$ is the gNobeB's height both in metres, $f_c$ denotes the carrier frequency in MHz. The shadow fading pathloss component is assumed to be a Gaussian random variable with zero mean and σ standard deviation in *dB*. The gain, $\mathrm{H^{g}_{u^{s,m}}}$, between the gNodeB $g$ and a user $u \in U$ is given by [135]:

$$H^{g}_{u^{s,m}} = 10^{-\frac{PL^{g}_{u^{s,m}(dB)}}{10}}. \tag{3.2}$$

The Signal-to-Noise Ratio (SNR) of the sub-channel c assuming there is no interference in the subcarrier is given by [135]:

$$\gamma^{c}_{u^{s,m}} = \frac{p^{c}\left|H^{g}_{u^{s,m}}\right|}{N_0 b^{c}}, \tag{3.3}$$

where $N_0$ is the noise power per unit bandwidth. From Shannon-Hartley theorem, using the SNR, $\gamma^{\mathrm{c}}_{\mathrm{u^{s,m}}}$, the data rate, $\mathcal{R}^{\mathrm{c}}_{\mathrm{u^{s,m}}}$ of user $u \in U$ subscribed to a slice $s \in S$ is given as:

$$\mathcal{R}_{u^{s,m}} = \sum_{c=C} [\delta^{c}_{u^{s,m}} * b^{c} \log_2\left(1 + \gamma^{c}_{u^{s,m}}\right)] \tag{3.4}$$

where $\delta^{c}_{u^{s,m}} \in \{0,1\}$ is the binary assignment index of a user $u \in U$ with a resource. The QoE of user $u \in U$ in the slice $s \in S$ is given by:

$$\mathbb{Q}^{c}_{u^{s,m}} = \frac{\mathcal{R}^{c}_{u^{s,m}}}{R^{max}_{s}} \tag{3.5}$$

## 3.4. Problem Formulation

The resource allocation problem taking into consideration the QoE of users is formulated as an optimisation problem. Therefore, the objective function is to maximize the overall QoE of users based on the total data rate of the set of users $U$ in the set of slices $S$ attached to sub-carriers $C$, associated with MVNO $M$ considering user priorities $r_{u^s}$ and slice priorities $p_{s^m}$. The optimisation problem is given by,

$$max \sum_{m \in M} \left[ \sum_{s \in S} \left( \sum_{u \in U} [\mathbb{Q}_{u^{s,m}}]^{r_{u^s}} \right)^{p_{s^m}} \right] \tag{3.6}$$

s.t

$$\sum_{m \in M} \sum_{s \in S} \sum_{u \in U} \sum_{c \in C} \delta_{u^{s,m}}^{c} * b^{c} \leq B \tag{3.7}$$

$$R_s^{min} \leq \mathcal{R}_{u^{s,m}}^{c} \leq R_s^{max} \qquad \forall c \in C, \forall u \in U, \forall s \in S, \forall m \in M \tag{3.8}$$

$$\delta_{u^{s,m}}^{c} \in \{0,1\}, \quad \forall c \in C, \forall u \in U, \forall s \in S, \forall m \in M \tag{3.9}$$

$$\sum_{u \in U} \delta_{u^{s,m}}^{c} = 1 \qquad \forall u \in U, \forall s \in S, \forall m \in M \tag{3.10}$$

$$\sum_{u \in U} r_{u^s} = 1 \qquad \forall s \in S \tag{3.11}$$

$$\sum_{s \in S} p_{s^m} = 1 \qquad \forall m \in M \tag{3.12}$$

Constraint (3.7) represents the bandwidth constraint by ensuring that the total number of allocated sub-channels cannot be more than the maximum bandwidth capacity $B$. Constraint (3.8) indicates that the data rate QoS requirement for user $u^{s,m}$ is guaranteed according to the associated slice data rate requirement. Meanwhile, constraints (3.9) and (3.10) which are the sub-channel association constraints and stress the fact that a sub-channel cannot be allocated to more than one user, i.e., $\delta_{u^{s,m}}^{c}$ is binary. Finally, constraints (3.11) and (3.12) ensure that the sum of the priorities must be equal to one.

## 3.5. Priority-Based Resource Allocation Algorithm

In this section, the proposed priority-based resource allocation is described. Fig. 3.3 illustrates a single InP having multiple tenants *M*, different slices *S*, with multiple users *U*. Each user and slice access the physical resources via the admission control scheme based on their different priorities.

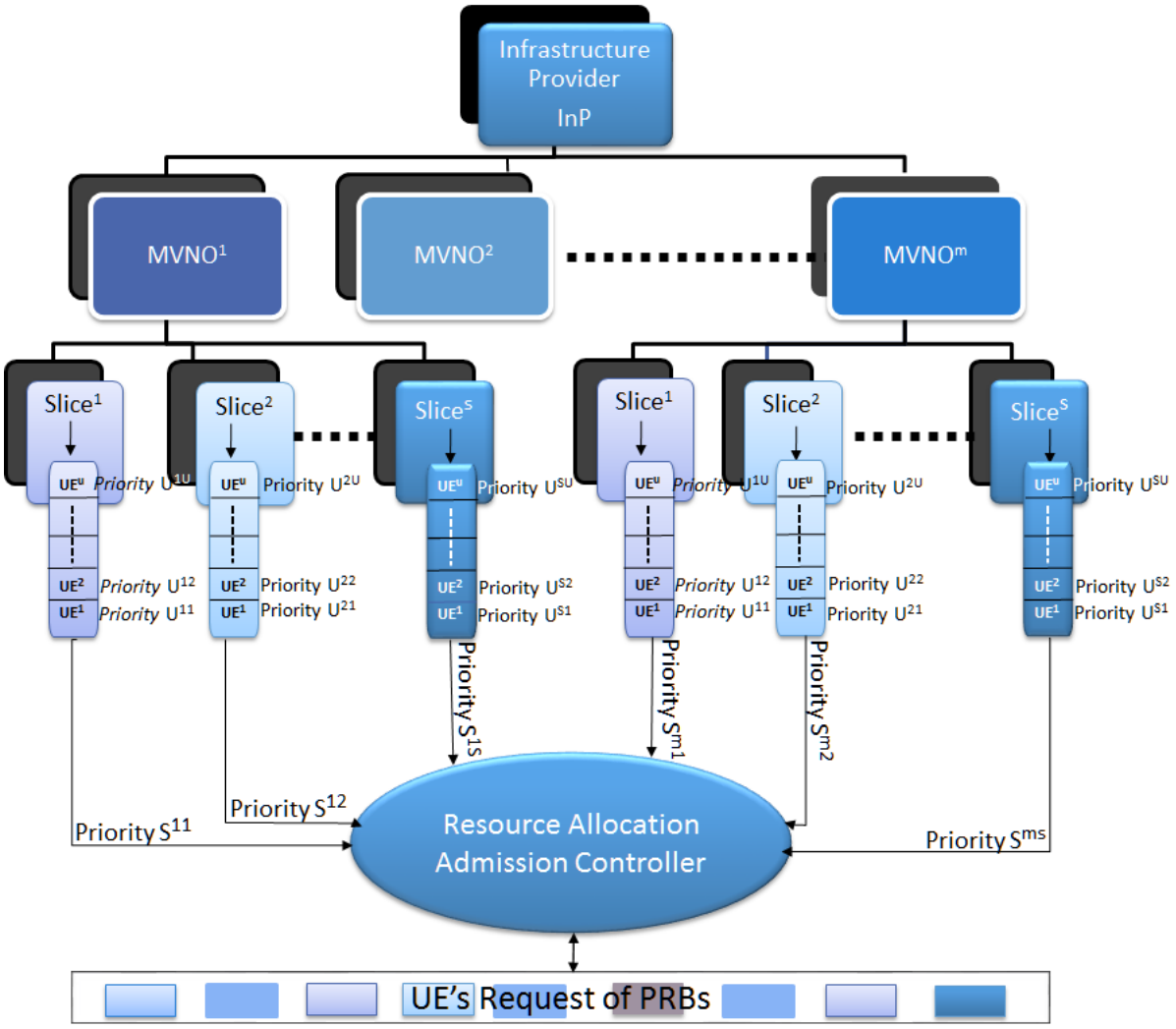


*Figure 3.3: Algorithm framework for prioritized slices and users admission control*

The algorithm solves and considers the users in the same slice and determines the acceptance possibility of a new user in the network taking into account the user's priority and the QoS (i.e., data rate) of the already served users. The newly arriving user(s) are be admitted into the network if the unused resources are enough to guarantee the minimum QoS for the slice.

Algorithm 1 shown in Table 3.2 solves the priority-based resource allocation problem while the admission control is performed using a pseudo-code of Algorithm 2 shown in Table 3.3.

*Table 3.2: Priority-based resource allocation algorithm*

**Algorithm 1** Priority-based resource allocation algorithm

**Inputs:** *S, C, M, P, B,* $f_c$, UEs, their positions and $H_{u^{s,m}}^{g}$.

**Outputs**: $\mathcal{R}_{u^{s,m}}^{c}$, $\mathfrak{Q}_{u^{s,m}}$

**I. Initialisation**:

1. **for** $m \in M$ **do** determine the number of MVNOs
2. **for** $s \in S$ **do** determine the slice priority
3. **for** $u \in U$ **do** determine the user distance and priority
4. **for** $c \in C$ **do** determine the PRBs allocated by InP

**II. Iteration**: **do**

5. **while** $R_{\mathrm{s}}^{min} \leq \mathcal{R}_{\mathrm{u}^{\mathrm{s,m}}}^{\mathrm{c}} \leq R_{\mathrm{s}}^{max}$ ∀u **do**
6. **calculate** UE data rate in (3.4)
7. **solve** max $\mathfrak{Q}_{\mathrm{u}^{\mathrm{s,m}}}$ with MINLP as in (3.6) where $\mathfrak{Q}_{\mathrm{u}^{\mathrm{s,m}}}$ takes values between [0,1]
8. **if** (3.8) is infeasible, **redo** step 6 adjusting the $\mathcal{R}_{\mathrm{u}^{\mathrm{s,m}}}^{\mathrm{c}}$. else denote the optimal solution with $\mathfrak{Q}_{\mathrm{u}^{\mathrm{s,m}}}$.
9. **end if**
10. **end while**
11. **end for**
12. **end for**
13. **end for**

Algorithm 1 considers the slices, MVNOs, the bandwidth, the carrier frequency, the sub-channels, the antenna height, the transmit power, the gains, the PLs, the priorities, and the various users' positions to maximize the QoE of the users as in Eq. (3.6) while solving for their data rates. The QoE was derived from Eqs. (3.1) to (3.5) before it was maximized in (3.6). The admission control is explained in Algorithm 2. Eq. (3.6) solves for the QoE of all users in the network. For every new user request, the scheme checks for the QoS target (i.e., the

minimum data rate $R_s^{min}$) required for the slice the UE belongs to. It determines if the network threshold $R^{TH}$ can accommodate this new request $R^{TH} \geq (\sum \mathcal{R}_{u^{s,m}}^{c} + R_s^{min})$; if so, the user is admitted and allocated to the network taking into account the inter-slice and intra-slice priorities. Else, the UE request is rejected and might go back to solving the optimisation problem in (3.6) while there are still request from UEs if within the TTI. Hence, the maximum achievable data rate is updated as in algorithm 2.

*Table 3.3: Admission control algorithm of new user(s)*

**Algorithm 2** Admission control algorithm of new users

**Inputs:** Set of UEs and their individual priorities ($p_{s^m}$, $r_{u^s}$) and QoS constraints ($R_s^{min}, R_s^{max}$).

**Outputs**: Set of admitted UEs. $u \in U$

1. **Solve** the MINLP (3.8) for all accepted UEs. $u\ u \in U$ with Algorithm 1. Calculate new QoE $\mathbb{Q}^{new}$
2. **for** every UE request $u \in U$, check the QoS target (in terms of $R_s^{min}$). Determine if $R^{TH} \geq (\sum \mathcal{R}_{u^{s,m}}^{c} + R_s^{min})$;
3. **if** so, a feasible solution has been found admit UE request
4. **for** each admitted UE $u \in U$, consider the slice priority order;
5. **for** each admitted UE $u^{s,m}$ in slice $s$, from MVNO $m$, consider the priority order within slice;
6. **if** priority order is higher, replace UE with the maximum achievable data rate, hence $(\max \mathbb{Q}_{u^{s,m}})$.
7. **else** replace with minimum achievable data rate hence $(\min \mathbb{Q}_{u^{s,m}})$.
8. **end if**
9. **end for**
10. **else** do not admit UE request.
11. **end if**
12. **repeat** the request in another TTI
13. **until** UE request is admitted or rejected when TTI≥ 2
14. **end for**

## 3.6. Non-Priority-Based Virtualised Resource Allocation Algorithm.

Herein, a non-priority-based virtualised resource allocation algorithm (NVRAA) that is inspired by the scheme in [136] is employed to benchmark the proposed algorithm. The NVRAA algorithm is the traditional scheme that is a non-priority based but provides virtualised services in the network. This has been deployed in the previous generations of wireless networks most especially in the LTE-A [47], [68], [122]. The traditional scheme services were modified to the various slices earlier used in this work. With the same performance metrics, the scheme was used to compare with the proposed scheme.

In this virtualised resource allocation algorithm, the InP dynamically allocates the network resources to the associated users of it serving MVNOs using the SLAs established with these MVNOs and the fairness among their users. The users fairness is derived as a function of the SINR between cell-edge users and cell-centre users.

The problem in (3.13), and its constraints is a MINLP problem. It is a modification of the formulated problem in (3.8) so as to have other constraints such as the fairness requirement as shown below.

$$max \sum_{m\in M}\sum_{s\in S}\sum_{u\in U}\sum_{c\in C}[\mathbb{Q}^{c}_{u^{s,m}}] \tag{3.13}$$

s.t

$$\sum_{m\in M}\sum_{s\in S}\sum_{u\in U}\sum_{c\in C} p^{t,c}_{u^{s,m}} \leq P^{\mathrm{T}}, \qquad \forall t \tag{3.14}$$

$$p^{tc}_{u^{s,m}} \geq 0, \qquad \forall m,s,u,t,c \tag{3.15}$$

$$\sum_{m\in M}\sum_{s\in S}\sum_{u\in \boldsymbol{U}} \delta^{t,c}_{u^{s,m}} = 1, \qquad \forall t.c \tag{3.16}$$

$$N^{m}_{PRB} = \sum_{u,t,c} \delta^{t,c}_{u^{s,m}} \geq R^{min}_{s^{m}} TC, \qquad \forall m \tag{3.17}$$

$$(1-\alpha)\frac{\mathcal{R}^{c}_{1^{s,m}}}{\gamma^{c}_{1^{s,m}}} \leq \frac{\mathcal{R}^{c}_{u^{s,m}}}{\gamma^{c}_{u^{s,m}}} \leq (1+\alpha)\frac{\mathcal{R}^{c}_{1^{s,m}}}{\gamma^{c}_{1^{s,m}}} \quad \forall m,s,u \tag{3.18}$$

Equations (3.14) and (3.15) are the total network power constraint and user power constraint, respectively. (3.16) is the orthogonality constraint which ensures that a sub-channel is not allocated to more than one user. (3.17) is the service-contract constraint that ensures the minimum required data rate is allocated. (3.18) is the fairness constraint that ensures reasonable signal ratios and sufficient transmit power [136] among the cell-edge users and the cell-centre users in the network.

A total of *TC* PRBs is available for scheduling and it is updated after a time *t*, of scheduling round of *T* duration. The algorithm uses the same system model and parameters as the proposed scheme. Other variables to be defined are; $N_{PRB}^{m}$ which is a minimum number of PRBs assigned to each MVNO to guarantee the minimum SLA for its users, $R_{s^m}^{min}$ is the agreed resource quota of MVNO $m$, such that $N_{PRB}^{m} \geq R_{s^m}^{min}$. $\gamma_{\mathrm{u}^{\mathrm{s,m}}}^{\mathrm{c}}$ is a set of predetermined values that ensure fairness among users of each slice and in each MVNO, and α the relaxation factor of the fairness constraint [136].
The scheme is proposed on this fairness rule as an MINLP optimisation problem with the objective to maximize the QoE of the users as in Eq. (3.15) and subject to constraints in (3.14) to (3.18).

Algorithm 3 shown in Table 3.4 solves the non-priority-based virtualised resource allocation problem. Similarly, this algorithm considers the slices, MVNOs, the bandwidth, the carrier frequency, the sub-channels, the antenna height, the transmit power, the gains, the PLs, and the various users' positions in their different slices. It takes into consideration the SLA with the different MVNOs and also considers the fairness among users of each MVNO as shown in Table 3.5.

*Table 3.4: Non-Priority-based virtualised resource allocation algorithm*

**Algorithm 3** Non-priority-based virtualised resource allocation algorithm **[136]**.

**Initialisation**:

1. **Set** $\mathcal{R}^{c}_{u s,m} = 0$, $\delta^{t,c}_{u^{s,m}} = \phi$ for $m = 1,2,\dots,M$, $s = 1,2,\dots,S$, $u = 1,2,\dots,U^{s,m}$, and $\{A = \{(1,1),(1,2),\dots,(t,c),\dots,(T,C)\}$
2. **for** $m = 1$ to $M$, $u = 1$ to $U^{s,m}$
3. **find** $(i,j)$ satisfying $\left|H^{ij}_{u^{s,m}}\right| \geq \left|H^{tc}_{u^{s,m}}\right|$, $\forall (t,c) \in A$
4. let $\Omega^{c}_{u s,m} = \Omega^{c}_{u s,m} \cup \{(i,j)\}$, $A = A - \{(i,j)\}$, **update** $\mathcal{R}^{c}_{u s,m}$ according to (3.5), and **update** $N^{m}_{PRB}$
5. **while** $A \neq \emptyset$,
6. find $m$ satisfying $N^{m}_{PRB}/R^{min}_{s^m} \leq N^{n}_{PRB}/R^{min}_{s^n}$, $\forall n, 1 \leq n \leq M$
7. **for** the found $m$, **find** $u$ satisfying $\mathcal{R}^{c}_{u s,m}/\gamma^{c}_{u s,m} \leq \mathcal{R}^{c}_{r^{s,m}}/\gamma^{c}_{r^{s,m}}, \forall r, 1 \leq r \leq U^{s,m}$
8. **for** the found $m$ and $u$, **find** $(i,j)$ satisfying $\left|H^{ij}_{u^{s,m}}\right| \geq \left|H^{tc}_{u^{s,m}}\right|$, $\forall (t,c) \in A$
9. **for** the found $m, u$, $i$ and $j$, let $\Omega^{c}_{u s,m} = \Omega^{c}_{u s,m} \cup \{(i,j)\}$, $A = A - \{(i,j)\}$, **update** $\mathcal{R}^{c}_{u s,m}$ according to (3.4), and **update** $N^{m}_{PRB}$.
10. **solve** max $\mathfrak{C}_{u^{s,m}}$ as in (3.13) to (3.18) and **find** the optimal solution.
11. **end for**
12. **end for**
13. **end for**
14. **end while**
15. **end for**

The algorithm above allocates the physical resource blocks to the different slices efficiently. It heuristically allows each slice to select a PRB having a high SNR and allocate it to one of its users considering the power constraints, the service-contract constraint and the fairness constraint in each slice.

With the initialisation of the algorithm, the initial data rate of all the users is set at zero (0), the sets of allocated PRBs are made an empty set (∅). The MVNOs $m$, slices $s$, users $u$, and set of (sub-channels and time frame) {(t,c)} are INITIALISED. In line 2, the channel state condition (time frame and sub-channel) satisfying the perfect channel gain $H^{t,c}_{u^{s,m}}$ needed for all users belonging to all MVNOs is found. $\Omega^{u^{s,m}}$ is the set of PRBs {(t,c)} assigned to the user $u^{s,m}$ such that $\delta^{t,c}_{u^{s,m}} = 1$. Allocated PRBs are removed from the set and the user data rates $\mathcal{R}^{c}_{u s,m}$ are UPDATED according to Eq. (3.5). Also, the minimum number of PRBs $N^{m}_{PRB}$ assigned for MVNO $m$ is UPDATED.

While available sub-channels and time slots are not empty, the algorithm finds the *m, u, i* and *j* that satisfy that allocated PRBs, channel gain and data rate are equal or greater than the minimum requirements. Also, the proportional fairness $\gamma^{c}_{u_{s,m}}$ ensure fairness among the users in each MVNO. Finally, with the found *m, u, i* and *j,* the allocated PRBs are once again removed from the set, the user data rates $\mathcal{R}^{c}_{u_{s,m}}$ are UPDATED according to Eq. (3.5). Also, the minimum number of PRBs $N^{m}_{PRB}$ assigned for MVNO $m$ is UPDATED. With these, the optimal solution is found by solving for max $\mathfrak{Q}_{u_{s,m}}$ as in (3.15) to (3.18).

*Table 3.5: System parameters for evaluated scenario*

| Parameter | Value |
|---|---|
| MVNOs/SPs | 2 each with 5 subscribers |
| SLA Vector | [0.6 0.4] |
| Fairness Ratios $\forall m$ (MVNOs) | [10 10 1 1 1] |

## 3.7. Result and Discussions

In this section, the performance of the proposed PRAAC is evaluated and the result is compared with respect to a non-priority based algorithm that does not put into consideration the chance of users having different slice priority. The simulation parameters used for the experiments, the performance metrics and the performance evaluation are discussed in the following sub-sections.

### 3.7.1. Simulation Parameters and Values

The performance of the proposed scheme was evaluated using a 5G network with a gNodeB as the InP having 2 MVNOs (i.e. $MVNO_1$ and $MVNO_2$) with 3 independent slices (denoted as $S_1$, $S_2$, and $S_3$) is considered. Each slice in the 5G network has a number of uniformly distributed users in a 500m by 500m coverage area of  of the gNodeB as shown in Fig. 3.4.

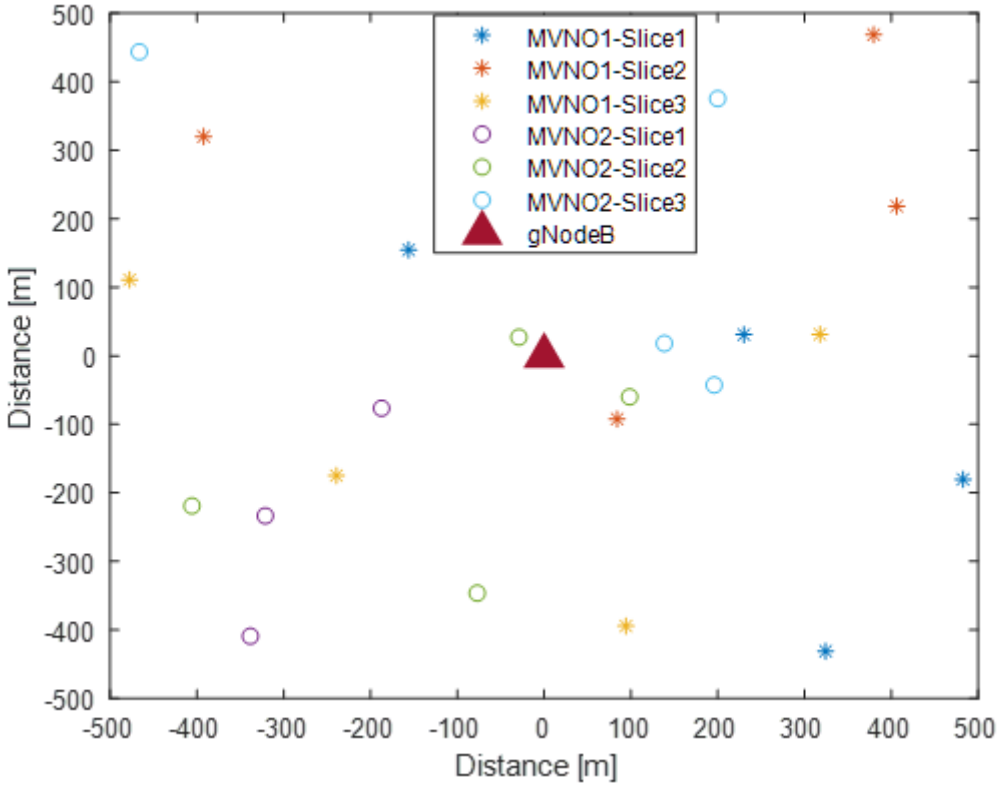


*Figure 3.4: Random users belonging to different slices and MVNOs within the coverage area.*

The simulation parameters used for the experiments are shown in Table 3.6. The algorithm allocates PRBs to maximize the overall QoE of users taking into consideration the UEs priorities as well as the minimum and maximum data rate of users, as the QoS constraints.

*Table 3.6: Simulation parameters and values*

| **Parameter** | **Value** |
|---|---|
| Number of Users/Slice | Varies (between 3 - 10) |
| Number of Slices | 3 |
| Number of MVNOs | 2 |
| Number of gNodeB | 1 |
| Spectrum allocation | 80 MHz |
| Carrier frequency | 6 GHz |
| Number of subcarriers per RB | 12 |
| Size of subcarrier | 30KHz |
| RB bandwidth | 12*30kHz = 360 kHz |
| Number of available RBs | 250 |
| Max gNodeB Tx power | 20 W [43dBm] |
| Slot duration | 0.5ms |
| Scheduling frame | 10ms |
| Overall interval | 20s |
| Cell-level user distribution | Uniform |
| Antenna height | 50m |
| Noise spectral density | -174 dBm/Hz |
| Log-normal shadow fading | 8 dB standard deviation |
| Cell coverage radius | 500m |

### 3.7.2. Priority Criteria

As explained earlier, prioritisation in 5G slice networks can be divided into inter-slice and intra-slice prioritisation. The inter-slice priority is the priority set among slices in the network while intra-slice priority is the priorities among users belonging to the same slice. Priorities are set fairly by the SP based on a pre-agreed contract so as to give preferences to certain slices or some users requesting access and resources.

Inter-slice priorities are set according to on-demand QoS requirements of the requesting slices such as latency, mobility, data volume, connection density, etc.

All these requirements are considered to ensure that priorities are fairly set. Similarly, the users' priorities are set according to payment plans/subscriptions established by the SP and the users. For example, users in the eMBB slices might have different subscriptions differentiated by prices. Users with a higher subscription price such as WhatsApp video calling will have a higher priority than users having WhatsApp chatting.

The slices used in this work is based on these broad use cases of (i) eMBB, as slice 1, (ii) mMTC, as slice 2, and (iii) uRLLC as slice 3. The major distinction between these use cases translate to a set of diverse requirements. In this scenario, the data rate is used [6] in performance evaluation. Setting the slice priority can be done randomly just like that of the users but for this work, the slice priorities are set as shown in Table 3.7.

*Table 3.7: Slice simulation parameters*

| **Parameter** | **Priority** | $R_s^{min}$ | $R_s^{max}$ |
|---|---|---|---|
| Slice 1 -eMBB | 0.3 | 1.0 Mbps | 2.0 Mbps |
| Slice 2 -mMTC | 0.2 | 0.6 Mbps | 1.0 Mbps |
| Slice 3 -uRLLC | 0.5 | 0.5 Mbps | 0.8 Mbps |

The inter-slice priority closer to zero is the lowest, while the one closer to one is the highest. i.e., slice 3 priority is the highest, followed by slice 1 and then slice 2. The justification for this is based on the reliability, latency, and the throughput required of these slices.

## 3.7.3. Performance Evaluation

In this sub-section, the performance of the proposed algorithm was compared with a previously proposed scheme [136] designed for virtualised LTE-A networks in the literature. The following subsections show and explain the results of the performance metrics employed in this work. The number, the throughput and the QoE of accepted UEs are considered and evaluated.

A. *Number of accepted UEs*

Figure 3.5 shows the evolution of the average QoE of UEs with a different number of users for both our proposed PRAAC scheme (using P-Slice 1, P-Slice 2,

and P-Slice 3) and the benchmark non-priority scheme (similarly, using NP-Slice 1, NP-Slice 2, and NP-Slice 3). It is observed that the average QoE of accepted UEs decreases with the increase in the number of users per slice. Compared to the proposed scheme, the non-priority scheme shows a steep degradation in the QoE of UEs as the average data rate increases in the network. The proposed PRAAC algorithm, as a result of the intra-slice and inter-slice priorities, can accommodate a reasonable decrease in the UEs' QoE. Also, the number of admitted UEs is higher in the proposed PRAAC scheme compared with the benchmarked algorithm.

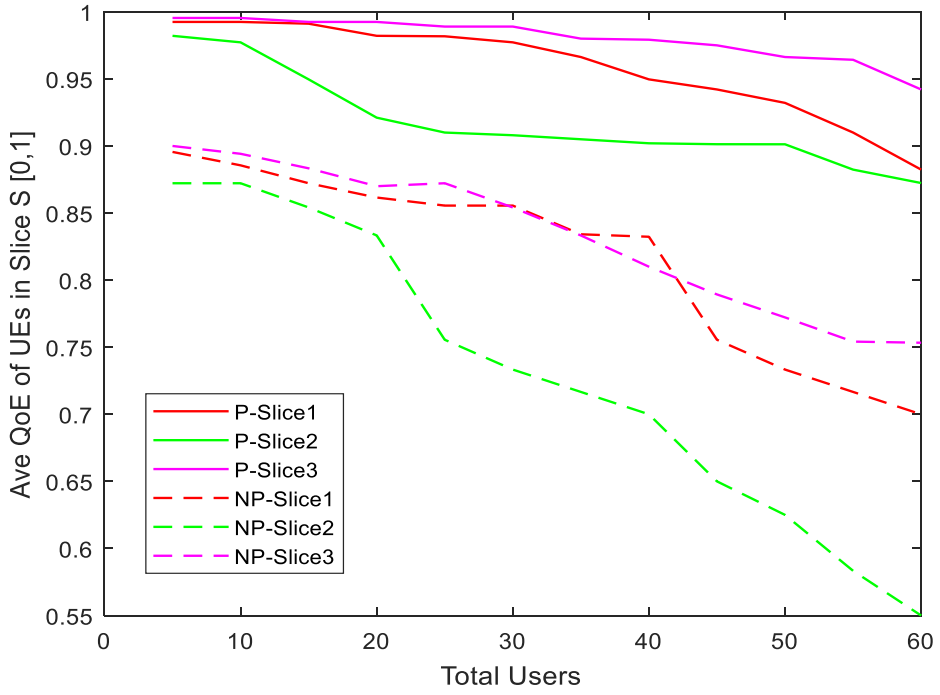


*Figure 3.5: Average QoE of UEs with different numbers of UEs.*

B. *Throughput of accepted UEs*

Figure 3.6 illustrates the average throughput of UEs in each of the slices. This figure demonstrates the effect of the priorities on both the QoS (i.e., throughput) and the derived users' QoE in the proposed algorithm. It depicts that the throughput of each of the users and slices are allocated according to the intra-slice and inter-slice priorities respectively. In the eMBB slice (Slice 1), the users' QoE varies between 0.89 to 1.00, while the users' throughput is between 1.00Mbps and 2.00 Mbps. Similarly, in the mMTC slice (Slice 2), the users' QoE varies between 0.87 to 1.00, while the users' throughput is between 0.60Mbps and 1.00 Mbps. Likewise, in the uRLLC slice (Slice 3), the users' QoE varies between 0.914 to

1.00, while the users' throughput is between 0.50Mbps and 0.80 Mbps. All these allocated QoS (i.e., data rates) are within the range of the slice's minimum data rate $R_s^{min}$, and the slice's maximum data rate $R_s^{max}$.

Slice 3, despite having the least QoS requirement in terms of data rate, but with the highest inter-slice priority, has most of its accepted UEs allocated with throughput closer to its associated slice's maximum data rate $R_s^{max}$ than its slice's minimum data rate $R_s^{min}$. Expectedly, this is followed by the eMBB slice, the QoS and QoE allocated to users of Slice 1 is higher than that of users of Slice 2 as a result of the higher priority of Slice 1.

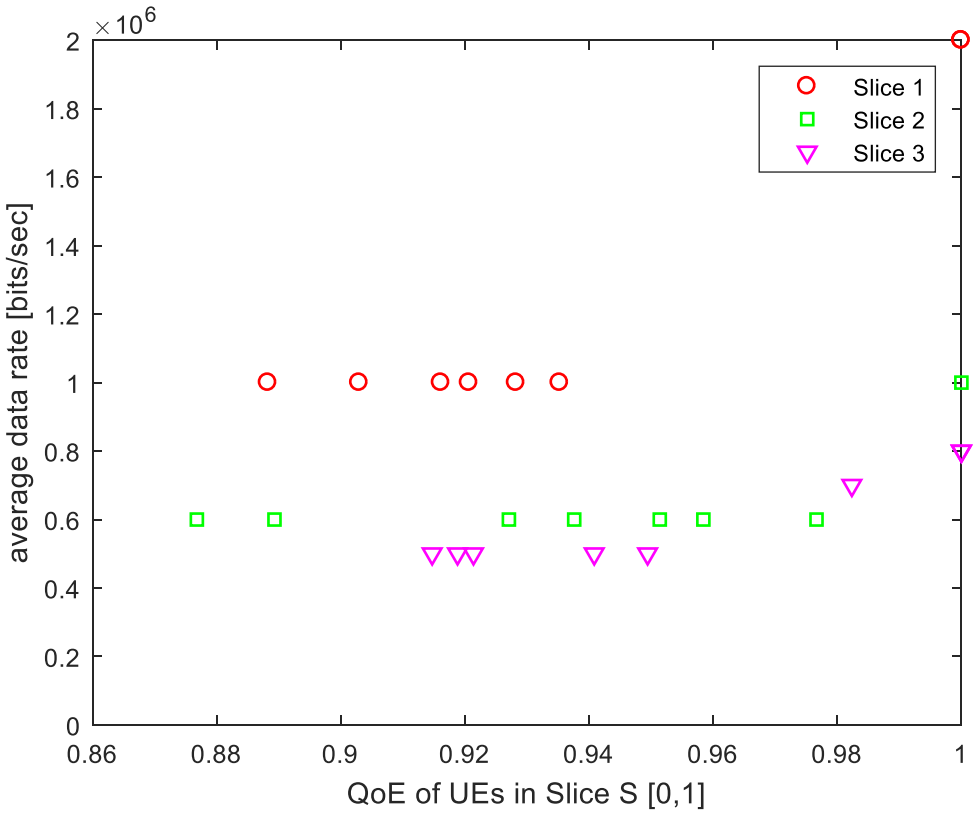


*Figure 3.6: Average throughput of UEs in different slices.*

C. *QoE of accepted UEs*

Here, the variations of the average QoE of users in each slice is studied. As shown in Fig. 3.7, with the plot of average QoE of users in each slice versus the slices in the network. The essence of this result is to compare the users' QoE of the

proposed algorithm with the QoE of users in the benchmarked algorithm. The proposed scheme gives more QoE for all the users in each slice (Slice 1, Slice 2, and Slice 3) than the non-priority scheme as a result of the slice priorities of the UEs. As depicted, Slice 3 with the highest allocated priority has the highest QoE, followed by slice 1, and then slice 2 with second-highest and least priorities respectively. This result shows the effect of enhancement of UE's QoE as stated in the contributions.

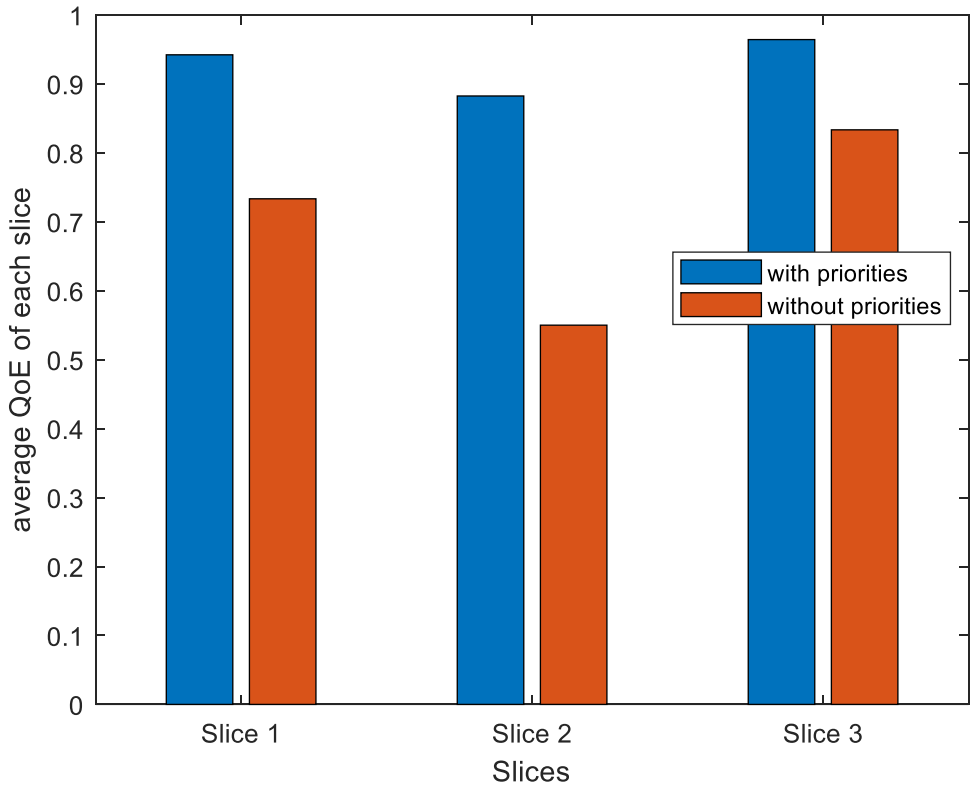


*Figure 3.7: Average QoE of UEs in different slices.*

Figure 3.8 presents the variation in the users' (UEs) QoE, showing the simulation result of 5 UEs per slice for the 3 slices and the 2 MVNOs. The slice (inter-slice) priorities are the same for all the users in a specific slice, however, the user's (intra-slice) priorities are not, as they are randomly allocated based on the service level agreement with the users. This is the main reason for the differences in the allocated QoE of users in a particular slice as shown in Fig. 3.8. It shows that the users' (intra-slice) priorities and the distances from the gNodeB (without downplaying the effect of pathlosses) play a major role in the overall QoE of UEs.

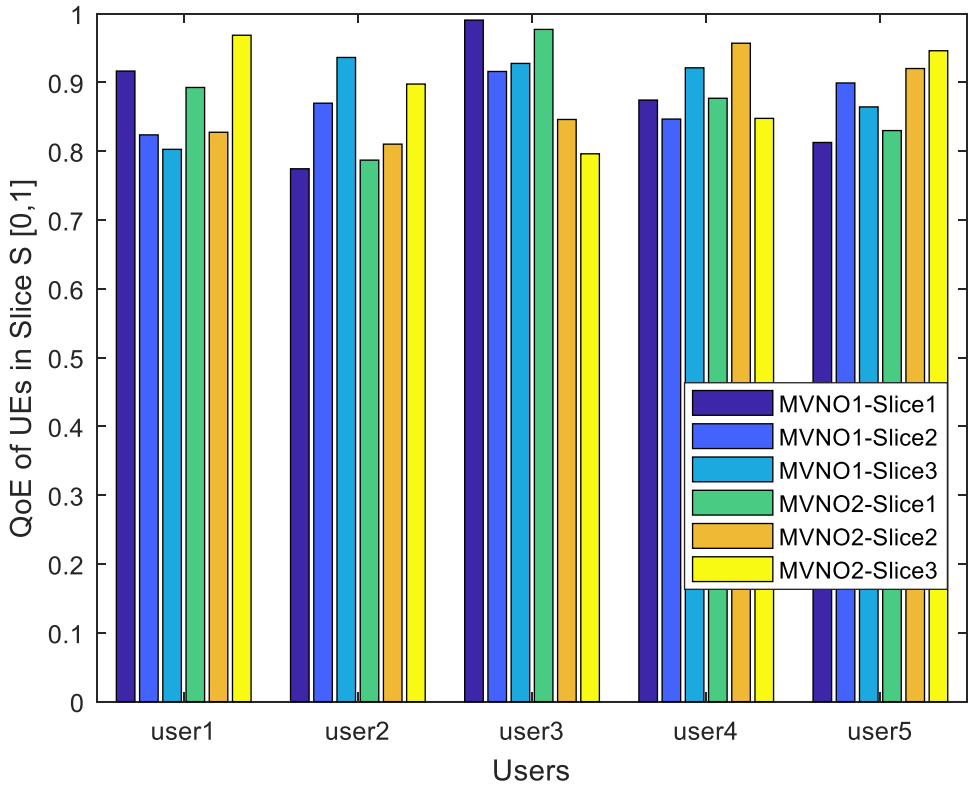


*Figure 3.8: Effect of users' intra-slice priority on QoE of UEs in each slice.*

The proposed resource allocation strategy for network slice in a 5G network using admission control has been considered. The proposed selection algorithm factors in both the inter-slice and the intra-slice priorities using an admission control mechanism. This is done while performing resource allocation to both slices and users in a multitenancy scheme to meet the on-demand requirements. The model was evaluated and compared considering the minimum and maximum QoS requirements, and the priorities of the user and slice it belongs to. Through numerical results, the performance of the proposed scheme in a 5G multitenant sliced network has been demonstrated and benchmarked with a non-priority–based scheme. Hence, the overall QoE of users and also the utilisation of scarce network resources have been enhanced by the proposed scheme.

## 3.8. Chapter Summary

This chapter presented a proposed RA and admission control scheme for 5G slice networks. It introduces the needs and motivations for dynamic resource allocation in a multi-tenancy sliced network as it maximizes network utilisation and system efficiency. It reviewed the related works in the literature regarding resource allocation in 5G networks and stated the contributions of this work. Also, the scheme system model was presented and an optimisation problem that maximizes the QoE of users was formulated subject to other factors.

Also, this chapter presented the scheme's framework and the PRAAC algorithms. These algorithms ensure that users are admitted and allocated resources based on their slice required data rate and that both their intra-slice and inter-slice priorities are considered. With the performance metrics set, the experiments were conducted and the scheme was compared with a Non-Priority-Based virtualised Resource Allocation scheme. The results showed a better performance with respect to the number of admitted users, individual user's throughput and the overall QoE of users.

# Chapter 4

# 4. Dynamic Slicing and Scheduling for 5G Network Using Joint Power and Sub-Channel Allocation.

## 4.1. Introduction

In wireless communication networks there is a need to meet the increasing demand of users' data rate and traffic. One of the most important challenges in meeting this demand in the 5G slice networks is how to flexibly, efficiently and dynamically assign both radio and core network resources to an isolated virtualised network. In solving this challenge, there is another challenge of interference being created [137], [138]. Interference is a great threat to communication in wireless networks, it limits the transmission quality [139], and this makes the interference intolerable. Interference is majorly caused by both spectrum resources sharing and the high transmit power of users as a result of their demanding QoS requirements for the slices/services they subscribed to. As a result, it is very important to regulate the transmit power in the channels to minimise the co-channel interference, taking into account the target data rate to increase the system performance and avoid intolerable interference.

Since 5G network will provide services based on virtualised slices tailored according to the use cases, and the QoS requirement of the use cases varies. This means that the transmit powers of the users in the network can be controlled according to the QoS requirements such as the data rates and latencies. Therefore, there is need for a 5G network slicing and scheduling scheme which centrally, intelligently, and dynamically; controls power and allocates network resources to users based on their QoS requirement of the slice they belong to.

Based on the QoS requirement of the use cases, it is expected that the various slices will require different transmit power. As illustrated in Fig. 4.1, an eMBB slice is envisaged to require the highest data rate compared to other slices, hence, demands the most power. A URLLC slice will require more data rate than the mMTC slice, hence a URLLC slice 2 requires more power than mMTC slice. Using other 3GPP use case requirements such as latency and connection rate, these requirements are categorised alongside the power required in gaining access, connection, and request resources from the 5G gNodeB. For instance, a slice that has a high data rate, a high connection rate and a high latency is expected to use more power and therefore, causes higher co-user interference among the users of the channel.

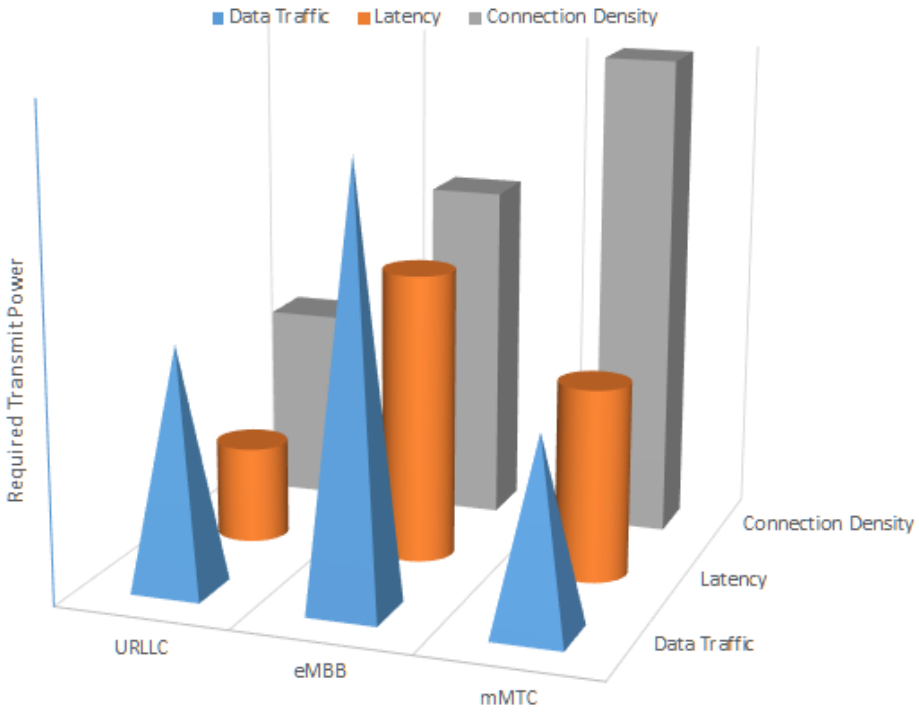


*Figure 4.1: 5G slice use case's QoS requirement analogy with transmit power.*

To meet the adaptive resource allocation problem and reduce the interference challenge, this chapter addresses these issues by proposing a dynamic slicing and scheduling scheme for virtualised 5G sliced network. In this scheme, an efficient joint power and subcarrier allocation algorithm is proposed. This algorithm assigns sub-channels to slice users based on their transmit power and subject to the QoS constraints and CSI of the sub-channel. Using orthogonality of the sub-channels, PRBs are allocated to users based on the slice they belong to. For example, if a UE $U_{11}$ that belongs to a slice that uses more power is allocated a sub-

channel, UE $U_{12}$ belonging to the same slice (and with equal or more power usage) with $U_{11}$ will not be allocated the neighbouring sub-channel or PRB. Rather, UE from another slice with less power consumption will be assigned the successive sub-channel.

The orthogonality constraint reduces interference, hence increases the SINR of the channel, increases the throughput and increases the overall network efficiency. This proposed dynamic scheme is made possible using a slice scheduler.

The main contributions of this chapter are summarised as follows:

- A Resource allocation optimisation problem is formulated in a 5G sliced network to minimise the total co-users' interference by minimising the downlink transmit power subject to QoS constraints, interference limit and the CSI.
- The idea of orthogonality in sub-channel is incorporated, and it is applied to the sliced network in allocating PRBs to slice users in order to minimise the co-user interference in the 5G network. This is based on the different QoS requirements of these slices.
- An algorithm that uses a centralised scheduler which dynamically and intelligently assigns sub-channels to slice users based on their required transmit power is proposed.
- Through simulation analysis, the performance of the proposed algorithm is evaluated. Moreover, the algorithm is benchmarked with a heuristic power control scheme with non-orthogonality constraint and equal transmit power for all sub-carriers.

The remainder of this chapter is organized as follows. Section 4.2 discusses the proposed system model and assumptions. The problem formulation is defined in Section 4.3. The proposed scheduling mechanism and the performance evaluation are presented in Sections 4.4 and 4.5, respectively. Finally, Section 4.6 concludes the chapter.

## 4.2. Notations

In this subsection, the relevant notations used in the entire chapter are described. Table 4.1 highlights the list of notations.

*Table 4.1: List of notations*

| Symbol | Description |
|---|---|
| $m$, $M$ | MVNO, MVNO set |
| $s$, $S$ | Slice, Slice set |
| $S_m$ | Slice $s$ in MVNO $m$ |
| $u$, $U$ | User, user set |
| $U_{s,m}$ | User $u$ in slice $s$ and MVNO $m$ |
| $g$ | gNodeB |
| $c$, $C$ | Sub-channels, set of sub-channels |
| $b^c$ | Bandwidth of the generic sub-channel $c$ |
| $B$ | Total Bandwidth of the InP |
| $P_T$ | Total transmit power of the gNodeB |
| $p_{u,s,m}^c$ | Allocated power of user $u$ of slice $s$ in the sub-channel $c$ |
| $P_s^{max}$ | Slice maximum transmit power threshold |
| $P_s^{min}$ | Slice minimum transmit power threshold |
| $\rho_{u,s,m}$ | Power metric |
| $R_s^{min}$ | Slice minimum data rate |
| $q_{u,s,m}$ | QoS metric |
| $\mathrm{I}_{\mathrm{s}}^{\mathrm{c,max}}$ | Maximum tolerable interference limit |
| $I_s^{c*}$ | Interference experienced in the sub-channel |
| $d_{g,u}$ | Distance between the user and the gNodeB |
| $\mathrm{l}_{\mathrm{g,u}}$ | Pathloss between the gNB and the user |
| $f_c$ | Carrier frequency in GHz |
| $N_0$ | Noise power per unit bandwidth |
| $x_{u,s,m}^c$ | Assignment binary variable of $u$ in the sub-channel |
| $CQI_{threshold}$ | CQI that guarantees the required throughput |
| $CQI_{u,s,m}$ | CQI of user u in slice s and MVNO m |
| $\mathrm{h}_{\mathrm{u,s,m}}^{\mathrm{c}}$ | Channel gain of user $u$ in slice $s$ and MVNO $m$ from the gNodeB |
| $\gamma_{\mathrm{u,s,m}}^{\mathrm{c}}$ | SINR of user $u$ in slice $s$ and MVNO $m$ |
| $\mathrm{R}_{\mathrm{u,s,m}}^{\mathrm{c}}$ | Data rate of user $u$ in slice $s$ and MVNO $m$ |
| $\mathrm{R}_{\mathrm{tot}}$ | Total network achievable data rate |
| $\acute{\Gamma}$ | constant SINR gap |

## 4.3. System Model and Assumptions

The system model considered is illustrated in Fig. 4.2. It shows the downlink of a single cell scenario of a 5G sliced networks. The 5G base station also known as gNodeB, is owned and managed by a single InP. There are several MVNOs sharing the physical network and the wireless spectrum. Each MVNO provides service to its set of UEs. In considering isolation, each MVNO is allocated a certain minimum share of the sub-channels which is required to efficiently serve their users and it is also based on the contract with the InP. The minimum allocated share changes accordingly with the change in the target rate and CSI.

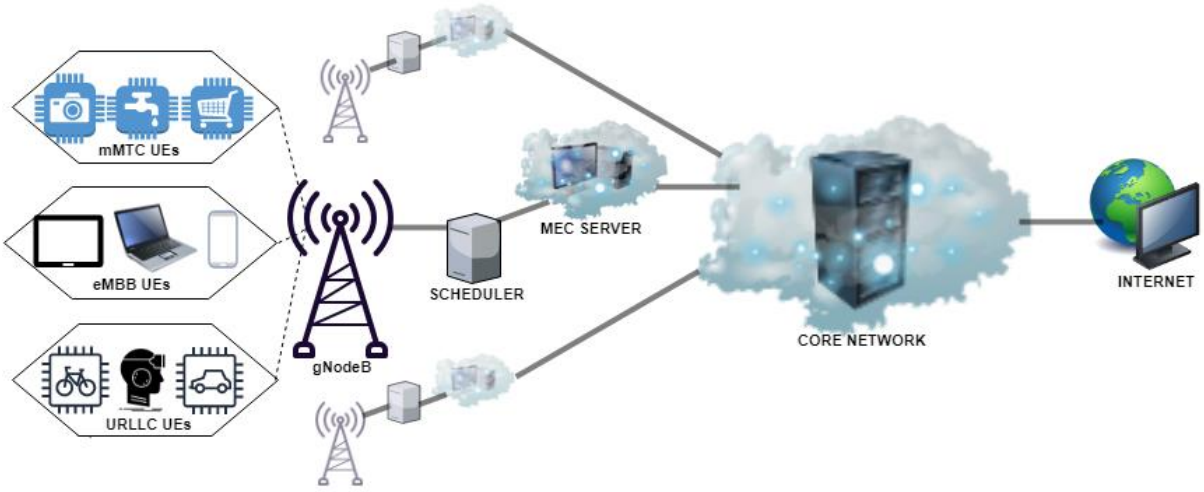


*Figure 4.2: System model with single gNB showing End-to-End slicing.*

The network services are virtualised into a specific set of slices, $S = \{1,2,\ldots,s\}$. The network also has a set of MVNOs denoted by $M = \{1,2,\ldots,m\}$. Each MVNO $m$ serves a set of users, $U = \{1,2,\ldots,u\}$ that are assigned to a particular slice $S_m$. ($S_m \in S$). The assigned $S_m$ from the virtual network resources is based on demand and provide services for the subscribers. In this chapter, the three slices considered are eMBB, mMTC, and URLLC, respectively. Also, there are $c \in C$ sub-channels in the frequency domain where the system bandwidth $B$ is divided into bandwidth $b_c = B/C$ of size 180 kHz each [140]. The $T$ sub-frames in the time domain refers to as TTI of 1ms which ten of which makes up the frame structure of the downlink air interface [141]. This total of $T*C$ PRBs is available for the network Scheduler in each duration of $T$. The minimum amount of the available PRBs of the 5G network

assigned to the MVNOs is based on the SLA with the InP and this will be updated after each duration of the scheduling round.

The gNB has a total transmit power of $P_T$ and let $p^c_{u,s,m}$ denotes the power allocated to user $u$ in the sub-channel $c$ belonging to slice $s$.

$$\sum_{m=1}^{M}\sum_{s=1}^{S}\sum_{u=1}^{U}\sum_{c=1}^{C} p^c_{u,s,m} \leq P_T \tag{4.1}$$

The channel gains depend on the distance $d_{g,u}$ (in m) between gNB and the user $u$ and it is expressed as

$$h^c_{u,s,m} = 10^{-\frac{l_{g,u(dB)}}{10}} \tag{4.2}$$

The pathloss [142] between the gNB and the users is modeled as

$$l_{g,u} = 36.8 log_{10}(d_{g,u}) + 43.8 + 20\, log_{10}(f_c/5) \qquad [dBm] \tag{4.3}$$

where $f_c$ is given in GHz and $d_{g,u}$ is the distance between gNodeB and the user $u$. in metres (m)

In the system model, slices are differentiated with the QoS demand (the required minimum data rate ($R_s^{min}$)) of the use cases, whereas users are differentiated based on the service contract they subscribed with their MVNOs. The SINR of the user $u$ occupying the $c^{th} \in \{1,2,\ldots,C\}$ sub-channel of the cell in slice $s^{th} \in \{1,2,\ldots,S\}$ can be expressed as:

$$\gamma^c_{u,s,m} = \frac{p^c_{u,s,m}\left|h^c_{u,s,m}\right|^2}{N_0 + \sum_{j=1,j\neq s}^{S}\left(p^c_{u,s,m}\left|h^c_{u,j,m}\right|^2\right)} \quad \forall j \in S \tag{4.4}$$

where $N_0$ is the spectral noise density, i.e., noise power per unit bandwidth. The summation in denominator is the sum of interference affecting the user. While, the numerator is the received signal of the user. To protect the user u from this interference, a maximum tolerable interference limit is set as $I_s^{c,max}$.

## 4.4. Problem Formulation

Based on Shannon's capacity, the achievable instantaneous data rate (i.e., the capacity) on the $c \in C$ sub-channel of the user u, in slice $s \in S$ can be given as:

$$R_{u,s,m}^{c} = b_c \, log_2\left(1 + \frac{\gamma_{u,s,m}^{c}}{\acute{\Gamma}}\right) \tag{4.5}$$

where $\acute{\Gamma}$ is denoted as the constant SINR gap as it is expressed as $\acute{\Gamma} = -\ln(5BER)/1.5$ [143] and $b_c$is the bandwidth of the sub-channel.

Also, $x_{u,s,m}^{c}$ is the binary assignment variable that indicates the allocation of the sub-channel to the user $u$ in slice $s$ during scheduling round $T$. Therefore,

$$x_{u,s,m}^{c} \in \{0,1\}, \qquad \forall c \in C, \forall u \in U, \forall s \in S, \forall m \in M \tag{4.6}$$

Also, a PRB must be allocated to exactly one user belonging to one slice, i.e., $\sum_{u,s,m} x_{u,s,m}^{c} = 1$. And each slice is assigned a minimum number of PRBs according to the agreed SLA in order to provide services for its users such that $R_s^{min} \leq R_{u,s,m}^{c}$.
The user transmit power $P_{u,s,m}^{c}$ should not be more than the maximum transmit power threshold, $P_s^{max}$ of its slice. i.e., $P_s^{max} \geq P_{u,s,m}^{c}$, $\forall s \in S$. Therefore, the power metric is set as $\rho_{u,s,m} = \left(\frac{P_{u,s,m}^{c}}{P_s^{max}}\right) \leq 1$.
The assigned data rate of a user is given as:

$$R_{u,s,m}^{c} = b_c \, log_2\left(1 + \frac{\gamma_{u,s,m}^{c}}{\acute{\Gamma}}\right) x_{u,s,m}^{c} \tag{4.7}$$

Hence, the total achievable instantaneous data rate of the network is:

$$R_{tot} = \sum_{m=1}^{M} \sum_{s=1}^{S} \sum_{u=1}^{U} \sum_{c=1}^{C} R_{u,s,m}^{c} \tag{4.8}$$

To establish this result and assume that the optimal solution is $P_{u,s}^{c}$. Hence, a given power allocation ($p_{u,s}^{c}$) can be expressed as follows [58]:

$$P_{u,s,m}^{c} = \left(\frac{b_c}{ln\, 2} - \frac{I_s^{c*} + N_0}{\left|h_{u,s,m}^{c}\right|}\right) \tag{4.9}$$

where $I_s^{c*}$ is the interference experienced in the sub-channel and it is expressed by:

$$I_s^{c*} = \sum_{j=1, j\neq s}^{S} (p_{u,j,m}^{c} \left| h_{u,j,m}^{c} \right|^2) \tag{4.10}$$

The objective of the joint power and sub-carrier allocation optimisation problem is to minimise the total downlink transmit power subject to UEs' QoS requirements, slice UE's interference limits and sub-channels orthogonality constraints. The optimisation problem is formulated and derived in (4.11), where the objective function is to minimise the total downlink transmit power and hence the interference of the users in the cell.

$$\min_{P_{u,s,m}^{c}} \sum_{m=1}^{M} \sum_{s=1}^{S} \sum_{u=1}^{U} \sum_{c=1}^{C} x_{u,s,m}^{c} \left| P_{u,s,m}^{c} \right|^2 \tag{4.11}$$

Subject to

$$\text{C1}: \sum_{c=1}^{C} \mathrm{b_c} \log_2 \left(1 + \frac{\gamma_{\mathrm{u,s,m}}^{\mathrm{c}}}{\acute{\Gamma}}\right) \geq R_{u,s,m}^{c} \qquad \forall u \in U$$

$$\text{C2}: x_{u,s,m}^{c} \left| P_{u,s,m}^{c} \right| \leq P_s^{max} \qquad \forall s \in S, \forall u \in U, \forall c \in C$$

$$\text{C3}: \sum_{c=1}^{C} x_{u,s,m}^{c} \leq q_{u,s,m} \rho_{u,s,m} \qquad \forall u \in U, \forall s \in S$$

$$\text{C4}: \sum_{u=1}^{U} \sum_{c=1}^{C} \left| P_{u,s,m}^{c} \right| \leq P_s^{max} \qquad \forall s \in S$$

$$\text{C5}: x_{u,j,m}^{c} \sum_{u=1}^{U} \left| \sum_{j=1, j\neq s} P_j^{c} \left| h_{u,j}^{c} \right| \right|^2 \leq I_s^{c,max} \qquad \forall \mathrm{c} \in C$$

$$\text{C6}: x_{u,s,m}^{c} \in \{0,1\}, \qquad \forall s \in S, \forall u \in U, \forall \mathrm{c} \in C$$

Constraint C1 ensures that the data rate for each slice user meets or exceeds the threshold. Constraint C2 ensures that sub-channels that are not assigned are not transmitting power. C3 ensures that the sub-channels are allocated to users based on the QoS requirement $q_{u,s,m}$ of their slice, where $q_{u,s,m}$ =

($\left|R^{c}_{u,s,m}\right|/R^{min}_{s}$). This prevents the scheduler from allocating neighbouring sub-channels to a user of the same slice. Constraint C4 ensures that the total power budget to the slice is less than the maximum power threshold. C5 guarantees that the interference threshold, $I^{c}_{j}$ is not exceeded. It places a limit on the total interference created by users on sub-channel *c*, it is only active if the same slice users are allocated neighbouring sub-channels. Lastly, constraint C6 ensures that a user is assigned a resource when the binary assignment variable is 1 or otherwise.

The problem (4.11) is formulated as an MINLP that solves the resource allocation problem by optimising the transmit power and as such limits interference among slice users.

## 4.5. Joint-Power and Sub-Channel Allocation Scheme

### 4.5.1. Slicing and Scheduling Scheme

In the proposed scheme, the frequency diversity offered by the multipath channel is exploited. Since a deep fade might hit a substantial number of subcarriers of a given slice. More importantly, the scheme uses a more flexible allocation strategy where a given slice can select the best subcarriers, which is one with the highest SINRs. This work considers a novel SCAS where the neighbouring sub-channels are not allocated to users of the same slice that the transmit power required to achieve the target rate is high enough to cause inter-user interference. However, there is no rigid association between the sub-channels and the users. As shown in Fig. 4.3, a neighbouring sub-channels are allocated to slice 1 (i.e., mMTC) because the users in the slice only need low transmit power based on their required data rate. Since the sub-carriers are at a lower data rate and therefore have longer symbol duration which is more robust against Inter-Symbol Interference (ISI). Therefore, the proposed SCAS allows dynamic resource allocation and provides more flexibility by considering alternating sub-channel allocation for the user $U_s$ on sub-channel $C_i$. i.e.. each sub-channel is allocated strictly to one user. Mathematically, constraint C3 in (4.11) assigns the neighbouring sub-channel $C_j$ to a different slice *s* if the power threshold is exceeded in according to C4 in (4.11).

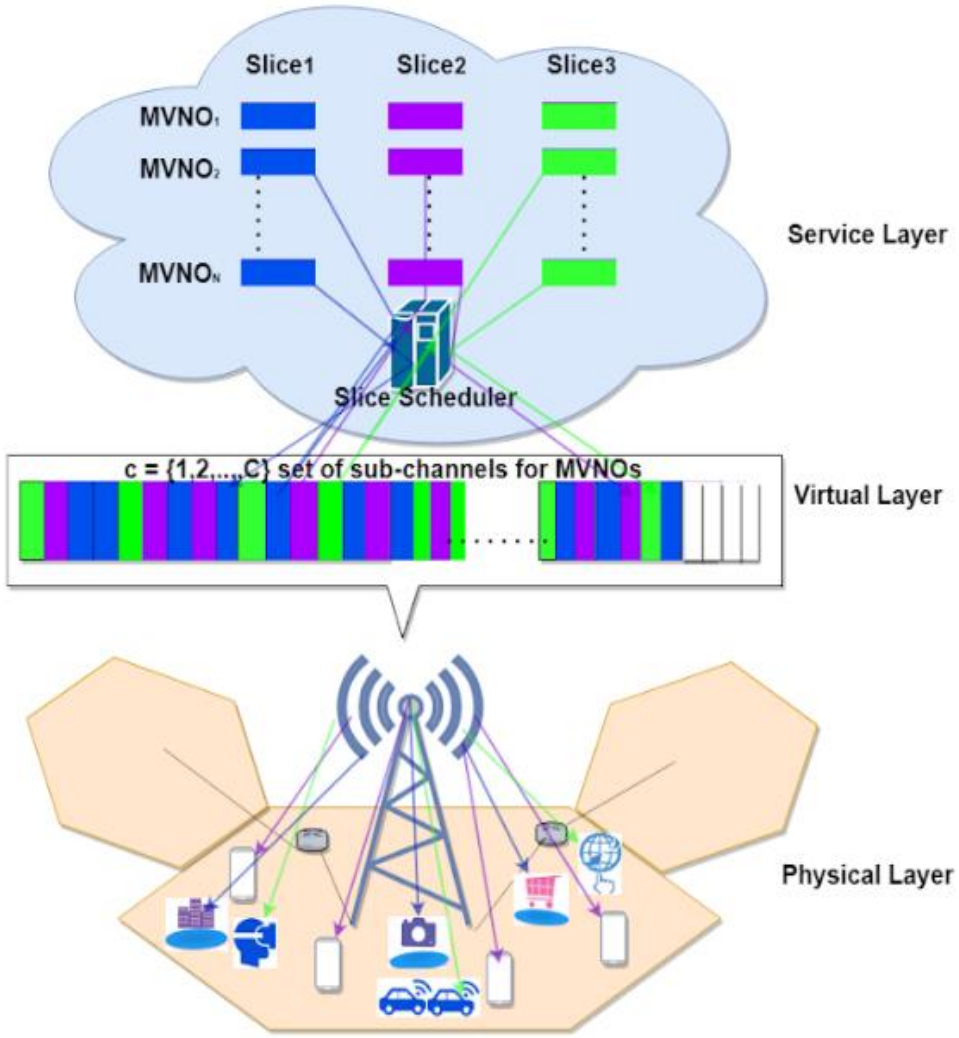


*Figure 4.3: NS and scheduling scheme with multiple MVNOs*

This also shows that the AP communicates with a user using the sub-channel with the least transmit power possible. Finally, the scheduler and in some cases called the controller (SDN controller), located at the MAC layer of the AP, gNB is to decide on how to assign the PRBs among users considering the QoS requirements and the channel conditions by solving for Algorithm 2 in Table 4.3 to determine the feasible power solution so as to allocate sub-channel(s) according to Algorithm 1 in Table 4.2. The assignment of these sub-channels is updated at each scheduling period.

## 4.5.2. Resource Allocation Algorithm

This subsection illustrates the sub-channel allocation algorithm and the optimal interference and power allocation algorithm used in solving the power problem in Eq. (4.11).

*Table 4.2: Sub-channel allocation algorithm*

**Algorithm 1** Sub-channel allocation algorithm

1. Given the set $C'$ where the set $C'$={c ∈ $C$: $x_{u,s,m}^{c} = 0,\ \forall s \in S$} as the set of sub-channels not allocated to $U_s$
2. **for** $s = 1{:}S$ **do** $u = 1{:}U$ **do**
3. Initialise $C_s = \emptyset$, as the set of sub-channel allocated to $U_s$, $\beta = C'$. $C'' = \{c{:}\, c \in C - C'\},\ C_s = C' \cup C'' = \emptyset$
4. Sort sub-channel in the set $\beta$ in descending order according to metric $\left|h_{u,s,m}^{c}\right|^2$
5. Sort QoS requirement $q_{u,s,m}$ of $s \in S$ in descending order according to metric $\left|R_{u,s,m}^{c}\right|$, where $q_{u,s,m} = (\left|R_{u,s,m}^{c}\right|/R_{s}^{min})$
6. **if** $q_{u,s,m} \leq |\beta|$ and $\rho_{u,s,m} \leq x_{u,s}^{c}$(i.e. $\rho_{u,s,m} \leq 1$) **then**
7. Allocate the highest $q_{u,s,m}$ sub-channels in the $\beta$ set to $U_s$ (i.e. $C^* = \underset{C \in \beta}{\operatorname{argmax}}\left|h_{u,s,m}^{c}\right|$)
8. **until** The QoS request $q_{u,s,m}$ of $U_{s,m}$ is met.
9. **else**
10. Allocate the next sub-channel in the set $\beta$ to the user of the slice with the next lowest $\rho_{u,s,m}$ and $q_{u,s,m}$ or till all sub-channels in the set $\beta$ are allocated
11. **end if**
12. Update $C_s$, $C_s = C_s + \{C^*\},\ \beta = \beta - \{C^*\}$
13. **end for**
14. **if** All UEs have their QoS requirement $q_{u,s,m}$ satisfied **then**
15. Terminate
16. **else**
17. Given the set $C'$
18. **for** $s = 1{:}S$ **do,** $u = 1{:}U$ **do**
19. Initialise $\beta = C''$
20. Sort sub-channel in the set $\beta$ in descending order according to metric $\left|h_{u,s,m}^{c}\right|^*$
21. Sort QoS requirement $q_{u,s,m}$ of $s \in S$ in descending order according to metric $\left|R_{u,s,m}^{c}\right|^*$
22. Assign sub-channels such that the next sub-channel is allocated to UE with the least transmit power and QoS requirement are satisfied.
23. Update $C_s$
24. **end for**
25. **end if**

*Table 4.3: Optimal interference and power allocation algorithm*

**Algorithm 2** Optimal interference and power allocation algorithm

1. Sort the set of all sub-channel $C = \{1,2, \dots, C\}$ in descending order channel gain $\left|h_{u,s,m}^{c}\right|$ such that $h_{u,s,m}^{1} \geq h_{u,s,m}^{2} \geq \dots h_{u,s,m}^{c}$
2. Initialise $C'$
3. Assume $I_s^{c'*} = I_s^{c,max}$ and find $P_{u,s,m}^{c'}$ using Eq.(4.11)
4. **if** $P_{u,s}^{c'} \leq P_s^{max}$ or $\rho_{u,s,m} \Rightarrow (P_{u,s}^{c'}/P_s^{max}) \leq 1$. **then**
5. Set $I_{u,s,m}^{c} = 0$, and $P_{u,s,m}^{c} = P_s^{max}, \quad \forall c = 2,3, \dots . C$
6. Terminate as the optimal solution is found
7. **else**
8. Increase $C'$
9. Set $P_{u,s,m}^{c} = P_s^{max}, \quad \forall c = 1,2,3, \dots . C - 1$
10. **repeat**
11. **until** A feasible solution is found else increase $C'$
12. **end if**

Algorithm 1 performs the sub-channel allocation process inside the scheduler. It defines $C' = \left\{c \in C: x_{u,s,m}^{c} = 0, \ \forall s \in S\right\}$ as the set of sub-channels that are not assigned to users of a slice $(U_{s',m)}$, for example, slice2 $(U_{2,m})$. The scheduler allocates the sub-channels in the set $C'$ to each user of slice1 $(U_{1,m})$. It sorts the sub-channels in the set $C'$ for each slice1 UE in descending order using the metric $\left|h_{u,s,m}^{c}\right|^2$, i.e., the scheduler allocates the best sub-channels first to each user of slice1 $(U_{1,m})$. If the sub-channels in the set $C'$ are not enough to satisfy the QoS request of the user of slice1 $(U_{1,m})$, the scheduler will allocate the remaining sub-channels in the set $C'' = \{c: c \in C - C'\}$, $(C' \cup C'' = C, \ C' \cap C'' = \emptyset)$ to the slice1 UEs. It will then sort the sub-channels in the set $C''$ in descending order using the metric $\left|h_{u,s,m}^{c}\right|^*$. The goal is to assign sub-channels to UEs of the slice with high QoS requirement with high gains which will cause low interference to the UEs of slices with low QoS requirements. The scheduler distinguishes between sub-channels allocated to all the different slices users.

The overall optimum interference and power allocation process are summarized in Algorithm 2. The set of allocated sub-channels is sorted in descending order using the channel gain metric. The minimisation problem in Eq. 4.11 is solved using the interference, power and QoS constraints, and the optimum power is found and allocated to UEs. The set of sub-channels is updated and iterations are repeated for each user of the different slices.

## 4.6. Downlink Heuristic Power Control Allocation Algorithm

In this section, a downlink heuristic power control allocation algorithm proposed in [144] is discussed and used to benchmark the proposed algorithm. This algorithm is one of the traditional schemes often used in wireless networks [58], [123], [145], [43], it is a distance-based algorithm and it works basically on power control that ensures that the $P_s^{min}$and $P_s^{max}$ are not exceeded.

The heuristic power-control algorithm aims to reduce the co-user's interference in the network by reducing the power wastage especially for Cell Centre Users (CCUs) that typically have good channel conditions and are less affected by pathloss. Also, the algorithm increases the downlink transmit power of the subcarriers assigned to Cell-Edge users (CEUs) that are usually affected by pathloss. To do these; the scheduler requires information in the form of feedback of CQI which are sent by the UEs to the gNodeB. In this case, the SINR measurements over the pilot signals received by the users are used as the CQI feedback to control the downlink transmit powers. The SINR measurements were averaged over time to reflect the true conditions of the users.

The algorithm, through the scheduler at the base station, performs both subcarrier and power allocation at each TTI. The idea is to mitigate the co-users interference by minimising downlink transmit power without degrading the throughput of the users. The transmit power is calculated using pathloss models. The received power is measured by the cell and the algorithm adjusts the transmit power incrementally or decrementally by a value known as the power control step. To provide the required throughput to the users, the algorithm increases the transmit power assigned for PRBs having low SINR values accordingly subject to its power constraints. If the SINR $\gamma_{u,s}^{pilot}$ is below the SINR threshold, the transmit power of the user $u$ in slice $s$ is increased, otherwise, the transmit power is reduced.

If the CQI feedback is lesser than $CQI_{threshold}$, the transmit power is increased as long as it is lesser than the required slice maximum transmit power $P_s^{max}$. However, if the received CQI feedback is greater than the agreed $CQI_{threshold}$, the transmit power is reduced as long as it is greater than the required slice minimum transmit power, $P_s^{min}$. $P_s^{min}$ and $P_s^{max}$ are predefined parameters that guarantee the

required data rate and tolerable interference. $CQI_{threshold}$ is the SINR that guarantees the required throughput. The total maximum transmit power assigned to all the PRBs is always less than or equal to the maximum transmit power of the gNodeB as in C4 in (4.6).

Algorithm 3 explains how downlink transmit power ascribed for each PRB is controlled by the scheduler according to the last received CQI feedback. Furthermore, this scheme minimises the downlink transmit power which is uniformly distributed among the subcarriers in the network using the same Eq. (4.11). Unlike the proposed scheme, the variance in the required power of different slice's users is not considered, therefore, subcarriers are not assigned to slice's users based on their different transmit powers.

*Table 4.4:* Downlink heuristic power control allocation algorithm

**Algorithm 3** Downlink heuristic power control allocation algorithm

1: Each user sends $CQI$ feedback about all available $PRBs$ to the serving base station
2: **for each** $PRB \in PRB_{pool}$ **do**
3: **if** (( $CQI_{u,s,m} < CQI_{threshold}$) **and** ($P_{T-TTI} < P_{\max per\ PRB}$ )) **then**
4: $P_T \leftarrow P_{T-TTI} + Power\ Control\ Step$
5: **else if** (($CQI_{u,s,m} > CQI_{threshold}$) **and** $P_{T-TTI} > P_{\min perPRB}$)) **then**
6: $P_T \leftarrow P_{T-TTI} - Power\ Control\ Step$
7: **end if**
8: **end for**

## 4.7. Result and Discussions

In this section, the simulation and performance evaluation of the proposed SCAS using Joint power and Sub-carrier Allocation algorithms is done and compared with the traditional algorithm, the Downlink Heuristic Power Control Allocation Algorithm.

### 4.7.1. Simulation Parameters and Values

Similar to the simulation performed in Chapter 3, using MATLAB [125], a wireless 5G network with a base station (gNodeB) provided by an InP is simulated.

The gNodeB deployed at $(0,0)$ provides services to 2 MVNOs ($MVNO_1$ and $MVNO_2$). Each has 3 independent slices ($S_1$, $S_2$ and $S_3$), which are categorized in this case as mMTC, eMBB and URLLC respectively. The MVNOs have several numbers of users uniformly distributed in the gNB's coverage area of radius 500m. These users request resources according to the slice they belong to and the assignment of sub-channels is done based on slice thresholds set for data rate, transmit power and interference as shown in Table 4.4. The assignment is regularly updated.

The other simulation parameters used for the experiments are as shown in Table 4.5.

*Table 4.5: Simulation parameters and values*

| **Parameter** | **Value** |
|---|---|
| Number of Users/Slice | (varies) |
| Number of Slices | 3 |
| Number of MVNOs | 2 |
| Number of gNodeB | 1 |
| Spectrum allocation | 80 MHz |
| Carrier frequency | 6 GHz |
| Number of subcarriers per RB | 12 |
| Size of subcarrier | 30KHz |
| RB bandwidth | 12*30kHz = 360 kHz |
| Number of available RBs | 250 |
| Set of sub-channels C' | 5 sub-channels (i.e. C' = 20) |
| Max gNodeB Tx power | 20 W [43dBm] |
| $R_s^{min}$ (Slice 1, 2 & 3) | 1Mbps, 2.5Mbps, 0.5Mbps respectively |
| $P_s^{max}$ (Slice 1, 2 & 3) | 0.05W [17dBm], 0.2W [23dBm], 0.1W [20dBm] respectively |
| $I_s^{c,max}$ (Slice 1, 2 & 3) | $10^3 N_0$, $10^5 N_0$, $10^4 N_0$, respectively |
| $I_s^{c,min}$ (Slice 1, 2 & 3) | $N_0$, $N_0$, $N_0$, respectively |
| Slot duration | 0.5ms |
| Scheduling frame | 10ms |
| Cell-level UEs distribution | Uniform |
| Antenna height | 35m |
| Noise spectral density ($N_0$) | $10^{-13}$W/Hz [-100 dBm/Hz] |
| Cell coverage radius | 500m |

### 4.7.2. Performance Evaluation

In this subsection, the performance of the proposed scheme is discussed with the simulation results. For comparison, the Downlink Heuristic Power Control Allocation Algorithm explained in Section 4.6 was used. This scheme which is henceforth referred to as Traditional Scheme, shares total signal power equally among the sub-channels [146], i.e., it does not assign sub-channels with respect to the target power of the slices. However, the algorithm adjusts the transmit power of these sub-channels based on the CQI feedbacks received from the UEs. The simulation results are presented with different performance metrics discussed below.

1) *Tolerable Interference Level*: In Fig. 4.4, the sum of the tolerable interference on users with the sub-channels with non-zero power is studied, that is, the allocated sub-channels versus the number of admitted users. The experiment is carried out by varying the number of users by considering 5, 10, 12, and 16 users each in 3 different slices belonging to 2 MVNOs. Fig. 4.4 shows that as the number of users in the network increases, the interference in the network also increases. However, the result shows that in the three slices (S1, S2, and S3), the proposed algorithm performs better than the benchmarked (traditional) algorithm. This is revealed by the level of increase in the interference, the rate of increase in the proposed scheme is minimal compared to that of the benchmark algorithm. The reason for this is quite evident in the scheduling of the users based on their transmit powers, this scheduling is done by the algorithm in the central scheduler. S1, S2, and S3 denote Slice 1, Slice 2 and Slice 3 respectively.

Figure 4.5 shows the effect of the scheduling algorithm. The sum of the tolerable interference on the users with the allocated sub-channels is studied in all the slices and the two MVNOs. In the traditional scheme, slices 2 and 3 with the highest and higher transmit power respectively have significant tolerable interference levels on their users. Compared with the proposed scheme, the interference levels of users in slices with high transmit power are low especially in slice 2. This significant decrease in the total network interference is as a result of the scheduling algorithm which takes into account the transmit power of the slice the user belongs to.

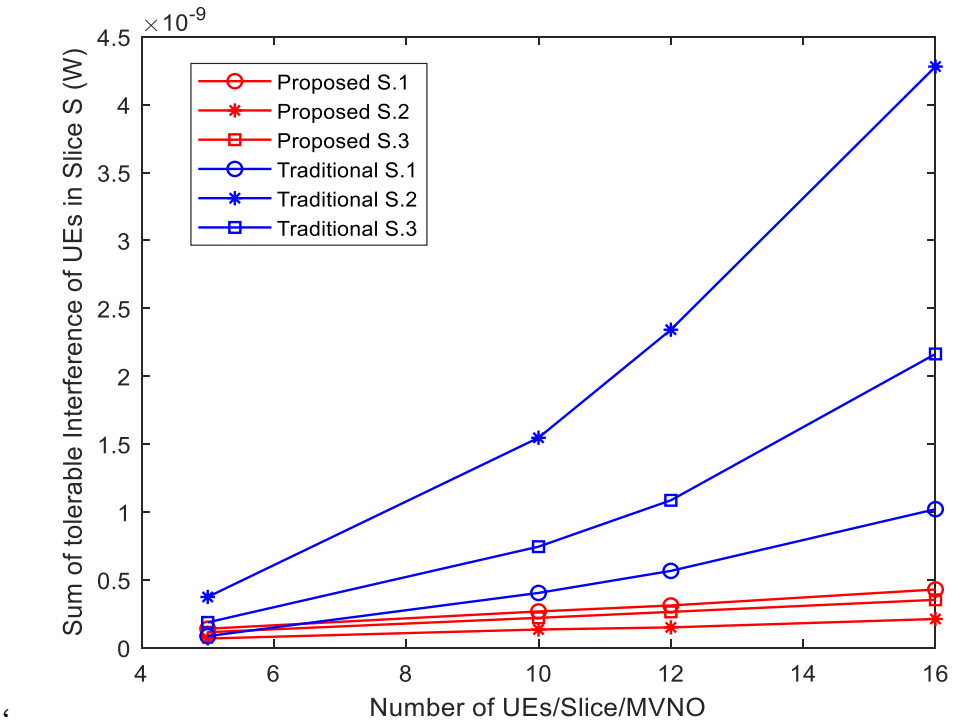


*Figure 4.4: Sum of tolerable interference of UEs in slice S vs number of UEs/Slice/MVNO*

The impact of the scheduling algorithm is further is shown with the increase in the number of users/slice/MVNO. In Slice1, with few numbers of admitted users, the traditional scheme gives less interference than the proposed scheme, this is as a result of the low transmit powers of the few UEs. But as the number of admitted UEs increases, our proposed scheme outperforms the benchmarked traditional method as shown in Fig. 4.5. M1 Slice1 stands for Slice1 in MVNO1, while M1 Slice2 stands for Slice2 in MVNO1, and M1 Slice3 stands for Slice3 in MVNO1. Likewise, M2 Slice1 stands for Slice1 in MVNO2, while M2 Slice2 stands for Slice2 in MVNO2, and M2 Slice3 stands for Slice3 in MVNO2.

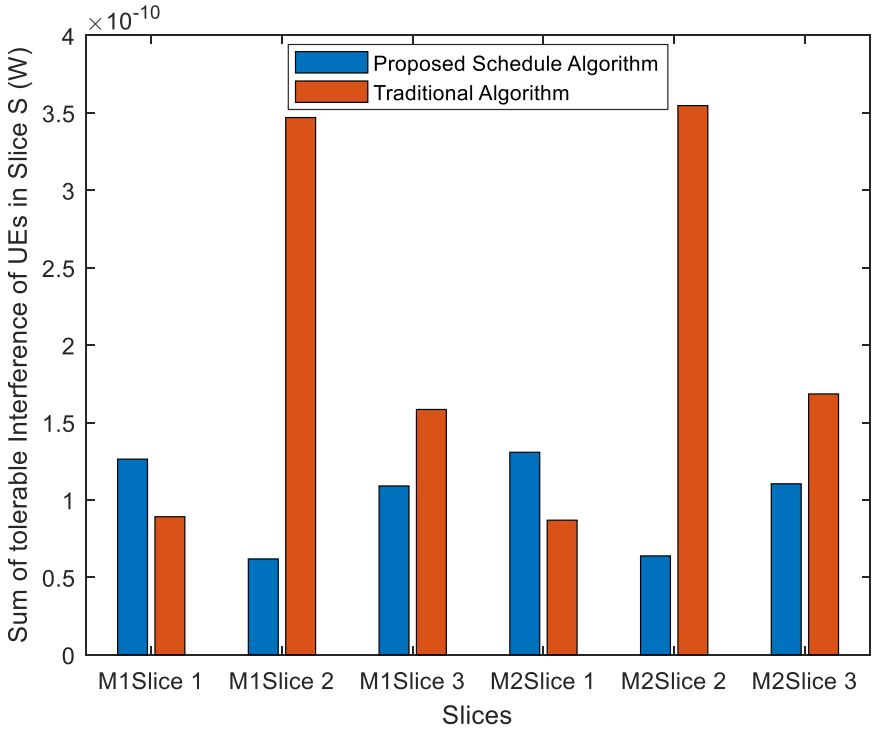


*Figure 4.5: Sum of tolerable interference of UEs in slices (S1, S2, and S3) in different slices and MVNOs.*

2) *Transmit* Power: In Fig. 4.6, the total transmit power of users in each slice is studied alongside the total generated data rate of users from each slice. Transmit power is required in the network to give the needed QoS and in this case, it is in terms of the threshold data rate to the users in the network. To avoid power wastage and to achieve energy efficiency, interference minimisation, as well as low radiation exposure. The power transmission between the gNodeB and the users should be as low as possible and should still give the required QoS values of the users. From the result in Fig. 4.6, it is obvious that even with the lower (minimised) transmit powers, the proposed scheme gives the users the throughput above the QoS threshold. While in the benchmarked algorithm, more transmit powers across the slices do not translate to more QoS for the users, the allocated QoS values are a little above little what the proposed scheme allocated. Therefore, the QoS is not compromised or traded-off for lower transmit power in the proposed scheme.

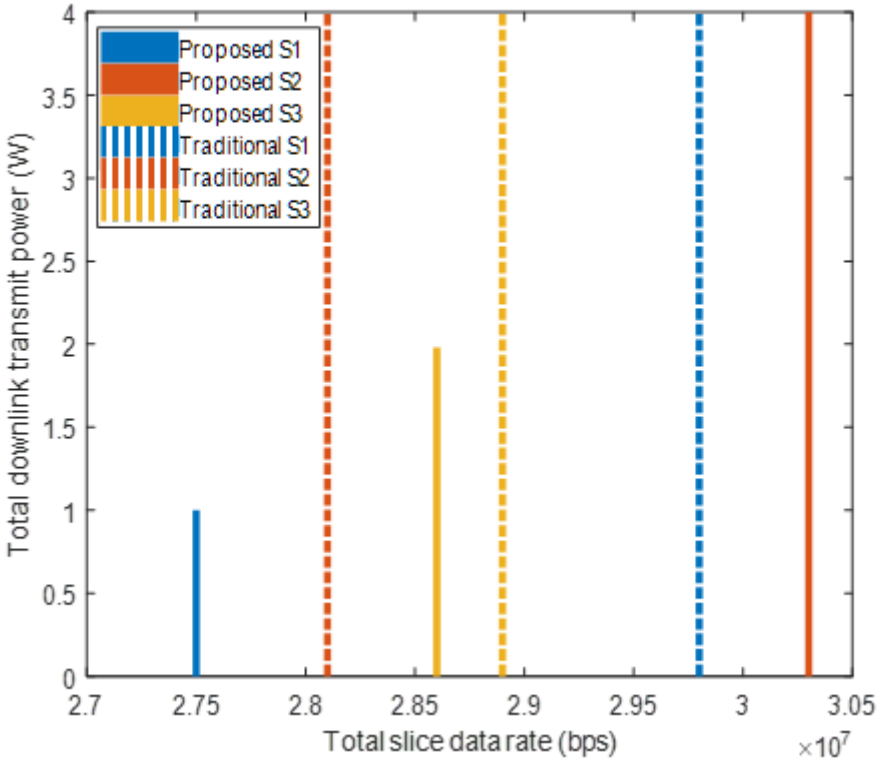


*Figure 4.6: Total downlink transmission power vs. Total slice data rate.*

3) *Number of admitted UEs:* Fig. 4.4 and Fig. 4.7 show that as the number of users increases in the slice and the network, the interference increases and the average data rate reduce respectively. Though with few users (expectedly at a low level of interference), the data rate of the benchmarked (traditional) scheme outweighs our proposed scheme (most especially at 5 users/slice) due to the high transmit power of the users, however, as the number of admitted UEs increases, the data rate values of the proposed scheme outruns that of the benchmarked scheme in all the slices (S1, S2 and S3). In Fig. 4.4, Fig. 4.5, Fig. 4.5, Fig. 4.7 and Fig. 4.8, the Proposed S1, Proposed S2 and Proposed S3 stand for proposed scheme Slice 1, Slice 2, Slice 3 respectively while Traditional S1, Traditional S2 and Traditional S3 stand for Traditional scheme Slice 1, Slice 2, and Slice 3 respectively. Moreover, for higher data rate requirements, the proposed model will support a higher number of slice's UEs with the maximized resources.

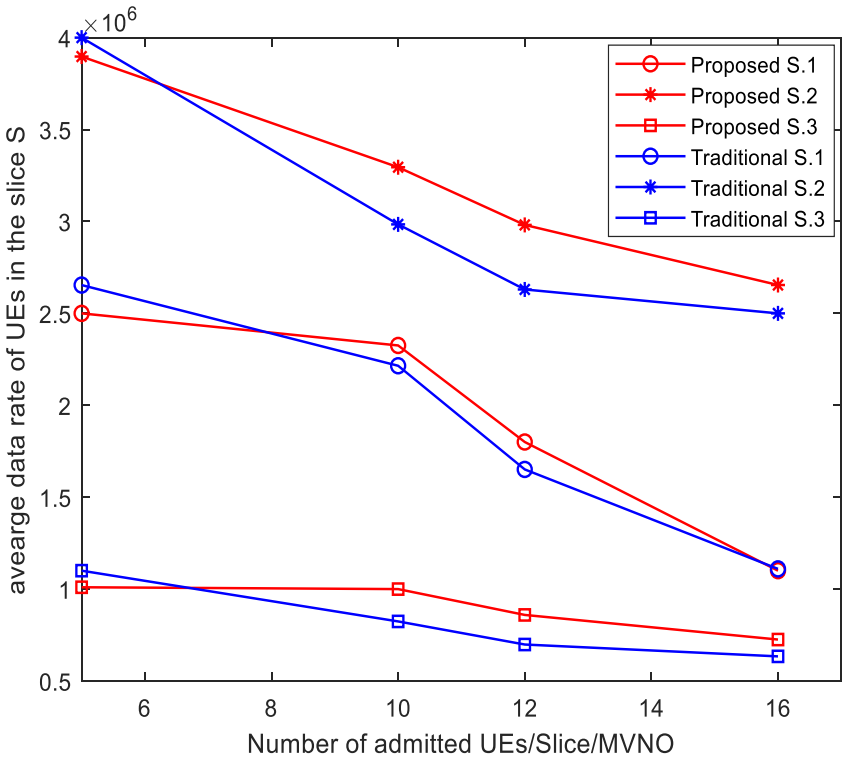


*Figure 4.7: Number of admitted UEs vs. average data rate.*

4) *QoS of admitted UEs:* Fig. 4.8 shows the effect of interference on the average data rate of the network. Despite having minimised transmit power, in all the slices (Proposed S1, S2 and S3), the proposed scheme still allocates resources with a data rate that is quite more value for each user than its slice's target requirement. This is in accordance with the slice threshold. This shows that the tolerable interference minimisation which is a by-product of the transmit power minimisation does not affect the needed throughput of the users in the network.

Additionally, Fig. 4.8 depicts that as the average data rate of users in the network decreases, the tolerable interference increases. This is because more users in the network are sharing the available radio resources, this means that the average data rate will drop as more users are admitted and allocated resources. Therefore, this causes more co-user's interference in the network. Moreover, comparing the two algorithms, the proposed scheme has lesser interference and also a less steep increase in the interference level compared with the benchmarked algorithm.

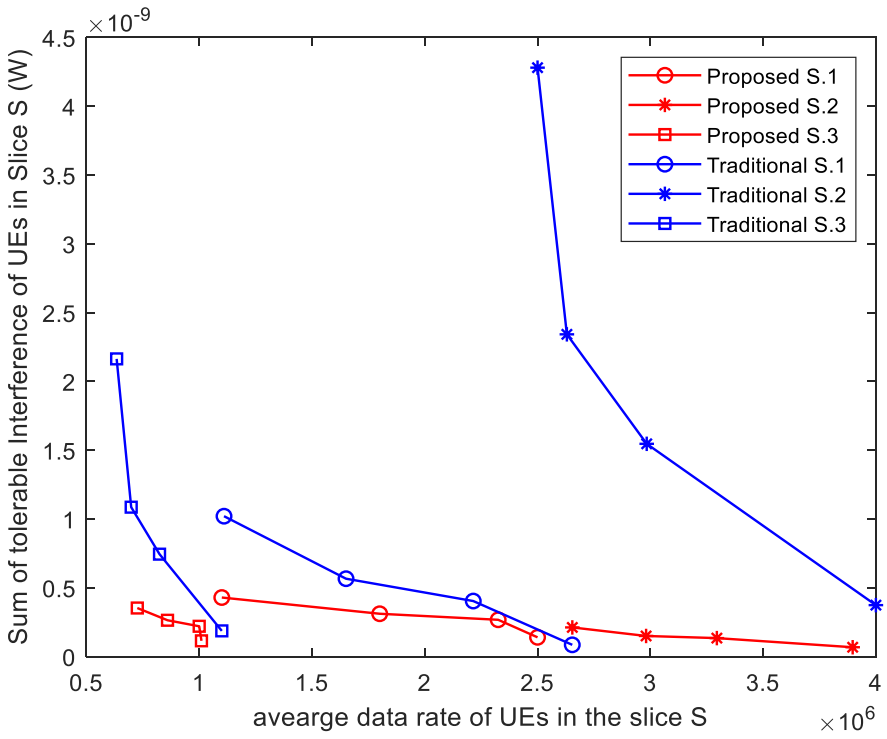


*Figure 4.8: Sum of UEs interference vs. average data rate.*

## 4.8. Chapter Summary

This chapter proposed a dynamic resource allocation (power and sub-channel) and slicing scheduling scheme for users in multitenancy 5G sliced networks. The algorithm is developed by formulating an MINLP optimisation problem, which minimises the total downlink transmit power of the network subject to the QoS constraints of users, capacity constraints and interference thresholds. The slicing scheduler accounts for sub-channels allocation and admission control which takes infeasibility into account. Through numerical simulation, the performance of the proposed scheme has been investigated. Results have shown the improvement of the proposed scheme over the benchmarked scheme.

# Chapter 5

# 5. RF-EMF Radiation Exposure Assessment of 5G Networks: Analysis, Computation and Mitigation Method.

## 5.1. Introduction

Since the evolution of cellular communication networks (GSM, UMTS, LTE, and 5G), the public concern about radio frequency (RF) electromagnetic (EM) fields health risks have rapidly grown. This is due to the drastic increase in the number of UE, increase in the number of RATs especially the concept of multiple-input-multiple-output (MIMO), and of course increase in the achievable users' throughput [7]. These health concerns have brought about many research and investigations [8], [9], [10] on the induced EM radiations originating from UEs (uplink) and the APs) (downlink).

However, the RF electromagnetic radiation has been classified as non-ionizing radiation as its photons do not have enough energy to break bonds or ionize biological molecules [11]. The photon's energy of an EM wave is given as the product of the Planck's constant and its frequency. The photon's energy of the radio frequency spectrum varies between approximately $4.1*10^{-6}$eV and $1.2*10^{-3}$eV for 1GHz and 300GHz, respectively. This is far lesser than (approximately 5eV) the minimum amount of energy required to cause ionisation in organic substances. Nevertheless, this fact, there is a need to investigate the level of EM radiations that causes human exposure in the various RATs of different generations of wireless networks and to also establish how safe they are, specifically in the 5G networks [9].

Moreover, there is a need to investigate the electromagnetic effect of mobile network transmitters and mobile receiver on humans. As it is a fact that the power level is notably higher in a transmitter compared to that of UEs. However, the distance of the transmitter to the exposed person is higher than the wavelength of it carrier frequency [147], and also notably higher when compared with the distance between UEs and their users. Results from experiments [147] show that the RF-EMF radiation exposures from base stations to users are significantly weaker compared to that of UEs to users.

In network planning [126], the concern for human exposure due to RF-EMF must be considered, as the transmit power is directly proportional to the RF-EMFs emitted from the user equipment. Therefore, a proper power control scheme [100] is required for both uplink and the downlink to dynamically adjust the transmit power of wireless communication networks and ensure target SNR level and minimise interference [21]. This is also important to regulate and be in compliance with the SAR limit.

SAR represents the transmitted energy absorption rate of the UEs placed close to human tissue [148], [104]. EI characterizes the most influencing parameter in global exposure, the power density of a particular point or location of single or several transmitters operating at different frequencies. SAR is an EMF exposure metric defined by the ICNIRP [12]. Also, EI is another metric developed by the LEXNET [15], is used to characterize the EMF exposure taking into account the SAR threshold by using both the *E* and *H*.

Therefore, it is vital that the required transmit power of user equipment is reduced by not always emitting at their maximum power when communicating with the microcell or macrocell APs. This lowers the power density of the user's location and by so doing reduces the SAR, as the power density is directly proportional to the *E* and the SAR. With the inverse square law principle in electromagnetic wave (energy decreases with distance squared), and pathloss principle in wireless networks communication, power density reduces as the UE move farther distance from the transmitter as shown in Fig. 5.1.

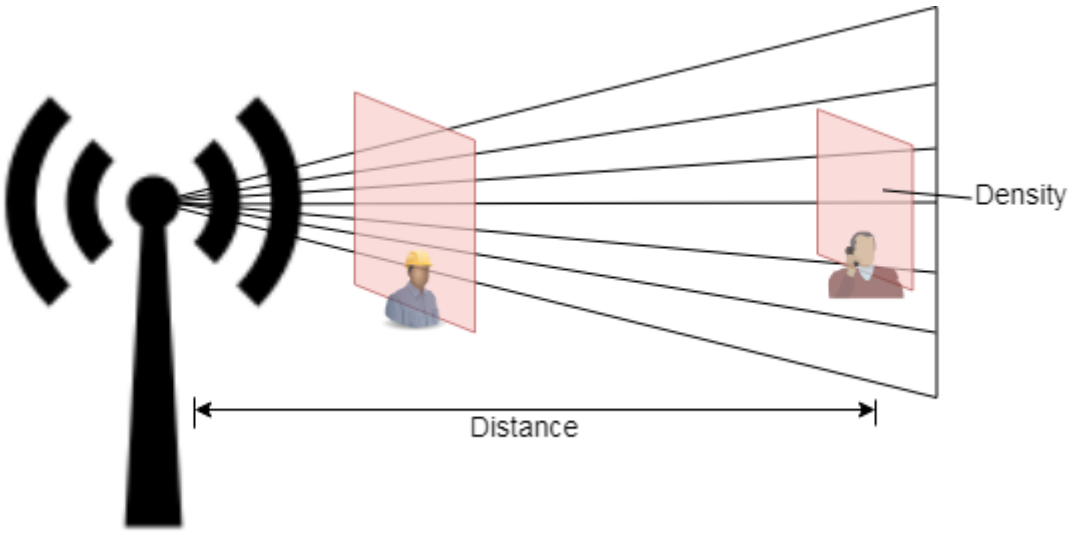


*Figure 5.1: Power density analogy in radio frequency propagation.*

In this chapter, the radiation exposure emitted by wireless networks is investigated by simulating the system models of heterogeneous 4G and 5G networks and characterize the data generated by the induced RF-EMF exposure of the given area. The distances ($d$ [m]) of the users to the APs; the effective antenna gain ($G$ [dBi]) of the APs; the pathlosses ($PL$ [dBm]) of users to the serving AP; the open-loop control transmit and received powers; the equivalent isotropically radiated powers ($P_{tx}$ and $P_{rx}$ [dBm]); the cross-sectional areas (CSA [m²]); spectral power densities ($S$ (W/m²)); the electric field strengths ($E$ [V/m]); and magnetic field strengths ($H$ [A/m]); respectively, are employed to evaluate the EI of the user. Lastly, an EOPCA scheme is used to mitigate the problem of RF-EMF exposure radiating from mobile uplink) and transmitting APs (downlink).

The main contributions of the chapter are summarized as follows:

- To the best of the authors' knowledge, this is the first evaluation and analysis of 5G wireless networks-induced RF-EMF using the computational method.
- An open-loop fractional power control concept (OLPC) that controls the UE transmit power $P_{tx}$ for the uplink transmission was incorporated. As a result, an exposure-index open-loop power control algorithm that controls and mitigates the EI if users in the network was proposed.

- The RF-EMF radiation exposures from the 5G network were compared with an existing RAT, i.e., 4G network. This was done to allay the fear of the “substantial health risk” 5G network might bring.

## 5.2. Notations

In this subsection, the relevant notations used in the entire chapter are described. Table 5.1 highlights the list of notations.

*Table 5.1: List of notations*

| Symbol | Description |
|---|---|
| $u$ | User, User set |
| $d_u$ | distance of a user to the interfering APs |
| $A_u$ | Cross-sectional area of this emitted radio wave |
| $B$ | Total bandwidth of the InP |
| $P_{Tx}$ | Transmit power from the users to the APs |
| $P_{Rx}$ | Received power by a UE from the APs |
| $P_u$ | Allocated power to a user $u$ as per its PRBs |
| $\mathrm{S_u}$ | Power density of user $u$ |
| $\mathrm{E_u}$ | Electric field strength of user $u$ |
| $H_{\mathrm{u}}$ | Magnetic field strength of user $u$ |
| $Z_o$ | Characteristic impedance of free space |
| $\mathrm{SAR_u}$ | SAR of user $u$ |
| σ | Electrical conductivity of the tissue |
| $\rho$ | Tissue density |
| $PL_u$ | Pathloss between the AP and the user |
| α | Pathloss compensator factor |
| $f_c$ | Carrier frequency in MHz |
| $h_g$ | Antenna height |
| $G_T$ | Antenna gain |
| $\in_{ant}$ | Antenna efficiency |
| D | Directivity of the antenna |
| $\lambda$ | Wavelength of the carrier frequency |
| $\mathrm{EI_{i,j}}$ | EI from the transmitters and receivers respectively |
| $\mathcal{M}$ | Number of PRBs allocated per user |
| $\mathrm{P}_{\mathrm{UE}}^{\mathrm{max}}$ | Maximum power allowed in uplink transmission |
| $\mathrm{P_o}$ | Power in one PRB |
| $\partial_{\mathrm{mcs}}$ | Modulation code scheme dependent offset |
| $\mathrm{f}(\Delta_{\mathrm{i}})$ | Closed-loop correction function |
| $\theta, \emptyset$ | Angle above the reference plane, angle between the projection and the reference plane |

## 5.3. System Model and Assumptions

The system is modelled as a network in a typical urban area as illustrated in Fig. 5.2, where the distributed networks consist mainly of 4G APs (i.e., eNBs) and 5G APs (i.e., gNBs).

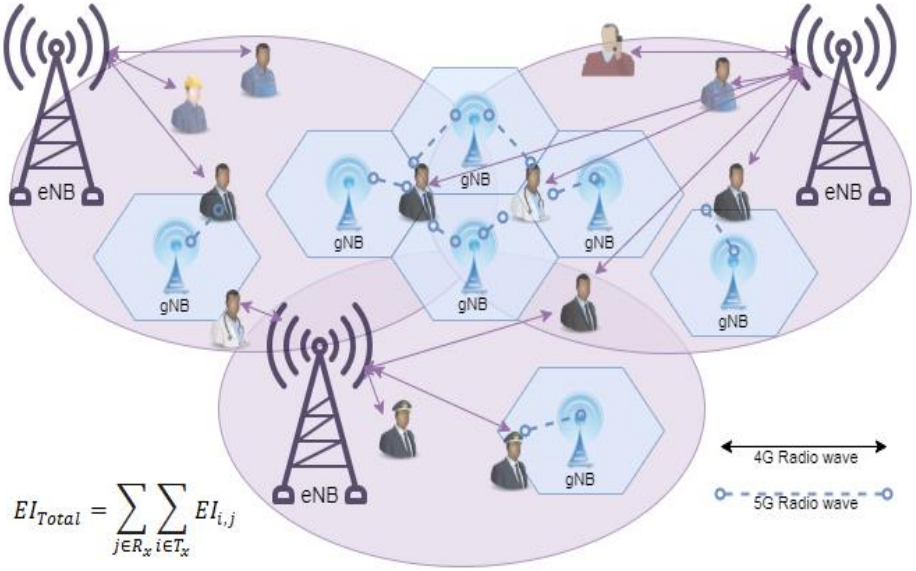


*Figure 5.2: System model of multiple 4G and 5G transceivers.*

These APs provide services to a set of users $U$ in a particular coverage area $A$ by propagating their radio wave within the geographical locations with radius $r$. Hence, the AP causes radiation within this area $A$. There is a set of UEs which are assumed to be held or used by humans within the networks' coverage area i.e., these hand-held devices cause exposure to their users. It is also assumed that all users are static. Hence, mobility is not considered in this study.

The total transmit power from all users to the APs (both gNBs and eNBs) is denoted as $P_{Tx}$, while the total received power by the UEs from the APs is denoted as $P_{Rx}$. Let $P_u$ represent the power allocated to user $u$ according to its PRBs. The power assignment for the UE is performed in such a way that each PRB contains an equal amount of power, the users' performance is only differentiated by their pathlosses and the required data rates. The carrier frequency of the APs is denoted by $f_c$ while the antenna height is $h_g$. In the frequency domain, the system bandwidth B is divided and shared by the sub-channels $C$ of size 180 kHz [149] for 4G networks and 360 kHz [150] for 5G networks, respectively.

The pathloss between the APs and the users $PL_u$ increases with the distance and makes the power density $S$ decrease. The EM radiation also decreases with the distance.

Environmental factors such as geographical region, network architecture, and temperature are assumed to be constant for all the scenarios considered in this chapter. Considering the near-field and far-field effects, it is established that the near-field effect is electromagnetic induction while the far-field effect is electromagnetic radiation. Therefore, for the users to experience an exposure due to electromagnetic radiation (in the far-field region), they are to be located beyond the distance $\frac{2D^2}{\lambda}$ and about a wavelength ($\lambda$) from the antenna. Where $D$ is the largest dimension of the antenna and $\lambda$ is the wavelength of the carrier frequency. The amount of exposure received by the user's device or the exposed person is equivalent to the sum of the power densities generated by the interfering APs as shown in Fig. 5.2, and can be expressed as:

$$EI_{Total} = \sum_{j \in R_x} \sum_{i \in T_x} EI_{i,j} \tag{5.1}$$

## 5.4. Methodology: RF-EMF Analysis, Computation, & Control

Herein, the users with UEs are simulated and the distance ($d_u$) of various users to the interfering APs are determined. The cross-sectional Area ($A_u$) of an emitted radio wave is expressed as:

$$A_u = 4\pi d_u^2 \tag{5.2}$$

The pathloss models employed in this work for all the users with UEs and the various 4G APs and 5G APs are given in Eqs. (5.3) and (5.4), respectively [71], [150].

$$PL_u = 36.8\log_{10}(\mathrm{d_u}) + 43.8 + 20\log_{10}(\mathrm{f_c}), \tag{5.3}$$

$$PL_u = 32.45 + 20\log_{10}(d_u) + 20\log_{10}(f_c), \tag{5.4}$$

where $f_c$ is the carrier frequency and it is given in MHz, $d_u$ is the distance in meters between the user u and the APs.

The antenna gain ($G_T$) of the transmitter is the product of the antenna efficiency, $\in_{ant}$ and the directivity, D of the antenna which is given as

$$G_T = \in_{ant} * D. \tag{5.5}$$

The directivity or the directive gain is $D(\theta, \emptyset)$, where $\theta$ is the altitude or angle above the reference plane and $\emptyset$ is the angle between the projection and the reference plane. Also, $\in_{ant}$ is the ratio of the output power and the input power of the antenna, respectively, and it is given as [10]

$$\in_{\boldsymbol{ant}} = \frac{\boldsymbol{P_o}}{\boldsymbol{P_{in}}}. \tag{5.6}$$

For an isotropic antenna, the D is equal to 1 and the gain equals its efficiency in every direction and, hence it is always at most 1. However, the gain of a directional antenna ideally should exceed 1. The gain in decibels for an isotropic antenna and a dipole antenna is expressed as $G_{dBi} = 10\log_{10}(G)$ and $G_{dBd} = 10\log_{10}(G/1.64)$, respectively, where i connotes for isotropic antenna and d stands for dipole antenna. The directivity of a half-wave dipole is known to be 1.64. An isotropic radiator is a theoretical lossless antenna that radiates power uniformly in all directions. The power radiated from the isotropic antenna will have a uniform power per unit area no matter where it is measured from. This fact motivates our decision to choose isotropic antennas.

The transmitted power is expressed based on the Effective Isotropic Radiated Power (EIRP). EIRP [11] is the product of transmitted power and the antenna gain in a given direction relative to an isotropic antenna of a radio transmitter given as:

$$EIRP_{dBm} = P_{TdBm} - Loss_{dB} + G_{T(dBi)} \tag{5.7}$$

$$EIRP_W = P_{Tx} * G_T \tag{5.8}$$

Powers are transmitted from both uplink (UEs to the base stations) and downlink (the base stations to UEs) transmissions. In this chapter, the downlink power (from the base stations to UEs) is referred to as the received power $P_{Rx}$ while the uplink power (from UEs to the base stations) as the transmit power $P_{Tx}$. Power control is important in network resource management to optimise the power of the desired received signals while limiting radiation and interference.

For downlink power, the controlled received power is expressed as [100]:

$$P_{Rx} = P_o + \alpha * PL_u \quad [d_{Bm}], \tag{5.9}$$

and for uplink power, the controlled transmit power is expressed and calculated as:

$$P_{Tx} = min\{P_{\underset{UE}{max}}; P_o + 10\,log_{10}\,\mathcal{M} + \alpha * PL_u + \partial_{mcs} + f(\Delta_i)\} \quad [d_{Bm}], \tag{5.10}$$

where $P_o$ is cell-specific and it is the power contained in one PRB. $PL_u$ is the pathloss between a user and the service AP given in Eqns. (5.3) and (5.4). $\alpha$ is pathloss compensator factor which is a cell-specific parameter that ranges between 0 and 1, for fractional power control, it is between 0.7 and 0.9 in practice. Herein, $\alpha$ was used as 0.7. $P_{max}$ depends on the UE and it is the maximum power allowed in uplink transmission. $\mathcal{M}$ is the number of PRBs allocated per user. $\partial_{mcs}$ is the modulation code scheme dependent offset and it is UE specific. $f(\Delta_i)$ is the closed-loop correction function.

With a power control scheme, UEs are designed in such a way that they don't transmit at their maximum, i.e., $P_{max}$, in real conditions. Therefore, $P_{max}$ can be ignored in the $P_{Tx}$ and $P_{Rx}$ equations. Also, the power expression based on which UE sets its initial transmitting power can be obtained from Eq. (5.10) by ignoring the modulation code scheme dependent offset $\partial_{mcs}$ and the closed-loop correction factor $f(\Delta_i)$. Therefore, Eq. (5.10) can be expressed as:

$$\begin{aligned} P_{Tx} = \quad & P_{Rx} - PL_u \\ & (P_o + \alpha * PL_u) - PL_u \\ & P_o + (\alpha - 1) * PL_u \end{aligned} \tag{5.11}$$

The spectral power density, S is the ratio of EIRP incident perpendicular to a surface and the cross-sectional area ($A_u$) of the surface of the radiated radio wave. The unit of power density is ($W/m^2$) and is computed as follows [127]:

$$S_u = \frac{P_{Tx} * G_T}{4\pi d_u^2} = \frac{P_{Tx} * G_T}{A_u} \tag{5.12}$$

Relating to the normalised value of the square of the of users' E-field strength ($E_u$) or the H-field strength ($H_u$) from the radiating source. User's power density $S_u$ can be computed as:

$$S_u = \frac{|E_u|^2}{Z_o} = |H_u|^2 * Z_o \tag{5.13}$$

where $Z_o$ is the characteristic impedance of vacuum which is 120πΩ = 377Ω. Therefore from Eq. (5.13), the $E_u$ and the $H_u$ of the radiated radiofrequency electromagnetic wave can be characterized as follow:

$$E_u = \sqrt{Z_o * S_u} \equiv Z_o * H_u \tag{5.14}$$

$$H_u = \sqrt{\frac{S_u}{Z_o}} \tag{5.15}$$

*SAR* [W/kg] is the rate of energy absorbed by or deposited per unit mass per unit time. It is proportional to the root-mean-square (RMS) value of the induced E-field strength ($E_u$) and also to the electrical conductivity (σ) of the tissue per tissue density (***ρ***) [11].

$$SAR_u = |E_u|^2 * \frac{\sigma}{\rho} \tag{5.16}$$

Therefore, *SAR* and *EI* are proportional to the $E_u$ or the $H_u$. We assume fixed electrical conductivity and density of the tissue and that they are constant for all users and all scenarios. Also, we assume an ideal non-thermodynamic circumstance [11] as SAR is related to an increase in temperature at a point by:

$$SAR_u = \frac{c\Delta T}{\Delta t}\Big|_{t=0,} \tag{5.17}$$

where $c$ is the specific heat capacity (J/kg ℃), $\Delta T$ is the temperature change (℃) and $\Delta t$ is the duration of exposure (s).

The *EI* is characterized as the ratio of the evaluated SAR (local or whole-body) taken for an average duration of 6 minutes and the corresponding maximum limit.

$$EI = \frac{SAR_{evaluated}}{SAR_{max\ limit}} \tag{5.18}$$

The ICNIRP *SAR* maximum limit for a local (i.e., EI from UEs) is 2 W/kg, while that of the whole-body (i.e., EI from the APs is 0.08 W/kg. The EIs are expressed as follows [127]:

$$EI_{mobile} \equiv \frac{SAR_{10g}\,[W/kg]}{2\,[W/kg]} \tag{5.19}$$

$$EI_{AP} \equiv \frac{SAR_{WB}[W/kg]}{0.08[W/kg]} \tag{5.20}$$

In a scenario where there are different number of transmitters ($N$) causing exposure to a user, the total $EI$ is can be expressed as:

$$EI_{Total} = \sum_{j=1}^{N} \frac{S_j(W/m^2)}{S_{jlimit}(W/m^2)}, \tag{5.21}$$

$$EI_{Total} = \sum_{j \in R_x} \sum_{i \in T_x} EI_{i,j}, \tag{5.22}$$

where $i$ and $j$ are the interfering transmitters and receivers respectively. $T_x$ is the transmitters (APs) while $R_x$ is the receivers (UEs).

## 5.5. A 5G Networks Exposure Analysis and Mitigation Method Using Power Control Scheme.

In this subsection, a RF-EMF exposure analysis and mitigation method is discussed. The open-loop transmit power-control scheme and the proposed exposure-index open-loop power control algorithm is investigated.

### 5.5.1. Open-Loop Power Control Scheme

The open-loop transmit power control ensures the target SINR level is achieved by making the network monitor and control the power emitted, especially the maximum transmit power in wireless communication. The downlink power limit $P_{max}$ is advised by 3GPP as 23dBm; however, lowering the value of $P_{max}$ might reduce UE battery life, interference and RF radiation. In the uplink power transmission, the UE manufacturers make sure that the devices do not transmit more than the maximum UE transmit power $P_{\underset{UE}{max}}$ as specified by 3GPP [9].

The scheme has the ability of the UE to set is transmit power to a particular value. When the AP is transmitting the reference signal, the UE's maximum

allowable power is also sent along to the UE. The UE detects and measures the power from the reference signal. The UE calculates the pathloss (PL) between the AP and the UE by comparing the measured power and the power information sent by the AP. From the calculated PL and the power information from the reference signal, the UE realises the amount of power it can actually transmit to the AP. The open-loop power-control ensures that the uplink power for any of the channels used in transmitting is not greater than the $P_{\underset{UE}{max}}$ as earlier explained in section 2.8.3 and with Eqs. 2.1 and 2.2.

The pathloss compensation factor α is set as a fractional power control scheme (less than 1), to avoid cell edge users transmitting at very high power to cater for their pathlosses. To evaluate the amount of exposure absorbed by humans, an open-loop power-control algorithm is employed in computing the SAR and the EI as shown in Algorithm 1 in Table 5.2.

### 5.5.2. Exposure-Index Open-Loop Power Control Algorithm.

This subsection illustrates the exposure-index open-loop power control algorithm. Algorithm 1 is a pseudo code that explains in step-by-step basis of using open-loop power control to mitigate the EI if users in the network.

*Table 5.2: Exposure-index open-loop power control algorithm*

**Algorithm 1** Exposure-index open-loop power control algorithm

**Inputs:** $Z_o$, $P_o$, $a$, $B$, $f_c$, $\lambda$, $h_g$, $r, D$, $U$, and their positions

**Outputs**: $S_u$, $|E_u|$, $|H_u|$, $SAR_u$, $EI_u$

1. Given the set $U$ where $u \in U$
2. **for** each user $u$ **do**
3. Initialise the values of $P_{\underset{UE}{max}}, \rho, \sigma$, and $SAR_{\max limits}$
4. Calculate the distance of users from the interfering APs.
5. **if** $\frac{2D^2}{\lambda} \leq d \leq \lambda$ **then**
6. Determine the pathloss $PL_u$ of UEs from the serving APs
7. **else**
8. RF-EMF radiation is not affecting user $u$.
9. **end if**
10. **for** each eNB and gNB **do**
11. Initialise the values of $P_{max}$
12. Calculate the downlink transmit power $P_{Tx}$ for each user from their interfering APs.
13. **while** $P_{Tx} \leq P_{max}$ $\forall$ APs **do**
14. $P_{Tx} \leq EIRP_{Tx}$
15. **end while**
16. **end for**
17. Solve for the Area of RF-wave to the point of user $u$
18. Calculate the uplink received power $P_{Rx}$ for each user from the interfering APs.
19. **while** $P_{Rx} \leq P_{\underset{UE}{max}}$ $\forall u$ **do**
20. $P_{Rx} \leq EIRP_{Rx}$
21. **end while**
22. Determine the spectral power density $S_u$ using Eq. (5.13)
23. Solve for the RMS values of $|E_u|$&$|H_u|$ using values from 22
24. Assume the values of $\rho$ and $\sigma$ are constant $\forall u$,
25. **then** find $SAR_u$ using Eq. (16)
26. Evaluate $EI_u = \frac{SAR_{evaluated}}{SAR_{\max limit}}$ Eqs. (5.18, 5.19, 5.20)
27. **end for**

## 5.6. Result and Discussions

In this section, the evaluation of the characterized, simulated, and computed power densities, the *SAR*s, and the *EI*s of users (humans) within the model is presented.

### 5.6.1. Simulation Environment and Parameters

The simulation parameters used for the experiment are as shown in Table 5.3. Using MATLAB [125], a typical 4G and 5G wireless network environment was simulated as shown in Fig. 5.3 with some eNodeBs having a coverage area of radius 500m each, and gNodeB having a coverage area of radius 30m each. These APs while serving the UEs held by some users for an average of 6 minutes, within the coverage area, causes RF-EMF radiation to the users. The SAR and exposure caused are evaluated using the radiation emitted from both the APs and UEs to the users (human beings).

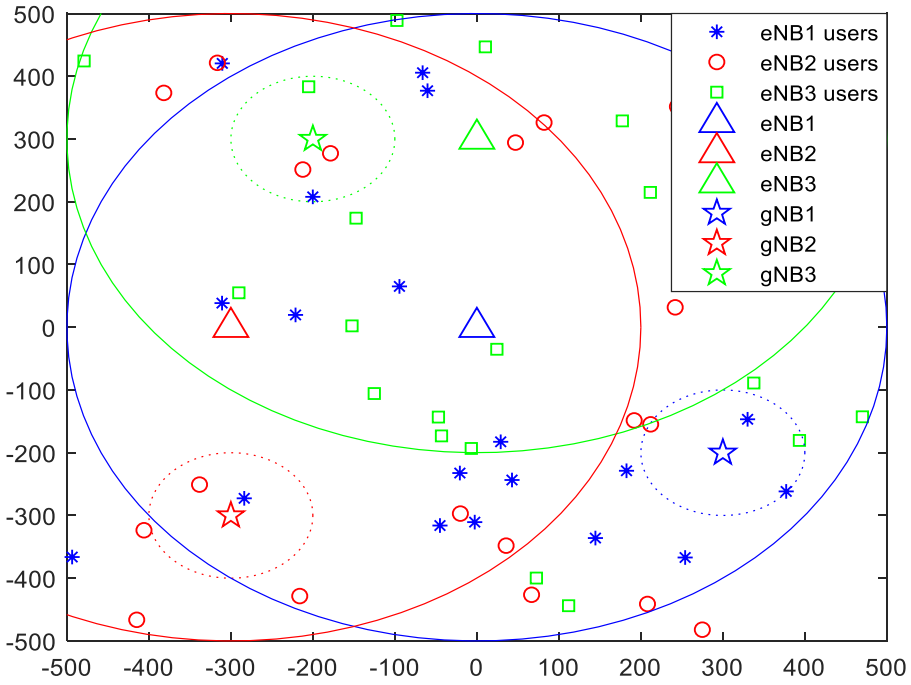


*Figure 5.3: Simulation scenario with multiple 4G and 5G transceivers.*

*Table 5.3: Simulation parameters and values*

| **Parameter** | **4G Value** | **5G Value** |
|---|---|---|
| Number of Users | Random | Random |
| Number of APs | 3 | 3 |
| Channel model | 3GPP | 3GPP |
| Spectrum allocation | 20MHz | 100MHz |
| Carrier frequency | 2GHz | 6GHz |
| Number of subcarriers per RB | 12 | 12 |
| Size of subcarrier | 15kHz | 30kHz |
| RB bandwidth | 12*15kHz = 180kHz | 360kHz |
| Number of available RBs | 100 | 250 |
| The conductivity of the tissue (σ) | 0.97S/m | 0.97S/m |
| Mass density of the tissue (***ρ***) | 1000kg/m³ | 1000kg/m³ |
| Characteristic Impedance ($Z_{o)}$ | 120$\pi\Omega$ = 377Ω | 120$\pi\Omega$ = 377Ω |
| Max AP $T_x$ power | 20W [43dBm] | 0.25W [24dBm] |
| Max UE emitted $R_x$ power | 0.25W [24dBm] | 0.25W [24dBm] |
| Power Control | Open-loop | Open-loop |
| Pathloss exponent (α) | 0.7 | 0.7 |
| Slot duration | 0.5ms | 0.5ms |
| Scheduling frame | 10ms | 1ms |
| Cell-level UEs distribution | Uniform | Uniform |
| Antenna height | 50m | 30m |
| UE height | 1.5m | 1.5m |
| Cell coverage radius | 500m | 30m |

## 5.6.2. Performance Evaluation

This sub-section analyses, compares and discusses the effects of RF-EMF radiations on the users who are carrying the UEs that are within the network coverage area of the APs. The analyses are done and presented in terms of different metrics such as power density, SAR and EI.

1) *Power density*:

Figure 5.4 gives the cumulative distribution function (CDF) plots of the power densities for the 4G and the 5G wireless networks. Power density characterizes the radiation experienced by a user at a point, therefore, the power density is a function of the SAR emitted from the different networks. It is evident from these results that the power densities of 4G networks are higher than that of the 5G network. This is largely due to the coverage distance and the cross-sectional area of the APs of the 5G networks which is shorter and smaller than that of the APs of the 4G networks. Hence, the RF-EMF radiation exposures from 5G networks are lower than those of 4G networks.

The power density cumulative distribution of the 5G networks ranges from 0.005 $mW/m^2$ to around 0.12 $mW/m^2$, while, that of 4G is from around 0.01 $mW/m^2$ to about 0.185 $mw/m^2$. These results are within the ERLs specified in the guidelines and as shown and explained in Section 2.8.4. The maximum power density from both the 4G and the 5G networks in Fig 5.4 is seen to be less than the recommended whole-body exposure limits of $10W/m^2$ for the general public and $50W/m^2$ for occupational or resisted environments for frequency between 2000 to 300000 MHz as shown in Table 2.4. It is also seen to be less than the recommended local exposure limits of $40W/m^2$ for the general public and $200W/m^2$ for occupational/resisted environments for frequency between 2000 to 6000 MHz as shown in Table 2.5.

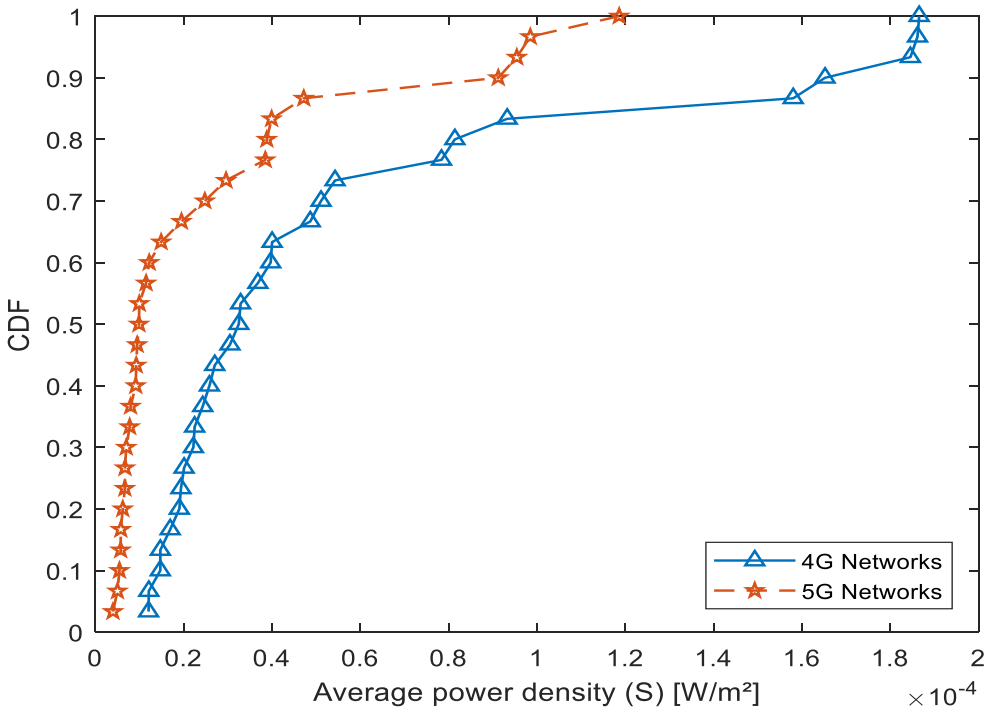


*Figure 5.4:* CDF graph showing average power density of the network.

The computed power density exposures are far below these limits and still lesser than the stricter ERLs imposed by some specific countries such as China, Germany and Belgium as explained in Section 2.8.4. Due to limitations, this study could not do any field measurements, however, the assessed power density exposures are in accordance with the measurements done in [82], [10].

2) *Pathloss Compensation factor (α)*:

Figure 5.5 shows the comparison of the power densities for both 4G and 5G networks when varying the pathloss compensation factors using the power control scheme. The pathloss compensation factor tends to compensate for the shortage caused by the pathloss. In the network, the cell edge users usually have more pathlosses than the cell centre users. Thus, the compensation factor makes the cell edge users transmit more power to make up for the pathloss. When α is 0, it means that is no power control and all the users are transmitting at equal power. Between 0 and 1, it means that there is the fractional power control and the users transmit power are different depending on their pathloss. Lastly, when α is 1, it means that there is full compensation, the users pathlosses is totally compensated for by transmit powers.

For the open-loop power-control scheme, the pathloss compensation factor in Eqs. (5.9) and (5.11) were chosen to be fractional and compared to a full pathloss compensation factor of 1. The choice of 0.7 was taken based on the experiment conducted in [100] which used the α between 0 (i.e., no power control) and 1 (i.e., full compensation).

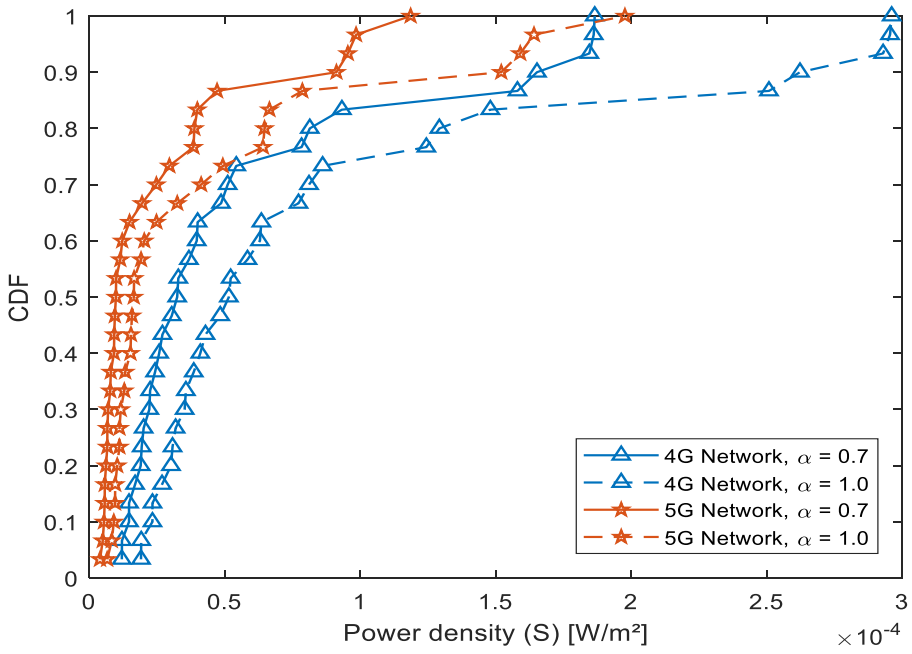


*Figure 5.5: Power density for different power control pathloss exponents.*

Clearly, the power density is reduced for both the 4G and the 5G networks when using fractional pathloss compensation factor (α) of 0.7 compared with full compensation where α is 1. The power density cumulative distribution of the 5G networks when the pathloss compensation factor is 0.7 ranges from 0.005 mW/m² to around 0.12 mW/m², while, that of 4G is from around 0.01 mW/m² to about 0.185 mw/m². It increased to between 0.008 mW/m² to around 0.2 mW/m² and 0.0135 mW/m² to about 0.3 mw/m² for 5G and 4G, respectively, when the pathloss compensation factor is (1) full.

The reason for this is that the cell edge users which usually have more pathlosses are compensated for with the full compensation of 1, thus, they are transmitting with more power in the network. Therefore, the power control scheme mitigates interference and reduces radiation due to the controlled transmit power translating to reduced power densities in the entire network.

*3) Specific Absorption Rate:*

In Fig. 5.6, the SAR against the number of transmitters in the networks was analysed. The explosion in data usage has brought about an increase in UEs, their apps, and a corresponding increase in the ultra-denseness of the APs in the network. Thus, it is essential to investigate the impact of the increase in the number of transmitters and receivers in the network. As explained in Chapter 2, the SAR is the measure of electromagnetic power absorbed in human tissue per unit mass. The value of SAR depends largely on the averaging mass or and the absorption of the electric field. So, the more the electric field generated in the network, the more the absorbed exposures.

From the results in Fig. 5.6, it can be seen that the SAR increases with the number of transceivers in the network. This is due to the increase in radiations caused by the close and interfering transmitters and receivers emitting more RF-EMF into the network area. The SAR increases from around 0.1 μW/kg to 80 μW/kg when the number of APs and UEs increase from 1 to 30 for the 4G network and from around 0.2 μW/kg to 73 μW/kg when the number of APs and UEs increase from 1 to 30 for the 5G network.

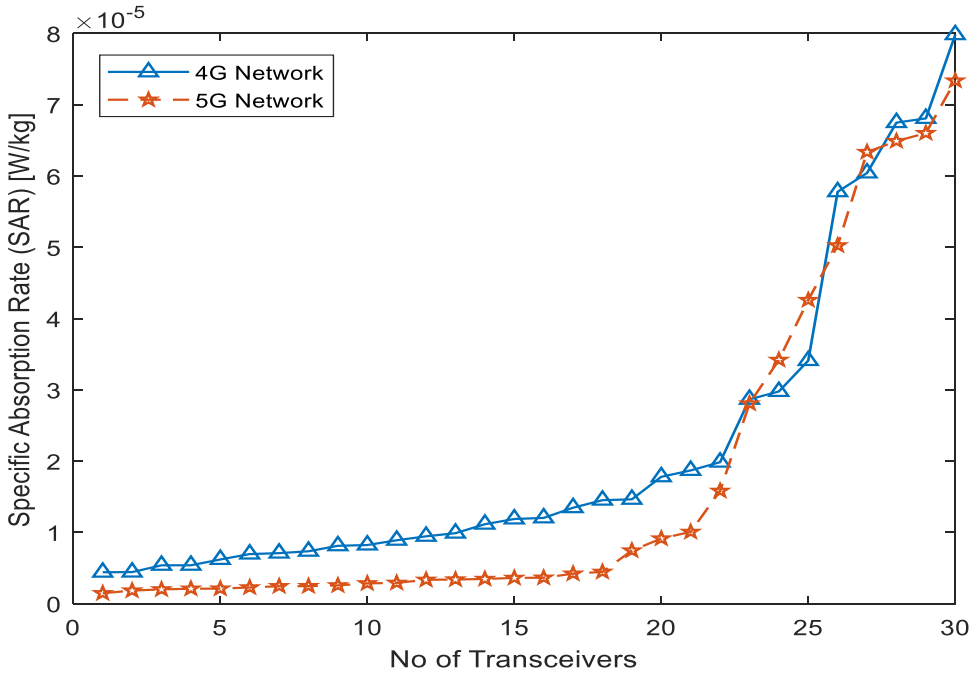


*Figure 5.6: The SAR against the number of transmitters.*

The results also show that SAR is higher in the 4G network compared with the 5G network especially when the number is between 1 and 24, after which the SAR values increase significantly for both networks. Meaning, as the number of transceivers increases, the difference becomes insignificant. The 4G and the 5G simulations were done together, i.e., the results show the effect of the heterogeneousness of both networks on each other.

Lastly, the results show that the maximum SAR values for both 4G and 5G networks (80 μW/kg and 73 μW/kg, respectively) are significantly lower than the recommended standard limit (0.08W/kg) of the ICNIRP.

4) *Exposure Index:*

Exposure indexes were evaluated by using the EI Eq. in [5.19] and [5.20]. The uplink exposures are the ones caused by mobiles devices to the head and are evaluated using the local exposure. Whereas, the downlink exposures are mainly caused by the APs and are evaluated using whole-body exposure. The EIs were evaluated as the ratio of the computed to the SAR's exposure reference limits. The standard limits for the general public local and whole-body exposures used are 2W/kg and 0.08W/kg, respectively.

In Fig. 5.7, the average EI caused by the APs and UEs in both the 4G and the 5G networks against their transmit powers were evaluated. For the downlink power and the EI, logically, the transmit power of the 5G APs are reduced and are below the (0.25W) 24dBm, while the broader 4G APs transmit at (20W) 43dBm power. Thus, the EI from the 4G eNB is approximately 0.0006, while that of the 5G gNB is approximately 0.000008. Looking at the uplink power and the EI, all the wireless UEs (from 2G to 5G) are thoroughly tested for exposure limits compliance and signalling power limit of (0.25W) 24dBm before they are sold out. Thus, the EI from the 4G UEs is approximately $10^{-5}$, while that of the 5G gNB is approximately $10^{-6}$.

The exposures caused by UEs are higher than the ones caused by the transmitters. This is as a result of the farther distance between the APs and their users compared with the distance between the users and their UEs, despite that these APs transmit more power to the users. The power densities of the emissions reduce with the distance as supported by pathloss and inverse square law theories.

Also, the EI is lower due to the values of the denominators (i.e., the local and the whole-body limits) in the EI's formula.

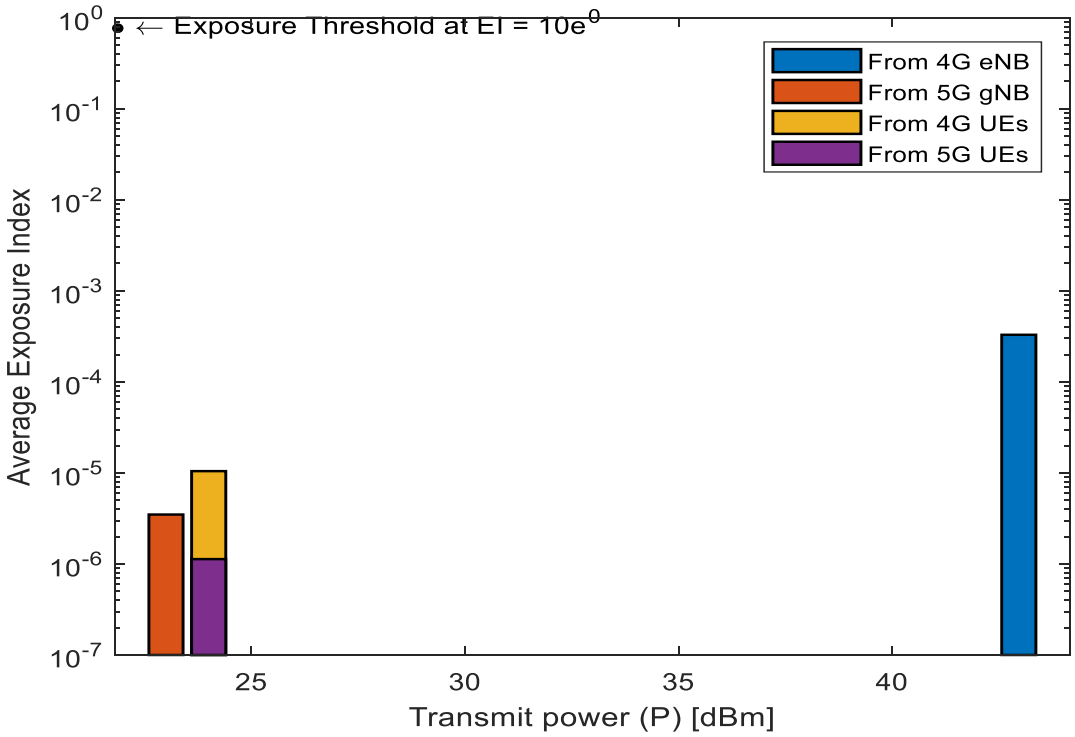


*Figure 5.7*: Average exposure index vs. transmit power.

It is also evident from the results that the exposure dosages of 5G networks are lower compared with that of 4G networks. Some of the reasons for this are that the 5G network uses a higher frequency band, brings higher densification; therefore it increases the capacity and reduces the coverage distance, thereby reducing power, transmission time and consequently the radiation exposure. Also worthy of note, is the threshold of EI derived to be $10^0 = 1$, based on the standard ERLs. All the 4G and the 5G networks EIs are found to be lower than this as depicted in Fig. 5.7 for both whole-body and the local RF-EMF exposures.

## 5.7. Chapter Summary

This chapter presents the impact of radiofrequency (RF) electromagnetic fields (EMF) radiation exposure induced by wireless networks, most importantly 5G cellular networks for both the uplink and downlink radio emissions using a novel simulation method that quantifies the realistic electromagnetic exposure of the human user. The EI is employed to characterize the EMF exposure taking into account the power density *S*, *SAR*; *E,* and *H* as well as considering the variability of other factors such as environment, the conductivity σ and the mass density of tissue $\boldsymbol{\rho}$. The simulated radiations emitted from the APs and UEs were analysed and compared with the threshold set by the ICNIRP to know the human exposure impact. The numerical simulation results reveal that the maximum radiation exposure emitted is far lower than the ICNIRP standard. It is shown that the exposure from UEs (uplink) is more compared with the ones due to the APs (downlink). EI can be minimised when there is an optimum power control scheme in the network as revealed in the power density received from the Aps as shown in Fig. 5.5. This is further revealed in the next chapter.

# Chapter 6

# 6. A Radiofrequency Electromagnetic Wave Radiation Exposure Minimisation Method in 5G Network: A Perspective of QoS Trade-Offs

## 6.1. Introduction

The 5G network is expected to improve the QoS of users in its network. To achieve this high gigabit-per-second (Gbps) data rate, 5G networks have been operating around the frequency of 6GHz. It is expected that future 5G networks will be deployed using the promising millimetre wave (mm-wave) communications band of 28 and 39 GHz. Operating in such high frequencies will reduce the coverage areas of the APs in the 5G network. Therefore, proper network planning is necessary and a large number of small cells is expected to make up for the reduced coverage area especially in crowded areas in the heart of the cities. This proliferation of APs and antenna such as massive MIMO brings about the needed SINR in the network along with a corresponding increase in the power density and unfortunately the challenges of the increase in the interference and exposure in the network as presented in Fig. 6.1 [82], [151]. However, compared to the previous generation of wireless generation networks, i.e., the existing third and fourth generation networks, the maximum transmit power is lower in 5G than the UE power levels [152].

RF-EMF exposure metric known as exposure index [15] is evaluated using the electric field strength, magnetic field strength, power density, SAR, as well as considering the variability of other factors such as environment, the conductivity and the mass density of tissue. The radiation emitted from APs and UEs is analysed and compared with the limits set by the ICNIRP [12].

*Figure 6.1: An architecture depicting radiation exposure in an ultra-dense 5G network*

In exposure management, there are many methods of reducing exposure such as transmission time reduction, power density minimisation, beamforming technique and data usage reduction etc. However, in 5G networks, it will be practically impossible to reduce the radiation exposure by minimising data usage since 5G is expected to solve the problem of data explosion. As established in Chapter 5, the impact of power control will great reduce UE transmit power and the RF-EMF radiations in the network. Thus, this chapter focuses on minimising further the transmission power/energy, hence, it minimises the EMF exposure and at the same time reduces the interference [21] in the network. The reduction factor for radiation EI in our work is evaluated as the power density. The proposed power control and optimisation algorithm minimises the characterized EI in the form of the power density in a simulated 5G network.

In this chapter, the RF-EMF radiation exposures induced in a 5G network is characterized by EI and evaluated with the power densities between the users and the APs in the network. To achieve a reasonable trade-off between radiation exposure and needed QoS amongst users in the network, the effects of lowering transmit power and lowering SINRs in the network were investigated by proposing an RF-EMF emission exposure reduction scheme that reduces the total EIs in the system. This scheme maintains the acceptable QoS with low EMF in both uplink

UL and DL transmissions. The proposed scheme uses an effective power control mechanism and optimisation solution in minimising the total EI in a 5G network subject to transmit power, QoS, interference and other constraints.

The performance of the proposed schemes was evaluated through simulations with RF-EMF and QoS metrics. The results show reduced users' interference and radiation exposure in the network while satisfying the users' target QoS. Also, the results are compared and discussed with the established global limits recommended by ICNIRP. This research work again increases the health awareness concerning radiation exposure of 5G wireless networks.

The main contributions of the chapter are as follows:

- Evaluation of the SAR and EI of the users in the 5G network using simulation analysis.
- Formulation of an optimisation problem that minimises the total EI of users in the network subject to some QoS constraints.
- Development of an EIPCA, a scheme that minimises the EI through the transmit and received powers in the network; and solves the radiation exposure problem.
- Evaluation and validation of the proposed algorithm by comparing its performance with a conventional 5G network power algorithm. Also, comparing the QoS and exposure results with the target QoS values and with the regulatory authorities' exposure thresholds, respectively.

## 6.2. Notations

In this subsection, the relevant notations used in the entire chapter are described. Table 6.1 highlights the list of notations.

*Table 6.1: List of notations*

| Symbol | Description |
|---|---|
| $l, L$ | AP, set of APs |
| $u$, $U$ | A user, User set |
| $c$, $C$ | Sub-channels, set of sub-channels |
| $b_{u,c}^{l}$ | Bandwidth of a subcarrier |
| $B$ | Total Bandwidth of the InP |
| $t, T$ | Time slot, time domain |

| | |
|---|---|
| $R_u^{min}$ | Minimum required data rate |
| $R_{u,c}^{l}$ | Data rate of user $u$ in AP $l$ |
| $I_u^{max}$ | Maximum interference limit |
| $I_{u,c}^{l}$ | Interference experienced by user $u$ in the sub-channel |
| $N_0$ | Noise power per unit bandwidth. |
| $x_{u,c}^{l}$ | Subcarrier allocation index of $u$ in the sub-channel |
| $h_{u,c}^{l}$ | Channel gain of user $u$ on subcarrier $c$ from the AP $l$ |
| $d_u^l$ | Distance of a user to the interfering APs |
| $A_u^l$ | Cross-sectional area of this emitted radio wave to the user |
| $P_{u,c,l}^{Tx}$, | Signaling power of user $u$ to the serving AP $l$ |
| $P_{u,c,l}^{Rx}$ | Received power of user $u$ from the serving AP $l$ |
| $p_{u,c}^{l}$ | Allocated power to a user $u$ as per its PRBs |
| $P_{ref}^{Tx}$ | Incident reference transmit power |
| $P_{ref}^{Rx}$ | Incident reference received power |
| $S_u^l$ | Power density of user $u$ |
| $E_u^l$ | Electric field strength of user $u$ |
| $Z_o$ | Characteristic impedance of free space |
| $SAR_{u,l}^{TX}$, $SAR_{u,l,}^{RX}$ | Averaged SAR of the $u$ user from UL, and from DL, respectively. |
| $T_{u,i,j,k}^{UL}$, $T_{u,i,j,k}^{DL}$ | Time of exposure in the uplink, time of exposure in the downlink |
| σ | Electrical conductivity of the tissue |
| $\rho$ | Tissue density |
| $PL_u$ | Pathloss between the AP and the user |
| α | Pathloss compensator factor |
| $f_c$ | Carrier frequency in MHz |
| $h_g$ | Antenna height |
| $G_T$ | Antenna gain |
| $\lambda$ | wavelength of the carrier frequency |
| $EI_u^l$ | EI of user $u$ from the transmitters and receivers |
| $\mathcal{M}$ | Number of PRBs allocated per user |
| $P_{UE}^{max}$ | Maximum power allowed in uplink transmission |
| $P_o$ | Power contained in one PRB |
| $\partial_{mcs}$ | Modulation code scheme dependent offset |
| $f(\Delta_i)$ | Closed-loop correction function |

## 6.3. System Model and Assumptions

The system model considered in this chapter is illustrated in Fig. 6.2. The considered scenario assumes a typical ultra-dense 5G network environment with a high number of APs $|L|$. $L$ is the set of APs serving various number of users as expected in any urban centre. These APs propagate radio wave signals to a set of users $U$ that are assumed to be static, hence, these users are susceptible to radiation exposure within a distance $d_u^l$, and cross-sectional area $A_u^l$ . We denote the signalling power of user $u$ to the serving AP $l$ in the uplink transmission as $P_{u,c,l}^{Tx}$, and $P_{u,c,l}^{Rx}$ is the received power of user $u$ from the serving AP $l$ in the downlink transmission. The exposure radiation on each of the users is equivalent to the sum of the interfering power densities generated by both the APs and the user's device at that particular location.

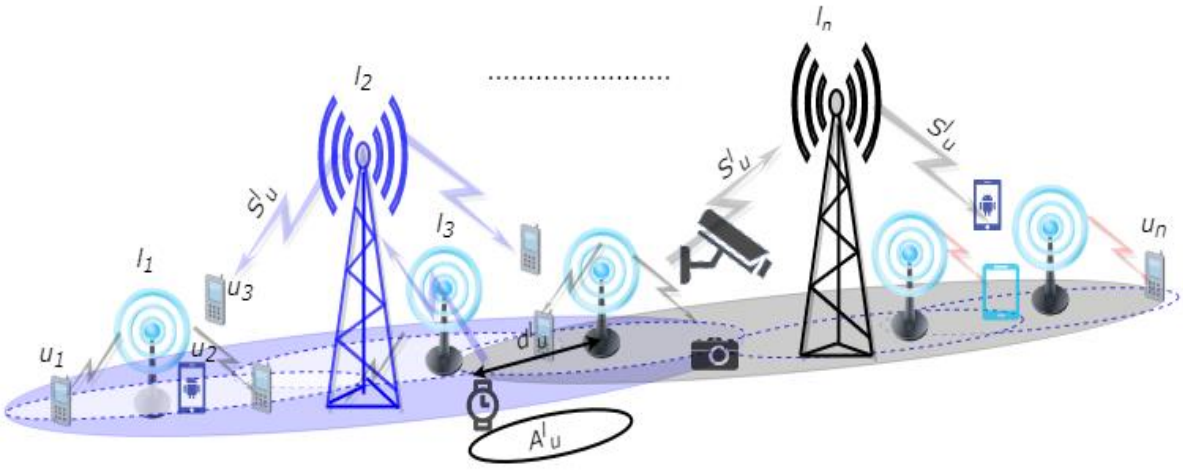


*Figure 6.2: System model of a typical ultra-dense 5G network.*

The spectral power density, $S_u^l$ $(W/m^2)$ is the ratio of EIRP incident perpendicular to a surface and the cross-sectional area $(A_u^l)$ of the surface of the radiated radio wave. The spectral power density closed-form expression is given as [11],

$$S_u^l = \frac{P_{Tx} * G_T}{4\pi {d_u^l}^2} = \frac{P_{Tx} * G_T}{A_u^l} = \frac{|E_u^l|^2}{Z_o} \tag{6.1}$$

where $Z_o$ is the characteristic impedance of vacuum which is 120πΩ = 377Ω. $E_u^l$ (V/m) is the user's E-field strength of the radiated radiofrequency electromagnetic wave. Therefore, $E_u^l$ is expressed as.

$$E_u^l = \sqrt{Z_o * (\frac{P_{Tx} * G_T}{4\pi {d_u^l}^2})}. \tag{6.2}$$

The $SAR$[W/kg] is the rate of energy absorbed by or deposited per unit mass per unit time and it is derived from the induced electric field strength using the electrical conductivity of the tissue σ (S/m) and the tissue density $\rho$ (kg/m³), which are assumed constant for all the users in the network. Consequently, $SAR_u^l$ is expressed as

$$SAR_u^l = |E_u^l|^2 * \frac{\sigma}{\rho} = \left| \sqrt{Z_o * \left(\frac{P_T * G_T}{4\pi {d_u^l}^2}\right)} \right|^2 * \frac{\sigma}{\rho}. \tag{6.3}$$

Finally, the EI is evaluated in Eq. (6.4) as the ratio of the evaluated SAR taken for an average duration of 6 minutes interval or local exposure or 30 minutes interval for whole-body exposure and the corresponding maximum limit [127].

$$EI_u^l = \frac{SAR_{u_{evaluated}}^l}{SAR_{max\ limit}} \tag{6.4}$$

The ICNIRP defined the SAR maximum limits to be 2W/kg for the local exposure and 0.08W/kg for the whole-body exposure

## 6.4. Problem Formulation

Herein, the uplink of a multiuser 5G network is considered as shown in Fig. 6.2 where single-antenna APs communicate with a set of users, $U$ randomly distributed and with a single-antenna UEs. The network uses a total bandwidth $B$ divided into $C$ equal subcarriers. The time is split into $T$, each of length $t$. A subcarrier can be assigned to at most one user in a time domain but a user can have more than one subcarrier in a $T$ i.e. more than one PRB ($T * C$). Hence, the throughput located to a user $u$ in RAT $l$ can be expressed as [149]:

$$R_{u,c}^{l} = \sum_{t=1}^{|T|}\sum_{c=1}^{|C|} x_{u,c}^{l}(t) b_{u,c}^{l}(t)\, log_2\left(1 + \frac{p_{u,c}^{l}(t)\left|h_{u,c}^{l}\right|^2(t)}{N_0 + I_{u,c}^{l}(t)}\right) \quad \forall u \in U, \forall l \in \mathrm{L} \quad (6.5)$$

where $b_{u,c}^{l}(t)$ represents the bandwidth of a subcarrier, $p_{u,c}^{l}(t)$ and $\left|h_{u,c}^{l}\right|^2(t)$ denotes the transmit power and channel gain, respectively, of user $u$ on sub-channel $c$ in RAT $l$ at time $t$.

The parameter $x_{u,c}^{l}$ represents the subcarrier allocation index of user $u$, such that $x_{u,c}^{l}(t) = 1$ if sub-channel $c$ is allocated to user $u$ in RAT $l$ at time $t$, otherwise, $x_{u,c}^{l}(t) = 0$. $N_0$ is the noise power per unit bandwidth. Additionally, $I_{u,c}^{l}(t)$ is the interference from users transmitting on sub-channel $c$ at time domain $t$ in the neighbouring cells such that

$$I_{u,c}^{l}(t) = \sum_{v=1, v\neq l}^{|L|} p_{u,c}^{v}(t)\left|h_{u,(v),c}^{l}\right|^2(t) \quad (6.6)$$

where $\left|h_{u,(v),c}^{l}\right|^2(t)$ denotes the channel gain of user $u$ on the sub-channel $c$ in cell $v$ to the AP in RAT $l$, while $|L|$ represents the number of RATs in the network.

The total EI exposure of the system can be expressed as in [128]

$$EI_{u}^{l} = \sum_{t}^{|T|}\sum_{u}^{|U|}\sum_{l}^{|L|}\left[T_{u,t,l}^{UL} * SAR_{u,l}^{TX}\frac{P_{u,c,l}^{Tx}}{P_{ref}^{Tx}} + T_{u,t,l}^{DL} * SAR_{u,l,}^{RX}\frac{P_{u,c,l}^{Rx}}{P_{ref}^{Rx}}\right] \quad (6.7)$$

where $EI_{u}^{l}$ denotes the contribution of user $u$ in sector RAT $l$ to the EI. $SAR_{u,l}^{TX}$ is the localised averaged SAR of the user $u$ mobile device (from UL). $SAR_{u,l,}^{RX}$ is the whole-body averaged SAR of the user $u$ mobile device (from DL), while $P_{ref}^{Tx}$ and $P_{ref}^{Rx}$ represent the incident reference transmit and received powers. $P_{u,c,l}^{Tx}$ is the signalling power of the user $u$ to the serving AP $l$ in the uplink transmission, $P_{u,c,l}^{Rx}$ and is the received power of the user $u$ from the serving AP $l$ in the downlink transmission. $T_{u,i,j,k}^{UL}$ is the time of exposure and posture accounted for in the uplink, while $T_{u,i,j,k}^{DL}$ is the time of exposure and posture accounted for in the downlink.

Moreover, the signaling power $P_{u,c,l}^{Tx}$ and the received power $P_{u,c,l}^{Rx}$ can be computed using power control as stated below [100]:

$$P_{u,c,l}^{Tx} = min\{P_{\underset{UE}{max}}; P_o + 10\,log_{10}\,M + \alpha * PL_u + \partial_{mcs} + f(\Delta_i)\} \quad [d_{Bm}] \tag{6.8}$$

$$P_{u,c,l}^{Rx} = P_o + \alpha * PL_u \qquad [d_{Bm}] \tag{6.9}$$

where $P_{max}$ depends on the UE and is the maximum power allowed in uplink transmission. $M$ is the number of PRBs allocated per user. $P_o$ is cell-specific and is the power contained in one PRB. $\alpha$ is the pathloss compensation factor and ranges between 0 and 1. $PL_u$ is the estimated pathloss for the UE. $\partial_{mcs}$ is the modulation code scheme dependent offset and it is UE specific. $f(\Delta_i)$ is the closed-loop correction function.

Consequently, the RF-EMF emission exposure minimisation scheme aims at decreasing the total EI in the network, the objective function of the optimisation problem is stated in Eq. (6.10),

$$\min_{P,t} \sum_{l}^{L} \sum_{u}^{U} (EI_u^l) \tag{6.10}$$

Subject to

$$\text{C1: } b_{u,c}^l \sum_{u}^{U} \sum_{c}^{C} x_{u,c}^l(t)\, log_2 \left(1 + \frac{p_{u,c}^l(t) \left|h_{u,c}^l\right|^2(t)}{N_0 + I_{u,c}^l(t)}\right) \leq B \qquad \forall l \in L, \forall t \in T,$$

$$\text{C2: } \sum_{u=1}^{U} \sum_{c=1}^{C} x_{u,c}^l(t) P_{u,c}^l(t) \leq P_u^{max} \qquad \forall l \in L, \forall t \in T,$$

$$\text{C3: } \sum_{u}^{U} x_{u,c}^l(t) \leq 1, \qquad \forall l \in L, \forall c \in C, \forall t \in T,$$

$$\text{C4: } x_{u,c}^l(t) \sum_{u}^{U} \left((I_{u,c}^l(t)\right) \leq I_u^{max} \qquad \forall l \in L, \forall c \in C, \forall t \in T,$$

$$C5\text{: } R_u^{min} \leq R_{u,c}^l \qquad \forall l \in L, \forall u \in U, \forall c \in C.$$

C1 is the bandwidth constraint, it ensures that the total PRBs allocated to all users do not exceed the network bandwidth. C2 is the power constraint, it indicates that

the total power budget is lesser than the maximum power threshold. C3 is the sub-channel allocation constraint. C4 is the interference constraint, it ensures that the interference threshold, $I_u^{max}$ is not exceeded, and C5 is the target data rate constraint for each user $u$. The objective function in Eq. (6.10) is formulated as a MINLP and the EI power control algorithm solves the problem by minimising the EI without compromising the QoS of the users.

## 6.5. Exposure Minimisation and QoS Trade-Offs using Power Control Methods in 5G Network.

### 6.5.1. Exposure Index Power Control Algorithm (EIPCA)

In the proposed algorithm, the optimisation problem in Eq. (6.10) is solved for by determining the feasible power solution needed to achieve the needed SINRs that give the required data rates for each user. Since EI is a function of power and time of transmission, the EI is minimised by optimising the transmit power and the transmit time. More importantly, for all users in the network, there is an agreed minimum data rate needed for the class of service/slice/use-case the UE is offered. Therefore, while the objective is to reduce both the transmit power and the transmission time of signals to minimise the total EIs of the user as given in Eq. (6.10), the required data rate must be satisfied according to constraint C5. The total bandwidth constraint set across the whole PRBs for all the users in the network must also be satisfied as in C1. The objective function in Eq. (6.10) also ensures that the total power budget is less than the maximum power limit as specified in C2. This is made possible with the pathloss compensation factor (α) and power control in Eqs. (6.8) and (6.9). Consequently, the subcarrier binary allocation and interference threshold constraints must be satisfied while optimising the EI as described in Algorithm 1 in Table 6.2. The defined objective function is solved until feasibility and optimality. The set constraints are evaluated at every MINLP solution, the MINLP problem is solved until all the constraints are satisfied.

*Table 6.2: EI power control algorithm.*

**Algorithm 1**. EI power control algorithm

**Inputs**: $G_T$, $Z_o$, $P_o$, α, $B$, $f_c$, λ, hg, $D$, $U$, $L$, $C$, $d_u$,

**Outputs:** $S_u^l$, $SAR_u^l$, $E_u^l$, $R_{u,c}^l$, $I_{u,c}^l$ , $EI_u^l$

1. Given the set $U$ where $u \in U$
2. **for** each user u **do**
3. Initialise the values of $P_u^{max}, \rho, \sigma$, and $SAR_{\max limits}$
4. Set $I_{u,c}^l = 0,\ t = T$, and $\forall c = 1,2,3,\ldots . C$
5. **while** $P_{u,c}^l \leq P_u^{max}$ ∀ APs and $u$ do
6. $I_{u,c}^l \leq I_u^{max}$
7. $\sum_c^C b_{u,c}^l(t) \leq B$
8. $R_u^{min} \leq R_{u,c}^l$
9. **end while**
10. Solve for the $EI_u^l$ as in Eq. 6.10.
11. **if** $R_u^{min} \leq R_{u,c}^l$ **then**
12. Determine $EI_u^l$
13. Terminate if the optimal solution is found
14. **else**
15. Increase $p_{u,c}^l$ or set $p_{u,c}^l = P_u^{max}$
16. **end if**
17. **end for**

## 6.6. A Conventional 5G Network Heuristic Power Algorithm

In this section, the benchmark algorithm which is a conventional 5G network power algorithm is considered in addition to the proposed EIPCA for comparison purposes. This reference algorithm is an idea adapted from [153] where equal power is allocated across all the PRBs.

In the approach, the resource allocation is proposed as an MINLP optimisation problem with fixed gain to the time-dependent channels. The objective is to minimise the total transmit power or to maximize total utility subject to rate and power constraints. This is required to satisfy all the requirements and optimally achieve the objective. As a result, all channels and users are allocated the required SNR-rate/utilities even despite bad channel conditions which can reduce the network efficiency such as the interference and RF-EMF exposure in the network. Unlike the proposed scheme/algorithm, the QoS requirements, or the average QoS requirements of some users might be optimal, however, the network challenges such as the RF-EMF might not be optimal. The conventional 5G network power allocation algorithm is presented in algorithm 2 in Table 6.3.

*Table 6.3: Conventional 5G network power algorithm [153].*

| Algorithm 2. Conventional 5G network power algorithm |
|---|
| Inputs: $G_{\boldsymbol{T}}$, $Z_o$, $P_{\boldsymbol{o}}$, ɑ, $B$, , $f_{\boldsymbol{c}}$, $\lambda$, $hg$, $D$, $U$, $L$, $C$, $d_{\boldsymbol{u}}$, |
| Outputs: $S_u^l$, $SAR_u^l$, $E_u^l$, $R_{u,c}^l$, $I_{u,c}^l$ , $EI_u^l$ |
| 1. Initialisation: $k = 0$, $p^k = p_{u,c}^l = P/C$ |
| 2. while sub-channel allocation changes, |
| 3. $u^k(c) = \max_{u \in U} b_{u,c}^l \, log_2\left(1 + \frac{p_{u,c}^l(t)\left\|h_{u,c}^l\right\|^2(t)}{N_0 + I_{u,c}^l(t)}\right), \ \forall c \in C.$ |
| 4. solve the optimisation problem in (6.10) |
| 5. $k = k + 1$ |
| 6. $(u^{\boldsymbol{k-1}}, p^k)$ is an optimal power allocation. |

## 6.7. Result and Discussions

In this section, the performance of the proposed EIPCA is evaluated and the results are compared with that of a conventional 5G network power algorithm for benchmarking the proposed algorithm. The simulation parameters used for the experiments, the performance metrics and the performance evaluation are discussed in the following sub-sections.

### 6.7.1. Simulation Environment and Parameters

In this section, the system model was simulated and the performance of the proposed EI power control algorithm was evaluated. The simulation parameters used for the experiment are as shown in Table 6.4.

*Table 6.4: Simulation parameters and values.*

| **Parameter** | **Value** |
|---|---|
| Number of RATs | 3 |
| Number of APs/RAT | 2 |
| Number of Users | Random |
| Spectrum allocation | 80MHz |
| Carrier frequency | 6GHz |
| Channel model | 3GPP |
| Data rate limit ($R_s^{min}$) | 2.5Mbps |
| Max UE power ($P_u^{max}$) | 0.25W [24dBm] |
| Max AP Tx power | 20W [43dBm], 0.25 W [24dBm] |
| $P_{ref}$ | 1W |
| Tolerable interference ($I_u^{max}$) | -116dBm |
| Slot duration (T) | 1ms |
| Scheduling frame | 10ms |
| Overall interval | 20s |
| Cell-level user distribution | Uniform |
| The conductivity of the tissue (σ) | 0.97S/m |
| The mass density of the tissue (***ρ***) | 1000kg/m³ |
| Characteristic Impedance ($Z_{o)}$ | 120πΩ =377Ω |
| Power Control | Open-loop |
| Pathloss exponent (α) | 0.7 |
| Antenna height | 35m, 50m |
| UE height | 1.5m |
| Noise spectral density (*No*) | 10-13W/Hz [-100 dBm/Hz] |
| Log-normal shadow fading | 8dB standard deviation |
| Cell coverage radius | 50m, 500m |

In performing the experiment, a wireless network with 5G RATs and 4G RATs as the umbrella network in a MATLAB [125] environment was simulated. A random number of users were uniformly distributed in the coverage area of radius 50m for the 5G APs (gNobeB) and 500m for the 4G APs (eNobeB). The radiated SAR, EI to each of the network users were evaluated using the system parameters. The proposed algorithm minimised the overall EI of these users taking into consideration the received and transmit powers, minimum data rate, and other QoS constraints

## 6.7.2. Performance Evaluation

In this sub-section, the performance of the proposed scheme is discussed. And for comparison, a conventional 5G network algorithm (C5GNA) where equal power is allocated across all the PRBs is used to benchmark our proposed algorithm. The simulation results are presented with different performance metrics below.

*1.) Impact of Network Interference Level on Users:*

The interference level and the radiation exposure level in the network are significantly related. Both are a function of the transmit power of both uplink and downlink transmissions. Likewise, the number of users in the network increases the total transmit power in the system, consequently, the increase in the number of users in the network leads to additional interference in the network which affects the users. The result in Fig. 6.3 compares the impact of the number of users in the network on the interference level of users for the proposed and the benchmarked schemes. The result shows that the interference level is higher in the conventional 5G network when compared with the optimised value for the same number of UEs/APs. The sum of tolerable interference increases from $10^{-11}$ W to $10^{-9}$ W for the proposed EIPCA and from around $10^{-9}$ W to $10^{-8}$ W for the C5GNA when the users per AP increase from 10 to 60 users/AP.

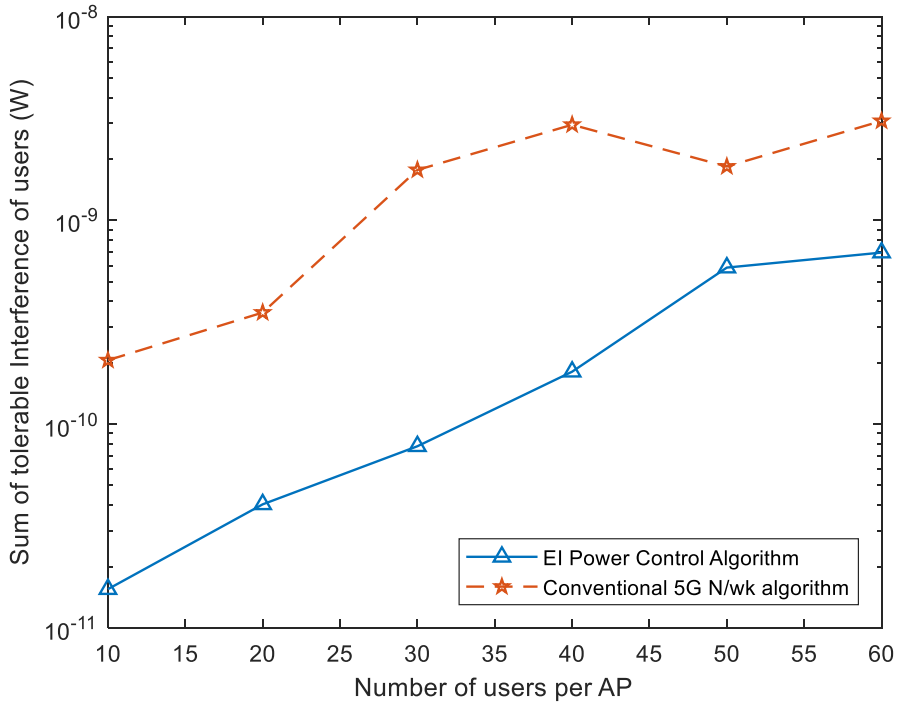


*Figure 6.3: Tolerable interference of users vs. the number of users.*

Also, the interference is lower than the tolerable interference limit of -116dBm ($2.5 * 10^{-15}$ W). This further shows that the interference is proportional to the RF-EMF radiation in the network. It means that minimising the RF-EMF radiation exposure reduces the interference in the network as well.

*2.) Effect of Power Density on the entire network:*

The power density of the network is the measure of the power transmitted within a particular area. The more the power in a location, the more the power density, and the more the radiation exposures absorbed by the body. The ultra-denseness and antenna proliferation of antennas of the UEs and APs in locations such as urban cities will increase the RF-EMF exposure. This is a rising complexity in the future of 5G and next-generation networks (NGN). Therefore, the result in Fig. 6.4 compares the effect of the number of users in the network on the total power density in the network for the proposed and the benchmarked schemes.

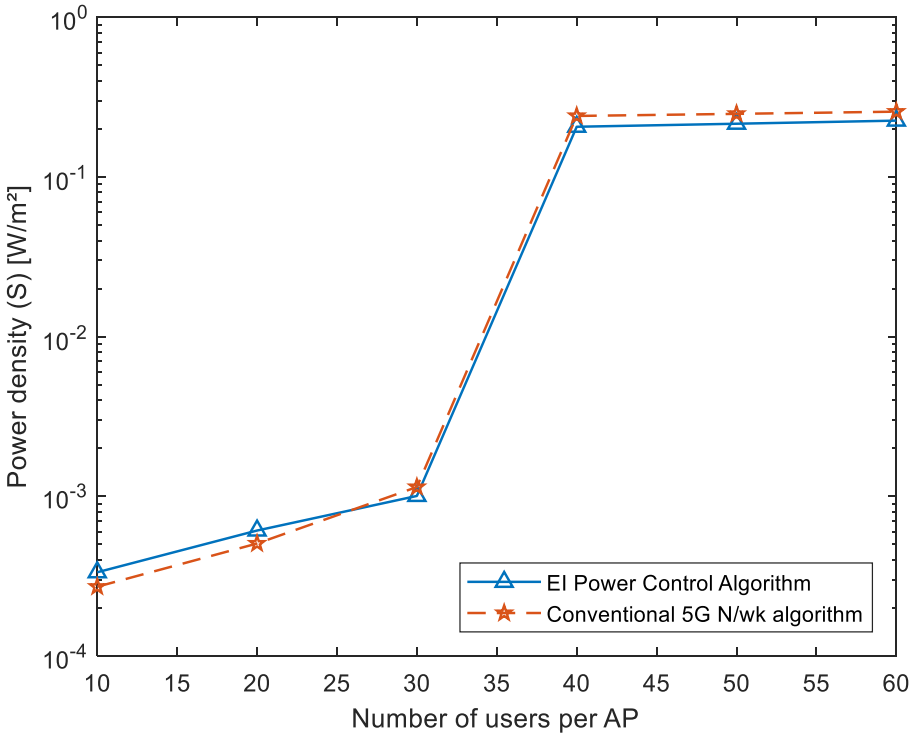


*Figure 6.4*: Tolerable power density of users vs. number of users per AP

It is evident from Fig. 6.4 that as the users and APs increase in the network, the power density experienced by a user at a point and the radiation exposure increase. The power density increases from about $0.3 * 10^{-3}$ W/m² to around $10^{-3}$ W/m² for both schemes. As the network becomes more crowded, there is a sharp increase in the power density from $10^{-3}$ W/m² to about 0.25 W/m² and 0.29 W/m² for the EIPCA and the C5GNA, respectively. As the network gets denser with users/AP, there is an insignificant increase in the power density from 0.25 W/m² to 0.27 W/m² and from 0.27 W/m² to 0.29 W/m² for the EIPCA and the C5GNA, respectively. Hence, the power density in the proposed EIPCA out-performed the bench-marked C5GNA scheme with its lower values as represented in the results.

From this, it can be concluded that the denser the network, the higher the power density and radiation exposure. Therefore, the main issue concerning RF-EMF radiation of an area is more of the ultra-denseness of the network (such as massive MIMO) than the radio access technology in that location. Although next-generation RATs use higher frequency in the radiofrequency C-band as well as the millimetre wave frequency range, however, it has been shown that the higher frequency is compensated for by its shorter wavelength [154]. Furthermore, Fig. 6.4

shows that the maximum power density experienced at any point in the network is lower than the limit of 10 W/m² set by the FCC for frequency above 6GHz [13] [155].

*3.) Impact of QoS (in terms of Data Rate) trade-offs on Users:*

QoS and QoE are the foremost metrics in wireless communication. In determining the efficiency of the network, QoS parameters such as throughput (data rate), latency, bit rate, jitter, packet loss, interference, radiation, etc., are important and are used to validate the performance of proposed schemes. In this chapter, the total EI in the network is minimised while guaranteeing the QoS requirement, which is the target data rates of the users. The result in Fig. 6.5 validates the impact on the QoS trade-off.

Figure 6.5 shows the graph of the data rate (i.e., QoS) of users in the network against the EI. The data rates are lower in the proposed algorithm as compared with the conventional 5G network algorithm. The users' data rates concentrate between 3 Mbps and 3.75 Mbps for the proposed EIPCA and between 4.45 Mbps and 5.3 Mbps for the C5GNA. However, the proposed algorithm offers more data rate than the needed QoS limit of 2.5Mbps for all the users.

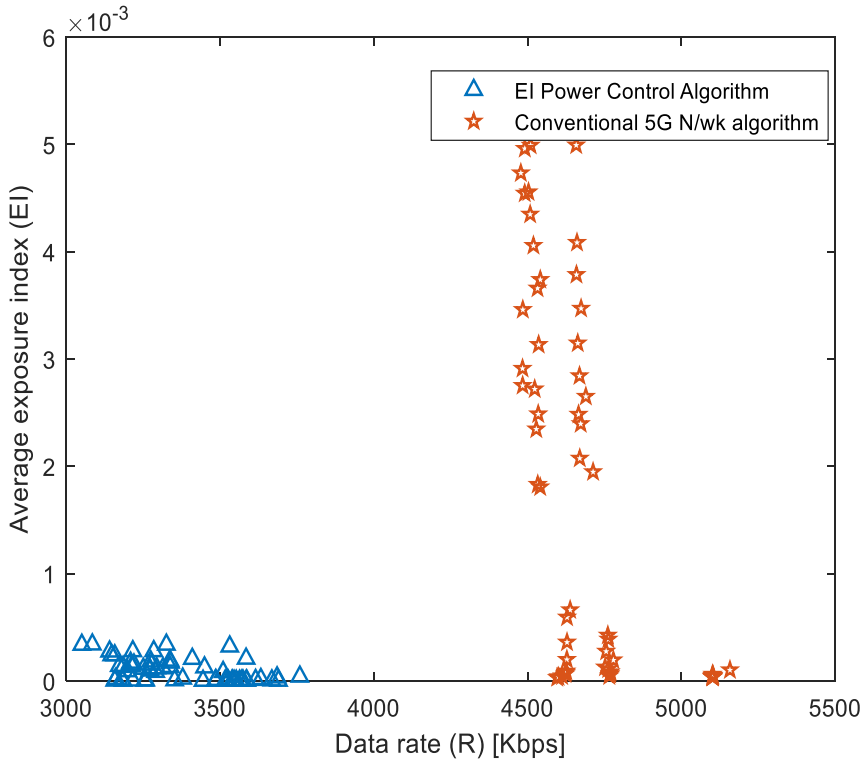


*Figure 6.5*: Average users' data rate (QoS) vs. users' EI.

Also, the EI is quite lower in the proposed algorithm as compared with the benchmarked algorithm. The average users' EI concentrate between $0.1 * 10^{-15}$ for the proposed EIPCA and $0.5 * 10^{-15}$ for the C5GNA. Furthermore, the C5GNA results demarcate the users into two. The users in the upper part of the graph are mostly the cell-edge users with lower data rates and higher EIs. This is because the cell edge users are transmitting at maximum power. Therefore, it can be inferred that the proposed algorithm offers good QoS (i.e., the required data rate and lower EI) in the network. It is worthy of note that all of the EIs calculated comply with the standard limits recommended by the IEEE Std. C95.1 [156] and the ICNIRP [101].

*4.) Impact of SAR on Network:*

Again, the SAR is the measure of electromagnetic power absorbed in human tissue per unit mass and depends largely on the radiated electric field. Fig. 6.6 presents the performance of the proposed scheme EIPCA and the C5GNA using the SAR in the network as the metric.

Similar to the QoS metric in Fig. 6.5, as the users and APs increase in the network, the SAR experienced by a user at a point and the total SARs in the network increase. Also, the SARs of the different users is reduced in the proposed algorithm compared with the conventional 5G network algorithm. The SAR is quite lower for the C5GNA when the user/AP in the network is between 10 and 25. The SAR increases from around $0.2 * 10^{-5}$ W/kg to $0.3 * 10^{-4}$ W/kg for the EIPCA and around $0.2 * 10^{-5}$ W/kg to $1 * 10^{-5}$ W/kg for the C5GNA when the number of APs and UEs increase from 10 to 20.

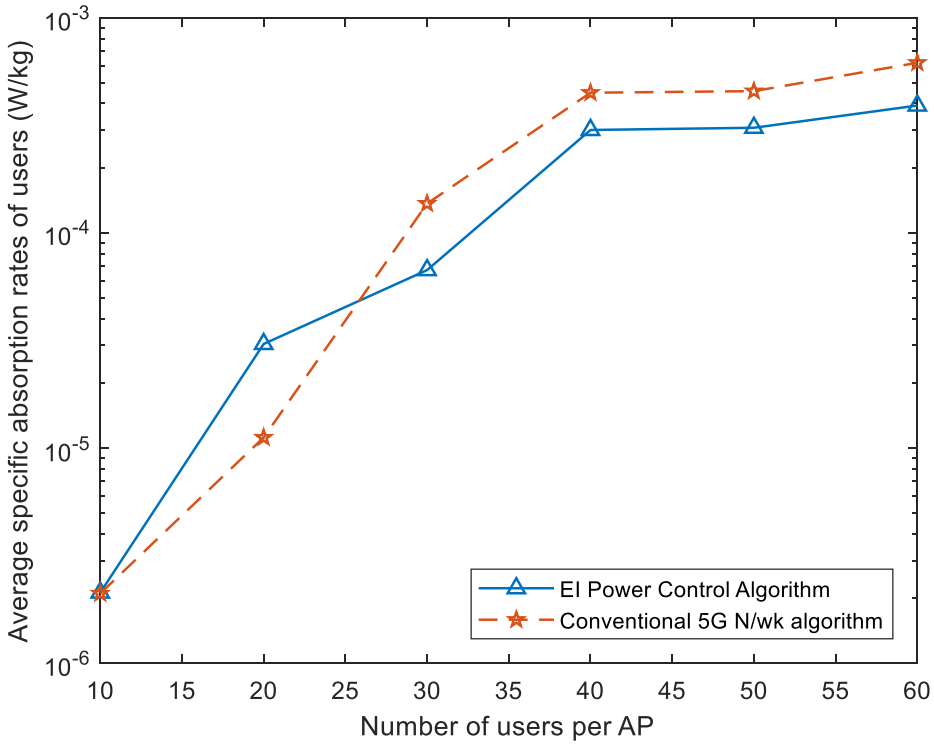


*Figure 6.6*: Specific absorption rates of users vs. the number of users.

However, when the network becomes denser, the C5GNA has a significant increase in the level of SAR especially from 25 users per AP. There is a sharp increase in the SAR values from $0.5 * 10^{-4}\text{W/kg}$ to $0.6 * 10^{-3}\text{W/kg}$ and $0.5 * 10^{-4}\text{W/kg}$ to $0.4 * 10^{-3}\text{W/kg}$ for the C5GNA and the EIPCA, respectively when the number increases from 25 users/AP upward. Meaning, as the number of transceivers increases, the EIPCA performance becomes substantial. This validates the performance of the proposed scheme in this chapter. It also shows the relationship between the power density ($\text{W}/m^2$), SAR ($\text{W}/kg$) and the EI radiated in wireless networks. More importantly, all the calculated SARs are in compliance with the standard and limit of $0.08\text{W/kg}$ advised by ICNIRP.

## 6.8. Chapter Summary

This chapter presented a proposed power control algorithm that minimised the radiation exposure in the 5G networks. The algorithm solves an optimisation problem that minimised the RF-EMF radiation in the network taking into account the QoS constraints such as the data rate, power and interference limits. The EI, power density, SAR and the data rate were employed in evaluating the performance of the proposed scheme. Simulation results showed that the EIs and SARs radiated in the network are minimised using the transmit power without compromising the QoS of the users. Results also demonstrated that the recommended exposure limits advised by the ICNIRP [101] and IEEE Std. C95.1 [14] are complied with in the simulated 5G network.

.

# Chapter 7

# 7. Conclusion

## 7.1. Introduction

In this chapter, a summary of what has been reported in the preceding chapters of this dissertation is presented. The chapter concludes the research work and discusses the extension that can be made on this work in the future to improve and evaluate the radiofrequency and resource management schemes proposed in this dissertation.

## 7.2. Final Conclusion

The 5G wireless network is expected to bring a lot of new network services with a large amount of variation in network resource requests. The current network model will not be able to meet these requirements. To cater for the requirements of emerging network services, it is necessary to employ Network Slicing as an enabling technology for managing resources flexibly and efficiently in 5G networks. However, resource management in network slicing has not been judiciously explored so as to provide satisfactory flexibility and efficiency.

Thus, this dissertation has explored new methods for radiofrequency EMF and resource management schemes in 5G sliced networks. And to that end, four schemes have been proposed. The first scheme uses the priorities of the users and that of the slice they belong to alongside their QoS requirements to admit users and allocate network resources. An admission control scheme is developed for effective allocation of network resources for sliced 5G network considering both the inter-slice and intra-slice priorities. The proposed admission control uses a heuristic mechanism to improve QoE, enhance resource utilisation efficiency and improve the throughput of users. Finally, the results obtained demonstrate the effectiveness of the proposed algorithm in terms of increase in QoE experienced by

users, improvement in the number of admitted users, and the positive effect of users' and slice prioritisation.

The second scheme addresses the problem of interference resulting from shared spectrum resources (co-channel interference among the users in the network) and takes into consideration the different slices transmit power as a result of the various slices QoS requirements to enhance the performance of the network. A novel slicing carrier assignment scheme has been developed where an optimisation problem is formulated to minimise the total transmit power while guaranteeing a minimum data rate requirement for each slice. The proposed SCAS technique has been formulated as an MINLP optimisation problem that minimises the DL transmit power subject to QoS constraints, interference thresholds, gNB power limits and the sub-channel orthogonality constraints. The scheme assigns sub-channels to users considering the transmit power level of the neighbouring sub-channel before allocating the sub-channel to a user by comparing the transmit power threshold of the slice the user belongs to. Simulation results show that the proposed scheme reduces the effect of tolerable interference on the users, increase the number of admitted users and provide the target data rate of the slice for its users.

The third scheme studied the challenges of RF-EMF radiation exposure induced by 5G networks and other wireless networks. The impact of RF-EMF-radiation exposure from the uplink and downlink radio transmissions was presented using a novel simulation method that quantifies the realistic electromagnetic exposure of the user. By using the calculated *E*, *H*, *S*, as well as the *SAR*; the EI was used to characterize the RF-EMF exposure considering other factors such as environment, the mass density of tissue, the conductivity. The simulated radiation exposure of the UEs and the APs were analysed and compared with the threshold set by the regulatory authorities such as FCC, IEEE, and ICNIRP to ascertain the level of the exposure impact. The numerical results show that the maximum radiation exposure emitted complies with these standards and limits. It also shows that EI in the network can be minimised when it employs an optimum power control scheme. The uplink and the downlink exposures were also compared in different RATs such as 4G and 5G networks.

Finally, the fourth scheme also addressed the challenges of RF-EMF radiation exposures induced by a 5G wireless network. It presented a proposed

power control algorithm that minimises the radiation exposure in a 5G network. This algorithm solved an optimisation problem that minimised the RF-EMF radiation in the network taking into account the QoS constraints such as the data rate, power and interference limits. The EI, power density, SAR and the data rate were employed in evaluating the performance of the proposed scheme. Simulation results showed that the EIs and SARs radiated in the network are minimised using the transmit power without compromising the QoS of the users. Results also demonstrated that the recommended exposure limits advised by the ICNIRP [101] and IEEE Std. C95.1 [14] are complied with in the simulated 5G network.

## 7.3. Future work

The following aspects of the proposed schemes can be considered for future work.

### 7.3.1. Resource Allocation Strategy for 5G Network Slices Using Admission Control with Prioritisation

Future works can be extended to a HetNet. This can involve multiple 5G gNB and 5G small cells belonging to different MVNOs. This will make it a multi-tier, multitenancy and heterogeneous network.

In this work, admission is performed and resources are allocated to users based on their assigned priorities using only one QoS parameter (minimum and maximum data rate). In the future, it is recommended that two or more QoS parameters (such as latency and data rate) be used in performing the experiment.

### 7.3.2. Dynamic Slicing and Scheduling for 5G Network Using Joint Power and Sub-Carrier Allocation

The scope of this dissertation is limited to a downlink transmission in the 5G wireless network. For future work, power allocation and the users' interference can be considered in both the uplink and downlink transmission channels. Additionally, future work can be carried out in a HetNet, considering both the co-channel interference and adjacent channel interference.

### 7.3.3. RF-EMF Radiation Exposure Assessment and Minimisation Method of 5G Network

This subsection covers the future work relating to Chapter 5's RF-EMF radiation exposure assessment of 5G network: analysis, computation and mitigation methods; and Chapter 6's A radiofrequency electromagnetic wave radiation exposure minimisation method in 5G network: a perspective of QoS trade-offs.

With the scope, time, resources available, the study was limited to computational analyses. For future work, it is recommended that some field measurements (the use of a SA or dosimeter) be done in the locations of the newly deployed 5G APs around Cape Town, South Africa. These field measurements would be ideal for comparison with the work already done in this dissertation. Although some field measurements in literature were used as a comparison as stated in Section 5.6.2.1.

The future work should also consider mobile UEs, as only static UEs were considered in the simulated experiments.

Lastly, it will be interesting to consider and analyse the RF-EMF exposure in a 5G network using the millimeter-wave frequency band, i.e., the above 6 GHz to 28 GHz frequency band.

# References


[1] Wikipedia, “Industrial Revolution,” April 2019. [Online]. Available: https://en.wikipedia.org/wiki/Industrial_Revolution. [Accessed 30 May 2019].

[2] Mohammad Meraj ud in Mir and Dr. Sumit Kumar, “Evolution of Mobile Wireless Technology from 0G to 5G,” *International Journal of Computer science and Infomation Technologies,* vol. 6, no. 3, pp. 2545-2551, 2015.

[3] Ericsson, “5G Wireless Access: An Overviews, White Paper,” January 2020.

[4] Cisco whitepaper, “Cisco Visual Network Index: Forecast and Methodology, 2016-2021,” pp. 1-17, 5 June 2017.

[5] Nokia Bell Labs, White Paper, “The Race to 5G and Enterprise Readiness,” July 2020.

[6] I. F. Akyildiz, S. Nie, S.-C. Lin, and M. Chandrasekaran, “5G Roadmap: 10 Key Enabling Technologies,” *Computer Networks,* vol. 106, pp. 17-48, 2016. https://doi.org/10.1016/j.comnet.2016.06.010.

[7] P. Mandl, P. Pezzei and E. Leitgeb, “Selected Health and Law Issues Regarding Mobile Communications with Respect to 5G,” in *2018 International Conference on Broadband Communications for Next Generation Networks and Multimedia Applications (CoBCom)*, Graz, 2018, pp. 1-5.

[8] S. Okuyucu, K. Yeğın, M. Seçmen and B. Özbakiş, “Parametric SAR study for 4G cellular phone applications,” in *2018 22nd International Microwave and Radar Conference (MIKON)*, Poznan, 2018, pp. 308-311.

[9] P. Joshi, D. Colombi, B. Thors, L. Larsson and C. Törnevik, “Output Power Levels of 4G User Equipment and Implications on Realistic RF EMF Exposure Assessments,” *IEEE Access,* vol. 5, pp. 4545-4550, 2017, doi: 10.1109/ACCESS.2017.2682422.

[10] Z. Kaijage and M. Kissaka,, “Assessment of Radio-Frequency Radiation Exposure Levels: A Case of Selected Mobile Base Stations in Dar es Salaam, Tanzania,” in *2018 IST-Africa Week Conference (IST-Africa)*, Gaborone, 2018, pp. 1-8.

[11] IARC, Non-ionizing Radiation, Part 2: Radiofrequency Electromagnetic Fields. IARC Monographs on the Evaluation of Carcinogenic Risks to Humans, vol. 102, Lyon: International Agency for Research on Cancer, 2013, pp. 1-481.

[12] The International Commission on Non-Ionizing Radiation Protection, “Guidelines for limiting exposure to time-varying electric, magnetic, and

electromagnetic fields (up to 300 GHz)," *Health Phys,* vol. 74, no. 4, pp. 494-522, 1998.

[13] FCC, "447498 D04 Interim General RF Exposure Guidance v01," United State (US) Federal Communications Communication (FCC), 2021.

[14] IEEE, "IEEE Standard for Safety Levels With Respect to Human Exposure to Electric, Magnetic, and Electromagnetic Fields, 0 Hz to 300 GHz, Standard IEEE C95.1-2019,," Oct. 2019 .

[15] N. Varsier et al., "D2.6: Global Wireless Exposure Metric definition v2," 2013. [Online]. Available: http://www.lexnet.fr/project-progress/publicdeliverables.html. [Accessed 23 01 2020].

[16] X. Foukas, G. Patounas, A. Elmokashfi, and M. K. Marina, "Network Slicing in 5G: Survey and Challenges," *IEEE Comms. Mag,* vol. 55, no. 5, pp. 94-100, May 2017.

[17] F. Boccardi, R. W. Heath, A. Lozano, T. L. Marzetta, and P. Popovski, "Five Disruptive Technology Directions for 5G," *IEEE Comms. Mag.,* vol. 52, no. 2, pp. 74-80, Feb. 2014.

[18] Xin Li, M. Samaka, H. A. Chan, D. Bhamare, L. Gupta, C. Guo, and R. Jain. "Network Slicing for 5G: Challenges and Opportunities," IEEE Internet Computing Mag., vol. 1089, no. 7801, p. 20–27, Oct. 2017.

[19] ITU-R, "IMT Vision — Framework and Overall Objectives of the Future Development of IMT for 2020 and Beyond," Sept. 2015.

[20] M. Y. Lyazidi, N. Aitsaadi and R. Langar, "Resource Allocation and Admission Control in OFDMA-Based Cloud-RAN," *IEEE Global Communications Conference (GLOBECOM),* Dec. 2016, pp. 1-6.

[21] A. T. Ajibare and O. Falowo, "Dynamic Slicing and Scheduling for 5G Networks Using Joint Power and Sub-Carrier Allocation," in *Southern Africa Telecommunication Networks and Applications Conference (SATNAC 2019)*, Hermanus, 2019. pp. 1-6.

[22] J. Ordonez-Lucena, P. Ameigeiras, D. Lopez, J. J. Ramos-Munoz, J. Lorca, J. Folgueira, "Network Slicing for 5G with SDN/NFV: Concepts, Architectures, and Challenges," *IEEE Communications Magazine,* vol. 55, no. 5, pp. 80-87, May 2017.

[23] 5G-PPP whitepaper, "Use Cases and Performance Evaluation Models," April 2016.

[24] L. Xu, M. Q. Meng, and H. Ren, "Effect of Subject Size on Electromagnetic Radiation from Source in Human Body Following 2450MHz Radio Frequency Exposure," *2007 IEEE International Conference on Integration Technology,* pp. 326-329, 2007.

[25] F. Hu, Opportunities in 5G Networks: A Research and Development Perspective, CRC Press, Taylor & Francis Group, ISBN 9780367574895, 2016, pp. 1-538.

[26] Nokia, "Dynamic end-to-end network slicing for 5G," *Nokia White Paper,* pp. 1-10, 2016.

[27] P. Demestichas, A. Georgakopoulos, D. Karvounas, K. Tsagkaris, V. Sta, J Lu, C. Xiong, and J. Yao., "5G on the Horizon: Key Challenges for the Radio-Access Network," *IEEE Vehicular Technology Magazine,* vol. 8, no. 3, pp. 47-53, Sept. 2013.

[28] Next Generation Mobile Networks Alliance, "NGMN 5G White Paper," 2015.

[29] Wireless Word Research Forum, "White Paper 3: End to End Network Slicing," Nov., 2017.

[30] P. Rost, C. Mannweiler, D.S. Michalopoulos, C. Sartori, V. Sciancalepore, N. Sastry, O. Holland, "Network Slicing to Enable Scalability and Flexibility in 5G Mobile Networks," *IEEE Communications Magazine,* vol. 55, no. 5, pp. 72-79, May 2017.

[31] P. Demestichas, A. Georgakopoulos, D. Karvounas, K. Tsagkaris, V. Stavroulaki, J. Lu, C. Xiong, J. Yao, "5G on the Horizon: Key Challenges for the Radio-Access Network," Vehicular Technology Magazine, vol. 8, no. 3, pp. 47-53, Sept. 2013, doi: 10.1109/MVT.2013.2269187.

[32] Open Networking Foundation, "Software-Defined Networking (SDN) Definition," [Online]. Available: https://www.opennetworking.org/sdn-resources/sdn-definition. [Accessed 18 April 2019].

[33] E. Kitindi, S. Fu, Y. Jia, A. Kabir, Y. Wang, "Wireless Network Virtualization With SDN and C-RAN for 5G Networks: Requirements, Opportunities, and Challenges," *IEEE Access,* vol. 5, pp. 19099-19115, 2017. doi: 10.1109/ACCESS.2017.2744672

[34] Open Networking Foundation. OpenFlow Switch Specification document ONF TR-025, ONF, 2015. [Online]. Available: https://www.opennetworking.org/wp-content/uploads/2014/10/openflow-switch-v1.5.1.pdf, [Online].

[35] Forwarding and Control Element Separation (ForCES). IETF, 2013, IEEE Standard RFC 5810, 2010., [Online].

[36] Path Computation Element (PCE), IETF, 2013, IEEE Standard RFC 5440, 2009, [Online].

[37] SDN Architecture Overview, document ONF TR-504, ONF, 2014.

[38] M. Richart, J. Baliosian, J. Serrat and J. Gorricho, "Resource Slicing in Virtual Wireless Networks: A Survey,," *IEEE Transactions on Network and Service Management,* vol. 13, no. 3, pp. 462-476, Sept. 2016.

[39] I. Sarrigiannis, E. Kartsakli, K. Ramantas, A. Antonopoulos and C. Verikoukis, “Application and Network VNF migration in a MEC-enabled 5G Architecture,” in *2018 IEEE 23rd International Workshop on Computer Aided Modeling and Design of Communication Links and Design of Communication Links and Networks (CAMAD)*, Barcelona, 2018.

[40] C. Casetti et al., “Network slices for vertical industries,” in *2018 IEEE Wireless Communications and Networking Conference Workshops (WCNCW)*, Barcelona, 2018.

[41] M. T Beck, M. Werner, S. Feld and T. Schimper, “Mobile Edge Computing: A Taxonomy,” in *AFIN 2014 : The Sixth International Conference on Advances in Future Internet*, IARIA, 2014', pp. 48-54.

[42] A. Ajibare and O. Falowo, “Resource Allocation and Admission Control Strategy for 5G Networks Using Slices and Users Priorities,” in *IEEE Africon Conference*, Accra, 2019, pp. 1-6.

[43] D. López-Pérez, X. Chu, A. V. Vasilakos and H. Claussen, “On Distributed and Coordinated Resource Allocation for Interference Mitigation in Self-Organizing LTE Networks,” *IEEE/ACM Transactions on Networking,* vol. 21, no. 4, pp. 1145-1158, Aug. 2013.

[44] H. Zhang, N. Liu, X. Chu, K. Long, A. Aghvami and V. C. M. Leung, “Network Slicing Based 5G and Future Mobile Networks: Mobility, Resource Management, and Challenges,” *IEEE Communications Magazine,* vol. 55, no. 8, pp. 138-145, Aug. 2017.

[45] M. Richart, J. Baliosian, J. Serrat and J. Gorricho, “Resource Slicing in Virtual Wireless Networks: A Survey,” *IEEE Transactions on Network and Service Management,* vol. 13, no. 3, pp. 462-476, Sept. 2016.

[46] B. Han, A. DeDomenico, G. Dandachi, A. Drosou, D. Tzovaras, R. Querio, F. Moggio, O. Bulakci and H. D. Schotten, “Admission and Congestion Control for 5G Network Slicing,” *2018 IEEE Conference on Standards for Communications and Networking (CSCN*), Paris, 2018, pp. 1-6.

[47] M. Monemi, M. Rasti and E. Hossain, “Low-Complexity SINR Feasibility Checking and Joint Power and Admission Control in Prioritized Multitier Cellular Networks,” *IEEE Transactions on Wireless Communications,* vol. 15, no. 3, pp. 2421-2434, March 2016.

[48] E. W. Knightly and N. B. Shroff, “Admission Control for Statistical QoS: Theory and Practice,” *IEEE Networks,* vol. 13, no. 2, pp. 20-29, Mar./Apr. 1999.

[49] M. H. Ahmed, “Call Admission Control in wireless Networks: A Comprehensive Survey,” *IEEE Commun. Surv. Tuts,* vol. 7, no. 1-4, pp. 50–69,, Feb. 2005.

[50] M. Ghaderi and R. Boutaba, “Call Admission Control in Mobile Cellular Networks: A Comprehensive Survey,” *Wireless Commun. Mobile Comput.,* vol.

6, no. 1, p. 69–93, Apr. 2006.

[51] Y. Fang and Y. Zhang, “Call Admission Control Schemes and Performance Analysis in Wireless Mobile Networks,” *IEEE Trans. Veh. Technology,* vol. 51, no. 2, p. 371–382, Aug. 2002.

[52] K. Park and C. Kim, “A Framework forVvirtual Network Embedding in Wireless Networks,” *4th Int. Conf. ACM Future Internet Technol.,* Jun. 2009, p. 5–7.

[53] D. Yun and Y. Yi, “Virtual network embedding in wireless multihop networks,” in *6th Int. Conf. ACM Future Internet Technol.,* Jun. 2011, pp. 30–33.

[54] M. Yang, Y. Li, L. Zeng, D. Jin, and L. Su, “Karnaugh-map like online embedding algorithm of wireless virtualization,” in *IEEE 15th Int. Symp. Wireless Pers. Multimedia Commun.*, May 2012.

[55] M. Yang, Y. Li, D. Jin, J. Yuan, L. Su, and L. Zeng, “Opportunistic spectrum sharing based resource allocation for wireless virtualization,” in *IEEE Seventh Int. Conf. Innovative Mobile Internet Serv. Ubiquitous Comput.*, Feb. 2013, pp. 51-58.

[56] M. Yang, Y. Li, J. Liu, D. Jin, J. Yuan, and L. Zeng, “Opportunistic Spectrum Sharing for Wireless Virtualization,” in *IEEE Wireless Commun. Netw. Conf. (WCNC)*, 2014, pp. 1803-1808.

[57] J. van de Belt, H. Ahmadi, and L. E. Doyle, “A dynamic embedding algorithm for wireless network virtualization,” in *IEEE 80th Veh. Technol. Conf. (VTC2014-Fall),* 2014, pp. 1-6.

[58] A. Abdelnasser and E. Hossain, “Resource Allocation for an OFDMA Cloud-RAN of Small Cells Underlaying a Macrocell,” *IEEE Transactions on Mobile Computing,* vol. 15, no. 11, pp. 2837-2850, Nov. 2016.

[59] L. Zanzi, J. X. Salvat, V. Sciancalepore, et al., “Overbooking Network Slices End-to-End: Implementation and Demonstration,” in *ACM SIGCOMM 2018 Conference on Posters and Demos. ACM*, 2018, pp. 144-146.

[60] M. R. Raza, C. Natalino, P. Öhlen, L. Wosinska and P. Monti, “A Slice Admission Policy Based on Reinforcement Learning for a 5G Flexible RAN,” in *44th European Conference and Exhibition on Optical Communication (ECOC)*, 2018, pp. 1-3.

[61] M. R. Raza, A. Rostami, L. Wosinska, et al., “Resource Orchestration Meets Big Data Analytics: The Dynamic Slicing Use Case,” in *44th European Conference and Exhibition on Optical Communication (ECOC)*, 2018, pp. 1-3.

[62] D. Bega, M. Gramaglia, A. Banchs, V. Sciancalepore, K. Samdanis and X. Costa-Perez, “Optimising 5G Infrastructure Markets: The Business of Network Slicing,” in *INFOCOM 2017-IEEE Conference on Computer Communications*, 2017, pp. 1-9.

[63] P. Caballer, A. Banchs, G. de Veciana, X. Costa-Pérez and A. Azcorra, "Network Slicing for Guaranteed Rate Services: Admission Control and Resource Allocation Games," in *IEEE Transactions on Wireless Communications*, 2018. vol. 17, no. 10, pp. 6419-6432, Oct. 2018.

[64] M. Mirahsan, G. Senarath, H. Farmanbar, N. D. Dao and H. Yanikomeroglu, "Admission Control of Wireless Virtual Networks in HetHetNets," *IEEE Transactions on Vehicular Technology,* vol. 67, no. 5, pp. 4565-4576, May 2018.

[65] J. Voigt-Antons, T. Hoβfeld, S. Egger-Lampl, R. Schatz and S. Möller, "User Experience of Web Browsing - The Relationship of Usability and Quality of Experience," in *2018 Tenth International Conference on Quality of Multimedia Experience (QoMEX)*, Cagliari, 2018, pp. 1-3.

[66] P. H. A. Rezende and E. R. M. Madeira, "An adaptive network slicing for LTE radio access networks," *2018 Wireless Days (WD)*, Dubai, 2018, pp. 68-73.

[67] Y. Zaki, L. Zhao, C. Görg and A. Timm-Giel, "LTE Mobile Network Virtualisation," *Mobile Networks and Application,* vol. 16, no. 4, pp. 424-432, August 2011.

[68] M. Hu, Y. Chang, Y. Sun and H. Li, "Dynamic Slicing and Scheduling for Wireless Network Virtualization in Downlink LTE System," in *19th International Symposium on Wireless Personal Multimedia Communications (WPMC)*, Shenzhen, 2016.

[69] J. Yang, J. Hu, K. Lv, Q. Yu and K. Yang, "Multi-Dimensional Resource Allocation for Uplink Throughput Maximisation in Integrated Data and Energy Communication Networks," *IEEE Access,* vol. 6, pp. 47163-47180, 2018.

[70] H. Hsu and K. Chen, "A Resource Allocation Perspective on Caching to Achieve Low Latency," *IEEE Communications Letters*, vol. 20, no. 1, pp. 145-148, Jan. 2016.

[71] A. Abdelnasser and E. Hossain, "On Resource Allocation for Downlink Power Minimization in OFDMA Small Cells in a Cloud-RAN," in *2015 IEEE Global Communications Conference (GLOBECOM)*, San Diego, CA, 2015, pp. 1-6.

[72] R. K. Raman and K. Jagannathan, "Downlink Resource Allocation Under Time-Varying Interference: Fairness and Throughput Optimality," *IEEE Transactions on Wireless Communications,* vol. 17, no. 2, pp. 722-735, Feb. 2018.

[73] S. Ismail, C. K. Ng and N. K. Noordin, "Fairness Resource Allocation for Downlink OFDMA Systems," *2009 IEEE 9th Malaysia International Conference on Communications (MICC),* 2009, pp. 575-579.

[74] J. C. Lin, "Telecommunications health and safety: Public exposure to radio frequency, microwave, and millimeter-wave electromagnetic radiation," *URSI*

*Radio Science Bulletin,* vol. 2016, no. 356, pp. 49-51, March 2016.

[75] W. H. Bailey et al., "Synopsis of IEEE Std C95.1™-2019 "IEEE Standard for Safety Levels With Respect to Human Exposure to Electric, Magnetic, and Electromagnetic Fields, 0 Hz to 300 GHz," *IEEE Access,* vol. 7, pp. 171346-171356, 2019.

[76] S. Romeo, A. Sannino, O. Zeni, L. Angrisani, R. Massa and M. R. Scarfì, "Effects of Radiofrequency Exposure and Co-Exposure on Human Lymphocytes: The Influence of Signal Modulation and Bandwidth," *IEEE Journal of Electromagnetics, RF and Microwaves in Medicine and Biology,* vol. 4, no. 1, pp. 17-23, 2020.

[77] D. Colombi, P. Joshi, B. Xu, F. Ghasemifard, V. Narasaraju, C. Törnevik, "Analysis of the Actual Power and EMF Exposure from Base Stations in a Commercial 5G Network," *Applied Sciences. 2020,* vol. 10, no. 15, pp. 1-10, July 2020.

[78] Ofcom, White Paper, "Electromagnetic Field (EMF) measurements near 5G mobile phone base stations," The Office of Communications (Ofcom), 1 March 2021.

[79] P. De Lellis, F. L. Iudice and N. Pasquino, "Time-Series-Based Model and Validation for Prediction of Exposure to Wideband Radio Frequency Electromagnetic Radiation," *IEEE Transactions on Instrumentation and Measurement,* vol. 69, no. 6, pp. 3198-3205, June 2020.

[80] W. Yang, Y. Chun, Y. Liu, B. Li and C. Cao., "The Correlation Analysis of Exposure to the Electromagnetic Field from Base Stations," *Progress in Electromagnetics Research,* vol. 65, pp. 23-30, 2017, doi:10.2528/PIERL16041201.

[81] S. Aerts, L. Verloock, M. V. D. Bossche, D. Colombi, L. Martens, C. Törnevik, and W. Joseph, "In-situ Measurement Methodology for the Assessment of 5G NR Massive MIMO Base Station Exposure at Sub-6 GHz Frequencies," *IEEE Access,* vol. 7, pp. 184658-184667, 2019, doi:10.1109/ACCESS.2019.2961225.

[82] A. M. El-Hajj and T. Naous, "Radiation Analysis in a Gradual 5G Network Deployment Strategy," in *2020 IEEE 3rd 5G World Forum (5GWF)*, 2020.

[83] A. Ahmad, R. Ariffin, N. M. Noor and M. A. Sagiruddin, "1.8 GHz Radio Frequency signal radiation effects on human health," *2011 IEEE International Conference on Control System, Computing and Engineering,* 2011, pp. 546-550.

[84] J. C. Lin, "Radio-frequency radiation safety and health: Current standards and their bases for safe human exposure to radio-frequency radiation," *URSI Radio Science Bulletin,* vol. 2004, no. 309, pp. 50-52, June 2004.

[85] M. H. Capstick, S. Kuehn, V. Berdinas-Torres, Y. Gong, P. F. Wilson, J. M. Ladbury, G. Koepke, D. L. McCormick, J. Gauger, R. L. Melnick, N. Kuster, "A Radio Frequency Radiation Exposure System for Rodents Based on

Reverberation Chambers," *IEEE Transactions on Electromagnetic Compatibility,* vol. 59, no. 4, pp. 1041-1052, Aug. 2017.

[86] J. W. Hansen, E. M. Swartz, J. D. Cleveland, S. M. Asif, B. Brooks, B. D. Braaten and D. L. Ewert, "A Systematic Review of In Vitro and In Vivo Radio Frequency Exposure Methods," *IEEE Reviews in Biomedical Engineering,* vol. 13, pp. 340-351, 2020.

[87] M. Cavagnaro and J. C. Lin, "Importance of Exposure Duration and Metrics on Correlation Between RF Energy Absorption and Temperature Increase in a Human Model," *IEEE Transactions on Biomedical Engineering,* vol. 66, no. 8, pp. 2253-2258, Aug. 2019.

[88] Jianqing Wang, O. Fujiwara and T. Uda, "New approach to safety evaluation of human exposure to stochastically-varying electromagnetic fields," *IEEE Transactions on Electromagnetic Compatibility 10.1109/TEMC,* vol. 47, no. 4, pp. 971-976, Nov. 2005.

[89] J. M. Paniagua, M. Rufo, A. Jimenez, A. Antolin and F. T. Pachon, "Estimation of Uncertainties in Electric Field Exposure From Medium-Frequency AM Broadcast Transmitters," *IEEE Transactions on Instrumentation and Measurement,* vol. 61, no. 1, pp. 122-128, Jan. 2012.

[90] M. R. Castellanos, Y. Liu, D. J. Love, B. Peleato, J. M. Jin and B. M. Hochwald, "Signal-Level Models of Pointwise Electromagnetic Exposure for Millimeter Wave Communication," *IEEE Transactions on Antennas and Propagation,* vol. 68, no. 5, pp. 3963-3977, May 2020.

[91] K. Taguchi, I. Laakso, K. Aga, A. Hirata, Y. Diao, J. Chakarothai, T. Kashiwa, "Relationship of External Field Strength With Local and Whole-Body Averaged Specific Absorption Rates in Anatomical Human Models," *IEEE Access,* vol. 6, pp. 70186-70196, 2018. doi: 10.1109/ACCESS.2018.2880905.

[92] R. D. Morris, L. L. Morgan and D. Davis, "Children Absorb Higher Doses of Radio Frequency Electromagnetic Radiation From Mobile Phones Than Adults," *IEEE Access,* vol. 3, pp. 2379-2387, 2015. doi: 10.1109/ACCESS.2015.2478701.

[93] W. Joseph and L. Martens, "Comparison of safety distances based on the electromagnetic field and based on the SAR for occupational exposure of a 900-MHz base station antenna," *IEEE Transactions on Electromagnetic Compatibility,* vol. 47, no. 4, pp. 977 - 985, 2005.

[94] H. Wang, "Analysis of Electromagnetic Energy Absorption in the Human Body for Mobile Terminals," *IEEE Open Journal of Antennas and Propagation,* vol. 1, pp. 113-117, 2020, doi: 10.1109/OJAP.2020.2982507.

[95] K. R. Foster, A. Lozano-Nieto, P. J. Riu, and T. S. Ely, "Heating of tissues by microwaves: A model analysis," *Bioelectromagnetics,* vol. 19, no. 7, pp. 420–428, , 1998 .

[96] K. R. Foster, M. C. Ziskin, Q. Balzano and A. Hirata, “Thermal Analysis of Averaging Times in Radio-Frequency Exposure Limits Above 1 GHz,” *IEEE Access,* vol. 6, pp. 74536-74546, 2018, doi: 10.1109/ACCESS.2018.2883175.

[97] C. Luo, J. Ji, Q. Wang, L. Yu and P. Li, “Online Power Control for 5G Wireless Communications: A Deep Q-Network Approach,” in *2018 IEEE International Conference on Communications (ICC),*, Kansas City, 2018, pp, 1-6.

[98] S. A. Saad, M. Ismail and R. Nordin, “Autonomous power control scheme for LTE-advanced macro-femto networks,” in *2013 IEEE Student Conference on Research and Developement*, Putrajaya, 2013, pp. 524-528.

[99] Z. Wang, W. Xiong, C. Dong, J. Wang and S. Li, “A novel downlink power control scheme in LTE heterogeneous network,” *2011 International Conference on Computational Problem-Solving (ICCP),* Chengdu, 2011, pp. 241-245.

[100] E. Tejaswi and B. Suresh, “Survey of Power Control Schemes for LTE Uplink,” *International Journal of Computer Scienece and Information Technologies,* vol. 4, no. 2, pp. 369-373, 2013.

[101] ICNIRP, “Guidelines for Limiting Exposure to Electromagnetic Fields (100 kHz to 300 GHz),” *Health Physics,* vol. 118, no. 5, pp. 483-524, 2020.

[102] J. C. Lin, “Radio-frequency radiation safety and health: Recent activities on radio-frequency exposure guidelines,” *URSI Radio Science Bulletin,* vol. 2014, no. 351, pp. 73-74, Dec. 2014.

[103] O. M. Dumin, O. O. Dumina, N. N. Kolchigin, D. D. Ivanchenko, Y. G. Shckorbatov and V. N. Pasiuga, “Simulation of microwave exposure of human cells by electromagnetic field of EMF band,” in *2011 VIII International Conference on Antenna Theory and Techniques*, 2011., pp. 312-314.

[104] IEEE, “IEEE Recommended Practice for Determining the Peak Spatial-Average Specific Absorption Rate (SAR) in the Human Head from Wireless Communications Devices Measurement Techniques, IEEE Std 1528,” 2013.

[105] B. Maes, “Evaluation guidelines for sleeping areas (sbm-2015). neuss, rosenheim (de): Baubiologie maes, ibn.,” Institut fur baubiologie+ nachhaltigkeit (ibn). Building Biology, pp. 1-4, May 2015.

[106] H. Chiang, “Rationale for setting emf exposure standards,” 2009.

[107] A. Ferikoğlu, O. Çerezci, M. Kahriman and Ş. Ç. Yener, “Electromagnetic Absorption Rate in a Multilayer Human Tissue Model Exposed to Base-Station Radiation Using Transmission Line Analysis,” *IEEE Antennas and Wireless Propagation Letters,* vol. 13, pp. 903-906, 2014.

[108] S. Iskra, R. McKenzie and I. Cosic, “Personal, Non-Invasive Dosimetry for Radio-Frequency Human Exposure Assessment,” in *Personal, Non-Invasive Dosimetry for Radio-Frequency Human Exposure Assessment," 2007 29th Annual International Conference of the IEEE Engineering in Medicine and*

*Biology Society*, 2007, pp. 2319-2322.

[109] S.O. Oladejo and O.E. Falowo, "Latency-Aware Dynamic Resource Allocation Scheme for 5G Heterogeneous Network: A Network Slicing-Multitenancy Scenario," in *2019 International Conference on Wireless and Mobile Computing, Networking and Communications (WiMob)*, Barcelona, Spain, 2019, pp. 1-7.

[110] S. Haryadi and D. R. Aryanti, "The fairness of resource allocation and its impact on the 5G ultra-dense cellular network performance," in *2017 11th International Conference on Telecommunication Systems Services and Applications (TSSA)*, Lombok, 2017, pp. 1-4.

[111] R. Xie, J. Wu, R. Wang and T. Huang, "A Game Theoretic Approach for Hierarchical Caching Resource Sharing in 5G Networks with Virtualization," *China Communications,* vol. 16, no. 7, pp. 32-48, July 2019.

[112] L. Miuccio, D. Panno and S. Riolo, "Joint Congestion Control and Resource Allocation for Massive MTC in 5G Networks Based on SCMA," in *2019 15th International Conference on Telecommunications (ConTEL)*, Graz, Austria, 2019, pp. 1-8.

[113] P. Liu, C. Wang, M. Lei, M. Li and M. Zhao, "Adaptive Priority-threshold Setting Strategy for Statistical Priority-based Multiple Access Network," in *2020 IEEE 91st Vehicular Technology Conference (VTC2020-Spring)*, Antwerp, Belgium, 2020, pp. 1-5.

[114] N. Bansal and M. Dutta, "Performance Evaluation of Task Scheduling with Priority and Non-Priority in Cloud Computing," in *2014 IEEE International Conference on Computational Intelligence and Computing Research*, Coimbatore, 2014, pp. 1-4.

[115] R. Pandey, A. Srivastava and R. Rathore, "An Efficient Resource Scheduling Algorithm using Dynamic Priority in Grid Computing," in *2017 International Conference on Current Trends in Computer, Electrical, Electronics and Communication (CTCEEC)*, Mysore, 2017, pp. 717-720.

[116] J. Zhu et al., "An Efficient Priority-Driven Congestion Control Algorithm for Data Center Networks," *China Communications,* vol. 17, no. 6, pp. 37-50, June 2020.

[117] V. Sciancalepore, K. Samdanis, X. Costa-Perez, D. Bega, M. Gramaglia and A. Banchs, "Mobile traffic forecasting for maximizing 5g network slicing resource utilization," in *IEEE INFOCOM 2017 - IEEE Conference on Computer Communications*, Atlanta, GA, May 2017, pp. 1-9.

[118] S. Kumar, R. Devaraj and A. Sarkar, "A hybrid offline-online approach to adaptive downlink resource allocation over LTE," *IEEE/CAA Journal of Automatica Sinica,* vol. 6, no. 3, pp. 766-777, May 2019.

[119] M. Jiang, M. Condoluci and T. Mahmoodi, "Network Slicing Management & Prioritization in 5G Mobile Systems," in *European Wireless 2016; 22th*

*European Wireless Conference,* 2016, pp. 1-6.

[120] V. K. Choyi, A. Abdel-Hamid, Y. Shah, S. Ferdi and A. Brusilovsky, "Network slice selection, assignment and routing within 5G Networks," in *2016 IEEE Conference on Standards for Communications and Networking (CSCN)*, Berlin, 2016, pp. 1-7.

[121] A. Devlic, A. Hamidian, D. Liang, M. Eriksson, A. Consoli and J. Lundstedt, "NESMO: Network slicing management and orchestration framework," in *2017 IEEE International Conference on Communications Workshops (ICC Workshops)*, Paris, 2017, pp. 1202-1208.

[122] S. Parsaeefard, V. Jumba, M. Derakhshani and T. Le-Ngoc, "Joint Resource Provisioning and Admission Control in Wireless Virtualized Networks," in *2015 IEEE Wireless Communications and Networking Conference (WCNC)*, New Orleans, LA, 2015, pp. 2020-2025.

[123] A. Pratap, R. Misra and S. K. Das, "Resource Allocation to Maximize Fairness and Minimize Interference for Maximum Spectrum Reuse in 5G Cellular Networks," in *," 2018 IEEE 19th International Symposium on "A World of Wireless, Mobile and Multimedia Networks*, Chania, 2018.

[124] Y. Huang and J. Wiart, "Simplified Assessment Method for Population RF Exposure Induced by a 4G Network," *IEEE Journal of Electromagnetics, RF and Microwaves in Medicine and Biology,* vol. 1, no. 1, pp. 34-40, June 2017.

[125] MATLAB, version 9.6.0.1072779 (R2019a). The Mathworks Inc., 2019..

[126] G. Koutitas and T. Samaras, "Exposure Minimization in Indoor Wireless Networks," *IEEE Antennas and Wireless Propagation Letters,* vol. 9, pp. 199-202, 2010, doi: 10.1109/LAWP.2010.2045870.

[127] A. Gati, M. Wong and J. Wiart, "Duality Between Uplink Local Downlink Whole-Body Exposures In Operating Networks," *IEEE Transactions on Electromagnetic Compatibility,* vol. 52, no. 4, pp. 829-836, 2010.

[128] T. Brown, "Containing exposure in 5G networks, a perspective from LExNet," in *5G Radio Technology Seminar. Exploring Technical Challenges in the Emerging 5G Ecosystem*, 2015.

[129] T. Sarrebourse et al., "Towards EMF exposure assessment over real cellular networks: An experimental study based on complementary tools," in *2014 11th International Symposium on Wireless Communications Systems (ISWCS)*, 2014.

[130] D. Plets et al.,, "Whole-body and Localized SAR and Dose Prediction Tool for Indoor Wireless Network Deployments," in *2014 11th International Symposium on Wireless Communications Systems (ISWCS)*, 2014.

[131] M. Popović, M. Tesanovic and B. Radier, "Strategies for Reducing the Global EMF Exposure: Cellular Operators Perspective,," in *2014 11th International*

*Symposium on Wireless Communications Systems (ISWCS)*, 2014.

[132] J. Stephan, M. Brau, Y. Corre and Y. Lostanlen, "Joint Analysis of Small-cell Network Performance and Urban Electromagnetic Field Exposure," in *The 8th European Conference on Antennas and Propagation (EuCAP 2014)*, 2014, pp. 2623-2627.

[133] M. Tesanovic E. Conil, A. D. Domenico, R. Aguero, F. Freudenstein, L. M. Correia, S. Bories, L. Martens, P. M. Wiedemann, J. Wiart, "The LEXNET Project. Wireless Networks and EMF: Paving the Way for Low-EMF Networks of the Future," *IEEE Vehicular Technology Magazine,,* vol. 9, no. 2, pp. 20-28, June 2014.

[134] Y. A. Sambo, F. Heliot and M. A. Imran, "A User Scheduling Scheme for Reducing Electromagnetic (EM) Emission in the Uplink of Mobile Communication Systems," in *2014 IEEE Online Conference on Green Communications (OnlineGreenComm)*, 2014, pp. 1-5.

[135] A. Moubayed, A. Shami and H. Lutfiyya, "Wireless Resource Virtualization With Device-to-Device Communication Underlaying LTE Network," *IEEE Transactions on Broadcasting,* vol. 61, pp. 734-740, Dec. 2015.

[136] M. Kamel, L. B. Le, and A. Girard, "LTE Wireless Network Virtualization: Dynamic Slicing via Flexible Scheduling," in *The 2014 IEEE 80th Vehicular Technology Conference (VTC Fall)*, Vancouver, Sept 2014, pp. 1-5.

[137] X. Xu, J. Luo and Q. Zhang, "Tolerable interference in multi-channel sensor networks: A measurement study," in *2010 IEEE 18th International Workshop on Quality of Service (IWQoS)*, Beijing, 2010.

[138] Y. Cheng, C. Chang, C. Lu and S. Kao, "Ensuring coverage quality with tolerable interference through optimizing the deployment of BSs in radio frequency communication," in *The 40th International Conference on Computers & Indutrial Engineering*, Awaji, 2010, pp. 1-5.

[139] Y. Matsumura, K. Temma, K. Ishihara, B. A. H. S. Abeysekera, T. Kumagai and F. Adachi, "Interference-aware channel segregation based dynamic channel assignment using SNR-based transmit power control," in *2013 International Symposium on Intelligent Signal Processing and Communication Systems*, Naha, 2013.

[140] S. Chadchan and C. Akki, "A Fair Downlink Scheduling Algorithm for 3GPP LTE Networks," *International Journal of Computer Network and Information Security (IJCNIS),* vol. 5, no. 6, pp. 34-41, 2013.

[141] 3GPP, "Further advancements for E-UTRA physical layer aspects (Release 9)," 3GPP, Nice, France, TR 36.814, Mar. 2010.

[142] O. Grondalen, A. Zanella, K. Mahmood, M. Carpin, J. Rasool and O. N. Osterbo, "Scheduling Policies in Time and Frequency Domains for LTE Downlink Channel: A Performance Comparison," *IEEE Transactions on*

*Vehicular Technology,* vol. 66, no. 4, pp. 3345-3360, 2017.

[143] Xiaoying Gan, Youyun Xu and Wentao Song, "A Feedback Reduction Algorithm for OFDM Based Transmit Power Adaptation," in *IEEE International Conference on Communications, ICC 2005* , 2005, pp. 2616-2620.

[144] M. Yassin, S. Lahoud, M. Ibrahim and K. Khawam, "A downlink power control heuristic algorithm for LTE networks," in *21st International Conference on Telecommunications (ICT)*, Lisbon, 2014, pp. 323-327.

[145] M. G. Shajan and P. V. Khushbu, "Minimizing Interference by Indoor-Cell of 4G LTE Networks," in *2015 Fifth International Conference on Communication Systems and Network Technologies*, Gwalior, 2015, pp. 249-252.

[146] A. Giovanidis, T. Haustein, E. Jorswieck, and D. Kim, "Maximization of the single user rate in OFDMA assuming equal power on allocated subcarriers," in *Vehicular Technology Conference, . VTC2007- spring. IEEE 65th*, April 2007, pp. 2751-2755.

[147] J. Gavan and M. Haridim, "Mobile Radio Base Stations and Handsets Radiation Effects: Analysis, Simulations and Mitigation Techniques," in *2007 International Symposium on Electromagnetic Compatibility*, Qingdao , 2007, pp. 15-18.

[148] European Telecommunications Standards Institute, "Digital cellular telecommunications system (Phase 2+); Radio transmission and reception (3GPP TS 45.005 version 11.3.0 Release 11)," 2015.

[149] A.T. Ajibare and O. Falowo, "Resource Allocation and Admission Control Strategy for 5G Networks Using Slices and Users Priorities.," *21st Southern Africa Telecommunication Networks and Applications Conference (SATNAC 2018),* Hermanus, 2018, pp. 1-2.

[150] S. -Y. Lien, S. -L. Shieh, Y. Huang, B. Su, Y. -L. Hsu and H. -Y. Wei, "5G New Radio: Waveform, Frame Structure, Multiple Access, and Initial Access," *IEEE Communication Magazine,* vol. 55, no. 8, pp. 64-71, June 2017.

[151] M. Celaya-Echarri, L. Azpilicueta, J. Karpowicz, V. Ramos, P. Lopez-Iturri and F. Falcone, "From 2G to 5G Spatial Modeling of Personal RF-EMF Exposure Within Urban Public Trams," *IEEE Access,* vol. 8, pp. 100930-100947, May 2020, doi: 10.1109/ACCESS.2020.2997254.

[152] B. Thors, D. Colombi, Z. Ying, T. Bolin and C. Törnevik, "Exposure to RF EMF From Array Antennas in 5G Mobile Communication Equipment," *IEEE Access,* vol. 4, pp. 7469-7478, 2016.

[153] H. Lee and S. Chong, "Downlink resource allocation in multi-carrier systems: frequency-selective vs. equal power allocation," *IEEE Transactions on Wireless Communications,* vol. 7, no. 10, pp. 3738-3747, October 2008.

[154] A. T. Ajibare, D. Ramotsoela, L. A. Akinyemi and S. O. Oladejo, "RF EMF Radiation Exposure Assessment of 5G Networks: Analysis, Computation and

Mitigation Methods," in *2021 IEEE Africon International Conference*, Arusha, 2021, pp. 1-6.

[155] R. Rodríguez-Cano, S. Zhang, K. Zhao and G.F. Pedersen, "User Body Interaction of 5G Switchable Antenna System for Mobile Terminals at 28 GHz," in *2019 13th European Conference on Antennas and Propagation (EuCAP)*, Krakow, 2019, pp. 1-4.

[156] IEEE, "IEEE Standard for Safety Levels with Respect to Human Exposure to Electric, Magnetic, and Electromagnetic Fields, 0 Hz to 300 GHz," *IEEE Std C95.1-2019 (Revision of IEEE Std C95.1-2005/ Incorporates IEEE Std C95.1-2019/Cor 1-2019)*, pp. 1–312, 2019.